Forensic Analysis of the NSTX-U PF1A-Upper Coil Failure

Rev. 0

November 18, 2016

Irving J. Zatz

Digitally signed by Irving J. Zatz
DN: cn=Irving J. Zatz, o, ou=PPPL, email=zatz@pppl.gov, c=US
Date: 2016.11.18 16:15:19 -05'00'

Irving J. Zatz

Joseph R. Petrella, Jr., PE

PPPL
PRINCETON PLASMA PHYSICS LABORATORY

Table of Contents

1.0 Executive Summary

On July 22, 2016, the NSTX-U project team suspended plasma operations due to the inoperability of the PF1A Upper (PF1A-U) coil. Preliminary indications evidenced that the PF1A-U coil experienced a coolant blockage. An external coolant leak developed from the PF1A-U coil pack after the blockage was attempted to be cleared. A post-mortem physics analysis indicated that an undetected gradual deterioration of coil inductance preceded the coolant blockage in the weeks leading up to the operational suspension.

PF1A-U is a conventionally wound de-ionized water-cooled copper conductor electromagnet. The coil conductor is electrically insulated with layers of fiberglass and Kapton tape and wound on a stainless steel mandrel. The coil pack is vacuum-pressure impregnated (VPI) with CTD-425 epoxy on the mandrel as an assembly. The coil conductor is approximately 440 feet long and has four (4) in-line induction braze joints. Turn density is maximized in the design by employing conductor joggles in turn transition regions.

Following the PF1A-U failure, a forensic team was formed to perform a non-destructive examination followed by destructive tests in order to determine the cause(s) of failure. The subsequent investigation, documentation, and analysis relative to the condition of the PF1A-U are the subject of this report. Relevant articles of evidence were thoroughly photographed during the investigation process. The photographs included in this report are a representative sample of the photographs recorded as part of the complete investigative record.

On August 24, 2016, the coil was removed from NSTX-U initiating the investigation. A comprehensive initial examination included visual inspection, low pressure testing, and electrical testing of the coil assembly. Initial non-destructive testing was followed by extensive non-destructive radiography. The radiographic study confirmed the locations of four braze joints and identified five anomalies. Further study of the identified features required access to the cooling paths of the conductors. Three coil pack cutting planes in feature-free benign regions were proposed based on the radiography results to provide access to the anomalous regions via the conductor cooling paths. A procedure was developed and approved by Peer Review to perform the minimally destructive task of sectioning the coil pack. The coil was cut into three sections on a horizontal Lucas Mill in the PPPL RESA building. Cuts were cautiously made in 0.03-inch depth increments. All efforts were made to comprehensively collect and catalog any debris from the milling procedure. Photographs were used to extensively document the process.

Two of the three coil sections were removed from the mandrel at the conclusion of cutting. The third section, containing the five anomalies identified in the radiographic study, the coil leads, and two braze joints, was left on the mandrel in order to minimize compromising evidence. All three sections were subjected to visual borescope/videoscope inspection through the cooling path, vacuum testing, and electrical testing of every conductor segment. One conductor cooling path visually evidenced a void through the sidewall of the cooling path. Vacuum testing

indicated that the cooling path with the void anomaly communicated pneumatically to atmosphere. Vacuum testing of all the remaining cooling path segments evidenced that there were no other detectable conductor cooling path leaks. The identified void in the conductor cooling path was not proximal to a braze or joggle. Electrical testing indicated that the voided conductor segment was a member of a group of 14 conductor segments that evidenced low-resistance connectivity. Electrical testing of the remaining conductor segments was unremarkable and evidenced no other reportable significant issues.

Two independent blockages were visually identified in conductor segments proximal to braze joints. The blockage material was removed from the blockage area and collected as evidence. Examination of the blockage material and braze joint interior surfaces indicated that the blockage material did not originate at the braze joint locations. The four braze joints and two lead segments were subjected to 400 psi hydrostatic pressure testing and evidenced that there were no detectable leaks in the tested cooling path segments. Helium leak testing was performed on two braze joints and both leads to confirm the hydrostatic test findings and reinforced the finding that there were no detectable cooling path leaks present in the tested cooling path segments.

Visual examination of the conductor electrical insulation system evidenced numerous un-wetted areas of fiberglass indicative of a lack of epoxy impregnation. Voids indicative of gaseous bubbles were identified in numerous locations in the sectioned portions of the insulation system. An absence and/or insufficient volume of fiberglass was evidenced by the observation of resin rich areas adjacent to exposed transitions. The observed deficiencies in the conductor electrical insulation system was noted in a total examined volume of approximately 2.34% of the coil pack, suggesting that the occurrence of the deficiencies may be significant. The sum of the anomalies noted in the conductor electrical insulation system indicated that the vacuum pressure impregnation (VPI) of the coil was deficient.

Based on the subject investigation observations, the writers' experience, training, and education, the writers conclude the following within a reasonable degree of engineering certainty:

1. The evidence indicates a single point of failure as indicated by a void in a conductor coolant path sidewall.
2. It is probable that electrical activity at the void location resulted in molten debris that blocked the cooling path at restrictions in the conductor braze joints.
3. Communication of debris into the conductor electrical insulation system most likely resulted in the observed low-resistance connectivity to 13 other conductor segments.
4. The most probable cause of the initiating event, by process of elimination, was a conductor electrical insulation system anomaly. An insulation anomaly may have been comprised of some combination of the following:
    a. Conductive material (debris or liquid)
    b. Exposed conductor
    c. Reduced insulation thickness

    d. Dry/unwetted insulation & voids
    e. Mechanical movement/abrasion
    f. Insulation wrapping inconsistencies
5. The exact characteristic(s) of the originating anomaly is indeterminate at this time and its nature may not be able to be determined due to the failure event itself potentially having destroyed the causal evidence.
6. Further non-destructive and destructive examination of the identified failure area would be necessary to potentially augment the characteristics of the initiating event anomaly.

The writers reserve the right to amend and/or supplement this report in the event that additional investigative steps are taken and/or additional information becomes available for review.

2.0 Background

PF1A Upper (PF1A-U) is an electromagnet that was fabricated for the NSTX Upgrade in 2013-2014 by Everson Tesla Incorporated (ETI) located in Nazareth, PA. The fabrication process was prescribed by a PPPL Statement of Work and Specification [1, 2]. ETI documented the fabrication process including providing weekly reports at PPPL's request as part of the contract [3]. Several non-conformance reports (NCRs) were reported during the fabrication process. The most notable NCR indicated that tested braze joint samples did not meet strength performance specifications [4]. PPPL deemed the braze joints met an acceptable stress safety margin as long as they were not installed within two turns of the coil leads. ETI conformed to this requirement by not placing braze joints within two turns of coil conductor leads. The shipping release for the PF1A-U coil was signed by PPPL on June 11, 2014.

The electromagnet design included the following noteworthy features:

- Four in-line induction braze joints located in coil conductors
- Half-hard copper conductor was used for the windings
- One half-lapped layer of spirally wound fiberglass insulation, reduced from two half-lapped layers due to dimensional limitations
- Joggles utilized in turn transition regions
- CTD-425 epoxy to be vacuum pressure impregnated (VPI) and cured

The coil conductors are wrapped around a stainless steel mandrel with upper and lower flanges that position the coil pack conductors and added stiffness during operations. The delivered coil is shown in Figure 1. A representative schematic of the coil is shown in Figure 2. The location of the PF1A-U coil on the center stack of NSTX-U is shown in Figure 3.

Stefan Gerhardt documented the in-service history of the PF1A-U prior to the subject investigation and his record serves as a basis for the historical summary included in this report [5]. The PF1A-U coil was first put into service in August 2015 via the PPPL ISTP-001 process.

Following re-commissioning issues unrelated to the subject investigation, the coil was put into service again in December 2015 via the PPPL ISTP-001 process. From January 2016 thru June 27, 2016, PF1A-U operated without any detected incident for approximately 1000 shots of varying length and power. At no time was the coil operated at the maximum design level. PF1A-U flexible bus deflections were observed on May 20, 2016. From May 23 through June 17, repairs were made to the PF1A-U flexible bus. Impact of the flexible bus deflections relative to the subject investigation was reviewed by the investigation team. It was determined after review of the physical evidence and theoretical calculations that the flexible bus deflections did not impact the subject investigation. The flexible bus deflection incident is included in this report for completeness, only.

On June 28, 2016, at approximately 16:05, the PF1A-U cooling path monitoring flow switch changed electrical condition and evidenced a lack of cooling liquid flow. Diagnostic evaluation determined that this was not an issue with the sensor but that the coiling path within the body of coil was blocked/compromised. The coil electrical and water temperature waveforms were unremarkable leading up to the last shot attempted prior to the flow blockage detection.

Between June 30 and July 5, attempts were made to clear the blocked cooling path by various means including reversing flow. Coolant water recovered from PF1A-U was observed to be cloudy and evidenced particulate matter and a 'charred' odor. A biological assay was performed on a sample of coolant liquid and evidenced levels of biological activity in initial samples [9]. Coolant water from other coils was also sampled, tested, and was unremarkable. The coolant path of PF1A-U was flushed with de-ionized water mixed with Dawn and subsequently Alconox. The blockage was reconfirmed to be within the body of the coil and not in the supply/return hoses. Each time the blockage appeared to have been cleared, the coil re-clogged. Any resulting flow was far less than normal flow rates. On July 5, 2016, during 600 psi hydrostatic pressure testing of PF1A-U, water was observed coming from the bottom of NSTX-U. A copper/carbon slug was recovered from water used to flush the coil cooling path (Figure 4) along with other debris (Figure 5). Chemical analysis of the slug showed that its component elements correspond with the composition of the conductor/epoxy/glass matrix, but not the brazes (which would have shown evidence of silver and other elements). The conclusion at that time was that while a leak may exist at a braze, the slug was formed elsewhere.

On July 6, 2016, 15 psi pressure testing indicated that at least one blockage still existed in the coil with some of the results implying that there may be a second blockage. As reported in Reference 5, drying of the NSTX-U vessel and coils proceeded following the leak event. Vacuum pumping on PF1A-U cooling paths yielded a frothy/bubbly liquid indicative of soapy water remaining within the cooling path of the coil. The decision was made to bake the entire center stack (CS), which includes PF1A-U. The bakeout process continued until July 19. During that time, periodic inspections evidenced frothy water within the PF1A-U cooling paths and water at the base of the CS.

From July 20 through July 22, 2016, limited operations resume including inductively energizing PF1A-U for the purpose of performing a diagnostic on the coil. Review of archived data shows a gradual deterioration of PF1A-U's resistance and inductance (Figure 6) going back several months. All data pointed to an internal electrical failure of the coil including a breached cooling path. Effective July 22, 2016, PF1A-U operations were suspended.

On July 28, 2016, a forensic analysis of the PF1A-U coil was commissioned with the charge to evaluate the coil and determine the cause of failure, first utilizing non-destructive means followed by destructive testing. Peer reviews would be held to evaluate the forensic plans ahead of each phase of the work. Outside experts would be invited to participate to ensure that the widest pool of expertise would be able to input ideas into the forensic study. The forensic team was to be led by Irving J. Zatz and Joseph R. Petrella, Jr, PE.

3.0 PF1A-U Removal from NSTX-U

The PF1A-U coil was removed from the NSTX-U Center Stack on August 24, 2016. It was safely lifted, without incident, out of the test cell and onto a platform in the South High-Bay. The coil was surveyed for radiation activity and cleared by HP. Figures 7 thru 10 illustrate the removal and lift activity.

4.0 Initial Visual Inspection and Electrical Tests

The PF1A-U was visually examined and extensively photographed (Figures 11 thru 13) in the South High Bay. It was noted that portions of the observable surfaces evidenced a powdered deposit indicative of dried sediment. An external visual inspection of the coil conductor leads was unremarkable (Figures 14 and 15). A majority of the electromagnet was not visible due to the shields that cover the perimeter of the coil. These shields are welded to the upper and lower flanges of the mandrel. Nevertheless, areas of surface delamination and discoloration were observable in the gaps between the shields. Prior to removal of the shields, the lead-to-lead electrical coil resistance was measured with a Megger 10A DLRO micro-ohmmeter to be 5.942 milliohms on August 24, 2016. High-pot electrical tests at voltages ranging from 500 to 5,000 volts were performed and the data recorded for comparative purposes (Table 1). The shields were then removed with a die-grinder, thereby exposing the overall circumferential surface of the coil pack (Figures 16 thru 19). Blue tape was placed over sharp mandrel edges left by the grinder process as a safety precaution. High-pot electrical tests at voltages ranging from 500 to 5,000 volts were repeated on the shield-less coil on August 26, 2016 and compared to the previous tests. The comparison of the electrical tests was unremarkable (Table 1).

Table 1 – PF1A-U Post-Removal Electrical Tests

Tests performed on 08/24/2016 & 08/26/2016								
No water connected to coil								
Coil Resistance		5.942 milliohms		(10A DLRO)				
The coil case was grounded and coil leads shorted. Then the coil was hipotted to the case.								
		8/24/2016				8/26/2016		
Volts		**Leakage uA**				**Leakage uA**		
500		40				21		
1000		60				39		
1500		90				60		
2000		110				75		
2500		125				95		
3000		140				100		
3500		155				100		
4000		170				105		
4500		180				120		
5000		230				140		
	decayed to	170	after one minute			120	after one minute	

It is noteworthy that on June 6, 2016, approximately one month prior to the blockage event, the leakage current was measured to be 9uA at 5kV.

Figures 20 thru 24 illustrate focused views of the outside surface of PF1A-U coil. Short, dark vertical lines were observed that evidence separations/tears in the ground layer wrap. An internal coolant path leak in the electromagnet may communicate with these separations as potential exit points for coolant. Removal of the shields evidenced numerous ground wrap delamination areas identified by their lighter color and confirmed by lightly tapping the areas with a tool that audibly noted hollows beneath the ground layer.

Following this initial evaluation, a Peer Review was held on August 29, 2016 that summarized the findings to date then outlined the proposed investigative path forward. The goal was established to complete the investigation as quickly and efficiently as possible while minimizing the risk of compromising any of the evidence. A causal analysis outlining potential failure modes for PF1A-U was presented including:

- Defective conductor material leading to a crack, leak and/or blockage
- Over-pressurization within the coil
- Defective braze joint
- Conductive material introduced during fabrication establishes turn-to-turn contact
- Improper VPI – dry areas

- Design issues – copper hardness/brazes/joggles/single half-lapped fiberglass insulation layer
- Material corrosion
- Excessive temperatures – charring of CTD 425

Consensus was reached that the next step would be additional non-destructive evaluation by radiographic techniques.

5.0 Radiography and Low Pressure Testing

On August 30, 2016, the PF1A-U coil/mandrel was transported by PPPL truck to Mistras Group, Inc. (Mistras) in Marcus Hook, PA, and staged for gamma radiographic examination. On September 1, 2016, Petrella traveled to Mistras to observe a radiographic study of the PF1A-U. Mistras personnel employed an Iridium-192 radioisotope source to irradiate 14"x17" photostimulable phosphor plates placed in angular segments around the exterior of the PF1A-U coil. The exposed phosphor plates were digitized in a Virtual Media Integration (VMI) model 5100MS-C plate scanner. The PF1A-U exterior circumference was marked with 8 angular regions labeled "0" through "7" and a symmetric centerline was designated proximal to the mid-plane of the coil pack (Figure 25). Image segments located above the mid-plane area toward the lead-out flange were designated "A" and images below the mid-plane proximal to the tapered end of the mandrel were designated "B". Correspondingly, recorded images were identified in segmental fashion, i.e., "image 0_1A". A total of nineteen (19) images were recorded during the September 1, 2016 imaging session with scale reference. Images were surveyed for anomalies by Mistras representatives using VMI Starrview 8.0 NDT software. The September 1, 2016 survey identified (4) anomalies with signatures indicative of in-line braze joints (Figures 26 thru 29). The locations of these anomalies corresponded proximally to the locations identified in the Manufacturing Process Outline/Traveler (MPO) provided by the coil manufacturer, Everson Tesla, Inc. [6]. Additionally, the September 1, 2016 survey identified an anomalous region proximal the mid-plane of the coil pack section at the angular proximity of the lead-in/out area (Figure 30).

On September 8, 2016, Petrella again traveled to Mistras to observe a re-survey of the anomalous region and employ a triangulation analysis method developed at PPPL for determination of the radial position of the anomalies. Scale paper templates were used to position reference indices and the iridium-192 radioisotope source to create an intentional 25-degree parallax of the anomalous region (Figures 31 thru 32). A total of thirteen (13) new images were recorded and were indexed in a similar fashion to the previous radiograph images with scale reference and the addition of a parallax notation. The scaled images were digitally imported into an AutoCAD drawing. The anomalous regions angularly proximal to the lead-in/out area were divided into visually perceivable density variations "alpha" through "epsilon". In-line braze joint number two (2) was visible in the imaging and was also included in the triangulation analysis. Circles

and rectangles were drawn over the observed density variations to optically determine an approximate center point reference for each area (Figure 33). A triangulation analysis was performed to determine proximate radial positions of the observed anomalies (Figures 34 thru 37). The analysis indicated that the regions alpha through gamma were proximal to conductor rows eight (8) and nine (9), and between conductor layers two (2) and three (3). The analysis also indicated that braze joint number two (2) was radially proximal to layer two (2). This geometric approximation corresponded to the ETI MPO [6] documentation for braze joint number two (2), validating the radial positional interpolation of regions alpha through epsilon.

Further validation of the triangulation method was performed by surveying in-line braze joint number one (1) with the triangulation approach and comparing the results with the ETI MPO. The geometric approximation using the triangulation imaging technique proximally identified braze joint number one (1) in the reported radial position, thereby further validating the triangulation method used (Figure 38 and 39).

The completed radiographic study was used to select locations to segment the coil for destructive evaluation. The features observed in the radiographic study allowed the investigation team to minimize the risk of compromising anomalies and critical areas such as brazes, joggles and leads.

Low pressure testing of the entire intact coil was the final non-destructive step prior to segmenting the coil pack. Nitrogen gas was used to charge the PF1AU cooling path to approximately 15 psi to determine if the cooling paths evidenced low-pressure leaks post-removal from NSTX-U. Four scenarios were tested and evidenced the corresponding observations as illustrated in Table 2.

Table 2 – Low Pressure (15 psi Nitrogen) Testing Results of the PF1A-U Coil

Low-pressure test set-up criteria	Observations
Lead-in charged to 15 psig and isolated for 20 minutes with lead-out valve closed	Negligible leaks to atmosphere, pressure on both lead-in and lead out
Lead-in at 15 psig and lead-out valve opened	Pressure drops to atmosphere when lead-out valve is opened
Lead-out charged to 15 psig and isolated for 20 minutes lead-out valve closed	Negligible leaks to atmosphere, pressure on both lead-in and lead out
Lead-out at 15 psig and lead-in valve opened	Pressure remains on lead-out when lead-in valve is opened after slight, quick (~1psi) drop. Lead-in valve pressure drops to atmosphere

The observed pressure behavior indicated that the coil cooling path did not have a gross leak to atmosphere, but that debris existed in the leak path causing the flow through the cooling path to be intermittent.

6.0 PF1A-U Sectioning

A Peer Review was held on September 19, 2016 to establish consensus on the proposed destructive testing plan based on the results of the radiography. Determination of the origin and extent of the internal anomalies observed in the radiographic survey necessitated visual and physical access to individual PF1A-U conductor segments. The combined observed and deduced locations of braze joints and anomalies guided the selection of three feature-free areas for segmentation of the coil pack. The three sectioning cuts were proposed and identified as cuts ‘A’, ‘B’ and ‘C’ as noted in Figure 40. Section A-B would be of the greatest interest because it contained the five principal anomalies, alpha thru epsilon, identified by radiography, plus the leads and two of the four braze joints.

The method of segmenting the coil pack was examined in parallel to the locations of segmentation and presented at the Peer Review. A decision matrix was developed to guide the segmentation method selection process (Table 3).

Table 3 – Segmentation Method Decision Matrix

			Method Attribute Score - Higher Score is Better						
	Method	Description	Cutting Depth of 6" and throat of 32" (0=no, 1=yes)	Cutting Capability of Copper, SS, Epoxy/Glass (0=no, 1=yes)	Lubrication Needed (1=no, 0=yes)	Chip Size (0-10) 0 is smallest	Cutting Temperature (0-10) 0 is hottest	Precision (0-10) 0 is the least precise	**Total Score**
1	**Wire Saw**	Continuous abrasive wire	*1*	*1*	*1*	1	10	5	**16**
2	**Band Saw**	Continuous saw blade	*1*	*1*	*1*	5	9	5	**19**
3	**Demo Saw**	Hand-Operated circular saw blade	*1*	*1*	*1*	2	4	2	**8**
4	**Die Grinder with Cutoff Wheel**	Circular grinding wheel	*0*	*1*	*1*	1	0	2	**0**
5	**Milling with End Mill**	Rotary cutting tool	*1*	*1*	*1*	5	8	9	**22**
6	**Milling with Slitting Saw**	Circular saw blade	*1*	*1*	*1*	4	8	8	**20**
7	**Wire EDM**	Electrical erosion of an area surrounding a continuous wire through conductive materials in a dielectric bath	*1*	*0*	*0*	0	9	9	**0**
8	**Water Jet**	Abrasive fluid at very high pressure	*1*	*1*	*0*	0	10	9	**0**
9	**Laser**	Focused melting/burning of material	*0*	*1*	*1*	0	0	9	**0**
10	**Plasma Cutting**	Melting/burning of material	*1*	*0*	*1*	0	0	3	**0**
11	**Reciprocating Saw**	Hand-Operated reciprocating saw blade	*1*	*1*	*1*	4	2	0	**6**

The highest (best) scoring option was determined through the decision matrix to be a milling process using a rotary end mill without lubrication (method number 5). The proposed segmentation process and destructive testing plan was agreed to by consensus at the Peer Review. Once segmented, the coil sections would be subjected to borescope inspections, electrical tests, vacuum tests, and pressure tests. Work Plan #2226 was initiated for the overall forensic analysis effort. Unique NEPA form 1615 was generated in addition to the existing generic NSTX NEPA form 1443. Procedure D-NSTX-IP-3878 [7] was written and approved to employ this milling segmentation technique and outline the steps to de-mandrel the milled coil pack sections. In addition to the procedure, a drawing set was generated to specify the cut locations, parameters, and fixtures [10]. All efforts were made to select coil pack cutting planes that avoided identified anomalies, braze joints, and joggle areas. Layer transitions were not able to be identified in the radiographic study due to the transition being out of plane with the imaging. The procedure D-NSTX-IP-3878 and associated documents were reviewed and approved at a work package review meeting on September 29, 2016.

The coil pack retention fixtures were mounted on the PF1AU and the assembly crane-lifted onto a horizontal Lucas Mill table (Figure 41) in RESA. Two dedicated, new, marked shop vacuums were used to collect milled debris from each cutting plane during the machining process (Figure 42). These shop vacuums were used to retrieve debris from their designated cutting plane throughout the segmentation process, with the exception of specific collections of noted debris. A ⅝ inch cobalt four-flute end mill was used to mill the cutting planes (Figure 43). The milling process removed approximately 31.9 cubic inches of coil pack volume at each of the three (3) cutting planes for a total of 95.83 cubic inches of removed material. The approximate total volume of the PF1A-U coil pack is 4,102.48 cubic inches. The amount of material removed during the milling process was therefore approximately 2.34% of the coil pack volume. Despite the small proportional amount of material removed from feature-free regions, each cutting plane was cautiously milled in 0.03” increments and inspected for anomalies after each milling pass. The machinist stopped milling as well as notified the ATI if any anomalies were observed. The observations recorded during the milling process are tabulated in Table 4.

Table 4 – Milling Observations

Cutting Plane A	Voids in the turn-to-turn insulation layer	Figures 44-45
Cutting Plane A	Voids in the insulation layer proximal to the bottom row	Figure 46
Cutting Plane A	Ballooning of the half-lap insulation layer	Figure 47

Cutting Plane A	Probable lack of adhesion of insulation layer to primed conductor	Figure 48
Cutting Plane A	Exterior ground-wrap to mandrel depth: approximately conductor row 1, conductor row 7, conductor row 16	Figures 49-51
Cutting Plane B	Resin rich area with crack/void in insulation space	Figures 52-53
Cutting Plane B	Delaminated and un-wetted insulation layer between conductor layers 2 and 3	Figure 54
Cutting Plane B	Unwetted insulation glass fibers between conductor layers 2 and 3	Figure 55
Cutting Plane B	Samples collected from delaminated insulation layer between conductors layers 2 and 3	Figures 56-58
Cutting Plane B	Debris observed suspended on surface of conductor layer 2 (from behind removed sample at 5”)	Figure 59
Cutting Plane B	Discolored area proximal to rows 14-16 on the surface of layer 2	Figure 60
Cutting Plane B	Delamination gap and depth measurements	Figures 61-63
Cutting Plane B	Insulation void/crack at bottom of conductor layer 3	Figure 64
Cutting Plane B	Exterior ground-wrap to mandrel depth: approximately conductor row 1, conductor row 7, conductor row 16	Figures 65-67
Cutting Plane C	Exterior ground plane insulation delamination	Figures 68-69
Cutting Plane C	Conductor layer 3 to layer 4 transition	Figure 70
Cutting Plane C	Exterior ground-wrap to mandrel depth: approximately conductor row 1, conductor row 7, conductor row 16	Figures 71-73

The segmented PF1A-U assembly was crane-lifted from the horizontal Lucas mill and placed on a Ransome rotary/tilt table (Figures 74 and 75). Fixtures were loosened/displaced to enable the radial displacement of coil pack sections B-C and C-A. Spacers and wedges fabricated from G-10 were inserted into the cutting planes to progressively force the coil pack section(s) away from the mandrel (Figures 76 thru 80). The removed coil pack sections were placed and cribbed on tables for examination and testing (Figures 81 and 82). After photographing the general conditions of the six exposed cutting plane surfaces, a conductor number was assigned to each

conductor segment at one side of the coil pack segment (Figure 83). The conductor number designated the 'starting' location at one cutting plane, whereas the connected, opposite conductor number would be the same conductor segment but not necessarily in the same vertical or radial relative location due to the winding pattern. The opposing matching conductor location was determined during subsequent electrical and vacuum tests and marked accordingly. Coil pack section A-B was not removed from the mandrel in order to limit any potential disturbance to the radiographed anomalies previously identified as alpha through epsilon located proximal to the lead-in/lead-out angular position.

Exterior visual examination of cutting planes A and C, left and right, evidenced similar insulation anomalies observed during the milling process (Figures 84 thru 87). Cutting plane B, left and right, evidenced a separation between conductor layers two (2) and three (3) from approximately conductor row three (3) to conductor row sixteen (16) (Figures 88 and 89). Observed conductor spacing, insulation characteristics, and conductor keystoning were noted and photographed (Figures 90 thru 93). Examination of the insulation wrap sequence evidenced that each conductor was wrapped with a half-lap co-wound glass/Kapton layer with the glass portion laid-up against the conductor surface (Figure 94). A glass-only half-lap layer was observed to be wound over the co-wound glass/Kapton layer (Figure 95). Each layer-to-layer region evidenced an additional flat-laid glass layer (Figure 96).

Subsequent borescopic/videoscopic, electrical, vacuum, and pressure testing of the three sections could now commence in accordance with Peer Reviewed procedure D-NSTX-IP-3879 [8].

7.0 Borescopic/Videoscopic Inspection of Coil Sections

Interior visual examination of each coil segment cooling path was performed with both fiber borescope and digital videoscope. The borescope used is a PPPL owned basic eyepiece device without recording capability with a limited viewing range. An Olympus IPLEX IV9435 RX videoscope was rented for a one week period. This Olympus videoscope had a focus range of 2 mm with both forward and side view attachments. In addition, the videoscope could be viewed on a screen with both still and video digital recording capabilities.

Each coil segment cooling path was surveyed for visual anomalies and photographed and videoed with the Olympus videoscope if anomalies were observed. It is noteworthy that the braze joints and anomaly "delta" (features visible from the cooling paths) radial positions predicted in the radiographic triangulation method were accurate and verified through the cooling path visual examination. The observations recorded during the internal visual examination are tabulated in Table 5.

Table 5 – Borescope/Videoscope Observations

Item	Location	Observations	Photographs
Braze Joint #1	C-A, conductor layer 1, row 15	Blockage Observed	Figures 97-99
Braze Joint #2	A-B, conductor layer 2, row 3	Void Observed	Figures 100-102
Braze Joint #3	A-B, conductor layer 3, row 13	Blockage Observed	Figures 103-105
Braze Joint #4	C-A, conductor layer 4, row 6	Misalignment Observed	Figures 106-107
Anomaly "Delta"	A-B, conductor layer 3, row 9	Void in sidewall of cooling path	Figures 108-112
Conductor 24	A-B, conductor layer 2, row 9	Discoloration along surface of cooling path	Figure 113

8.0 Electrical Testing of Coil Sections

Each conductor segment was measured for segment resistance using a micro-ohm meter and tabulated in Table 6.

A grounding harness consisting of copper wire and banana plugs was inserted into the cooling path of each conductor along one side of each coil pack section for megger testing (Figure 114). The conductor under test was electrically disconnected from the grounding harness during the test. Each conductor segment was megger tested at 250VDC per the Generic Megger and Hipot Procedure - PTP-GEN-01. The observed conductor insulation resistance varied from 1.81 Mohm to greater than 750Gohm in un-shorted conductor segments. Results were tabulated for future analysis and are listed in Table 7.

A total of fourteen (14) conductor segments were observed to be effectively shorted in coil pack section A-B. Additional turn-to-turn resistance measurements were performed between these electrically communicating turns as tabulated in Table 8.

Table 6 – Conductor Segment Resistance Measurements

Coil Section A-B — Individual Testing: Alexis Sanchez, Elliot Baer — Test Date: 10/27/16

Conductor Segment Resistance (mohm) — Individual Recording: Weiguo Que

Turn	Reading	Turn	Reading	Turn	Reading	Turn	Reading
1	0.0366	17	No copper	33	0.0393	49	0.0421
2	0.0362	18	0.0382	34	0.0391	50	0.042
3	0.036	19	0.0386	35	0.0398	51	0.0417
4	0.0359	20	0.0382	36	0.0397	52	0.0415
5	0.0354	21	0.0378	37	0.0396	53	0.0418
6	0.036	22	0.0385	38	0.0397	54	0.0416
7	0.0364	23	0.038	39	0.0399	55	0.0415
8	0.0365	24	0.0378	40	0.0404	56	0.0416
9	0.037	25	0.0377	41	0.0406	57	0.042
10	0.0367	26	0.0376	42	0.0403	58	0.0418
11	0.0368	27	0.038	43	0.0405	59	0.0417
12	0.037	28	0.0382	44	0.0403	60	0.0415
13	0.0368	29	0.0379	45	0.0405	61	0.0413
14	0.0371	30	0.0384	46	0.0408	62	0.0406
15	0.0369	31	0.0378	47	0.0402	63	0.0412
16	0.0384	32	0.0375	48	0.0403	64	

Coil Section B-C — Individual Testing: Alexis Sanchez, Elliot Baer — Test Date: 10/25/16

Conductor Segment Resistance (mohm) — Individual Recording: Weiguo Que

Turn	Reading	Turn	Reading	Turn	Reading	Turn	Reading
1	0.0245	17	No Copper	33	0.0261	49	0.0283
2	0.0252	18	0.026	34	0.0272	50	0.0284
3	0.0249	19	0.0257	35	0.0267	51	0.0285
4	0.0236	20	0.0266	36	0.0275	52	0.0281
5	0.0239	21	0.0255	37	0.0268	53	0.0286
6	0.0247	22	0.0263	38	0.0269	54	0.0287
7	0.0252	23	0.0261	39	0.0272	55	0.0284
8	0.0246	24	0.026	40	0.0274	56	0.0288
9	0.025	25	0.0256	41	0.0268	57	0.0284
10	0.0246	26	0.0259	42	0.0276	58	0.0287
11	0.0241	27	0.0255	43	0.0274	59	0.0285
12	0.0244	28	0.0261	44	0.027	60	0.0284
13	0.0235	29	0.0263	45	0.0273	61	0.0282
14	0.0243	30	0.0255	46	0.0274	62	0.0281
15	0.0238	31	0.026	47	0.0273	63	0.028
16	0.0248	32	0.0256	48	0.0272	64	0.0285

Coil Section C-A — Individual Testing: Alexis Sanchez, Elliot Baer — Test Date: 10/26/16

Conductor Segment Resistance (mohm) — Individual Recording: Weiguo Que

Turn	Reading	Turn	Reading	Turn	Reading	Turn	Reading
1	0.0373	17	0.0393	33	0.041	49	0.0433
2	0.0375	18	0.0397	34	0.0413	50	0.0428
3	0.0381	19	0.0396	35	0.0415	51	0.0431
4	0.0377	20	0.0394	36	0.0407	52	0.0429
5	0.0376	21	0.0393	37	0.0413	53	0.0432
6	0.0373	22	0.0391	38	0.0411	54	0.0434
7	0.0362	23	0.0395	39	0.0413	55	0.0425
8	0.0374	24	0.0393	40	0.0412	56	0.0431
9	0.0373	25	0.0392	41	0.041	57	0.0428
10	0.0374	26	0.039	42	0.0413	58	0.0433
11	0.0381	27	0.0391	43	0.0411	59	0.0434
12	0.0375	28	0.0394	44	0.041	60	0.0433
13	0.0374	29	0.0395	45	0.0409	61	0.0436
14	0.037	30	0.0399	46	0.041	62	0.0433
15	0.0383	31	0.04	47	0.0412	63	0.0431
16	0.0376	32	0.0395	48	0.0409	64	No Copper

Table 7 – Coil Pack Section Megger Test Results

Coil Section A-B — Individual Testing: Alexis Sanchez, Elliot Baer — Test Date: 10/27/16

Insulation Test (250 V, 1 min) — Individual Recording: Weiguo Que — when the resistance below 10 kohm, it is measured by the multimeter (fluke 87 V)

Turn	Resistance	Current	Turn	Resistance	Current	Turn	Resistance	Current	Turn	Resistance	Current
1	597 Gohm	0.42 nA	17	No copper		33	17.5 Mohm	14.1 uA	49	2.44 Mohm	102 uA
2	7.79 Gohm	32 nA	18	761 Mohm	328 nA	34	9.09 Mohm	27.2 uA	50	319 Gohm	0.78 nA
3	629 Gohm	0.4 nA	19	211 Gohm	1.18 nA	35	3.0 ohm		51	436 Gohm	0.57 nA
4	701 Gohm	0.35 nA	20	24.9 Mohm	9.97 uA	36	1.0 ohm		52	477 Gohm	0.52 nA
5	711 Gohm	0.35 nA	21	764 Mohm	325 nA	37	15.2 ohm		53	609 Gohm	0.41 nA
6	713 Gohm	0.35 nA	22	15.5 Gohm	16.0 nA	38	3.7 ohm		54	750 Gohm	0.08 nA
7	698 Gohm	0.36 nA	23	326 Gohm	0.76 nA	39	1.2 ohm		55	471 Gohm	0.53 nA
8	737 Gohm	0.34 nA	24	8 ohm		40	1.7 ohm		56	466 Gohm	0.53 nA
9	750 Gohm	0.29 nA	25	0.6 ohm		41	6.9 ohm		57	545 Gohm	0.45 nA
10	750 Gohm	0.29 nA	26	0.4 ohm		42	4.75 Mohm	52.0 uA	58	561 Gohm	0.44 nA
11	747 Gohm	0.33 nA	27	0.5 ohm		43	2.78 Mohm	89.1 uA	59	350 Gohm	0.71 nA
12	4.69 Gohm	52.9 nA	28	0.6 ohm		44	192 Gohm	1.29 nA	60	605 Gohm	0.41 nA
13	4.99 Gohm	49.7 nA	29	0.5 ohm		45	5.39 Mohm	46.2 uA	61	526 Gohm	0.47 nA
14	486 Gohm	0.51 nA	30	0.7 ohm		46	25.4 Mohm	9.77 uA	62	537 Gohm	0.46 nA
15	7.68 Mohm	32.3 uA	31	69.1 Mohm	3.58 uA	47	13.8 Mohm	18.0 uA	63	634 Gohm	0.39 nA
16	1.81 Mohm	137 uA	32	15.1 Mohm	16.4 uA	48	2.33 Mohm	106 uA	64	510 Gohm	0.49 nA

Coil Section B-C — Individual Testing: Alexis Sanchez, Elliot Baer — Test Date: 10/25/16

Insulation Test (250 V, 1 min) — Individual Recording: Weiguo Que

Turn	Resistance	Current	Turn	Resistance	Current	Turn	Resistance	Current	Turn	Resistance	Current
1	31.6 Mohm	7.9 uA	17	No Copper	No Copper	33	9.29 MOhm	26.5 uA	49	1.26 Mohm	196 uA
2	737 Gohm	0.34 nA	18	121 Mohm	2.04 uA	34	1.24 MOhm	197 uA	50	6.98 Mohm	35.3 uA
3	750 Gohm	0.29 nA	19	1.7 Gohm	145 nA	35	132 Gohm	1.87 nA	51	456 Gohm	0.54 nA
4	750 Gohm	0.23 nA	20	107 Mohm	2.32 uA	36	12.0 Gohm	20.6 nA	52	565 Gohm	0.44 nA
5	750 Gohm	0.28 nA	21	61.7 Mohm	4.01 uA	37	911 Mohm	271 nA	53	584 Gohm	0.33 nA
6	750 Gohm	0.28 nA	22	158 Mohm	1.56 uA	38	362 Mohm	682 nA	54	750 Gohm	0.32 nA
7	750 Gohm	0.25 nA	23	83.3 Gohm	2.97 nA	39	105 Mohm	2.34 uA	55	627 Gohm	0.39 nA
8	750 Gohm	0.27 nA	24	547 Gohm	0.45 nA	40	121 Mohm	2.04 uA	56	660 Gohm	0.37 nA
9	750 Gohm	0.21 nA	25	21.1 Gohm	11.7 nA	41	337 Mohm	732 nA	57	750 Gohm	0.32 nA
10	750 Gohm	0.18 nA	26	229 Gohm	1.08 nA	42	69.3Mohm	3.56 uA	58	719 Gohm	0.34 nA
11	750 Gohm	0.31 nA	27	57 Gohm	4.33 nA	43	1.65 Gohm	150 nA	59	750 Gohm	0.28 nA
12	675 Gohm	0.37 nA	28	133 Gohm	1.86 nA	44	524 Gohm	0.47 nA	60	750 Gohm	0.24 nA
13	750 Gohm	0.30 nA	29	16.6 Mohm	14.8 uA	45	639 Gohm	0.39 nA	61	750 Gohm	0.09 nA
14	750 Gohm	0.23 nA	30	2.86 Gohm	86.2 nA	46	601 Gohm	0.41 nA	62	750 Gohm	0.28 nA
15	750 Gohm	0.29 nA	31	2.11 Gohm	117 nA	47	391 Mohm	632 nA	63	750 Gohm	0.30 nA
16	17.5 Mohm	14.2 uA	32	315 Mohm	783 nA	48	6.72 Mohm	367 uA	64	47 Mohm	5.24 uA

Coil Section C-A — Individual Testing: Alexis Sanchez, Elliot Baer — Test Date: 10/26/16

Insulation Test (250 V, 1min) — Individual Recording: Weiguo Que

Turn	Resistance	Current	Turn	Resistance	Current	Turn	Resistance	Current	Turn	Resistance	Current
1	148 Gohm	1.69 nA	17	180 Mohm	1.38 uA	33	281 Gohm	0.89 nA	49	516 Gohm	0.48 nA
2	509 Gohm	0.49 nA	18	690 Gohm	0.36 nA	34	561 Gohm	0.44 nA	50	421 Gohm	0.59 nA
3	654 Gohm	0.38 nA	19	750 Gohm	0.01 nA	35	449 Gohm	0.55 nA	51	436 Gohm	0.57 nA
4	592 Gohm	0.42 nA	20	442 Gohm	0.56 nA	36	525 Gohm	0.47 nA	52	424 Gohm	0.58 nA
5	717 Gohm	0.35 nA	21	566 Gohm	0.44 nA	37	750 Gohm	0.3 nA	53	554 Gohm	0.45 nA
6	263 Gohm	0.95 nA	22	482 Gohm	0.51 nA	38	463 Gohm	0.53 nA	54	474 Gohm	0.52 nA
7	750 Gohm	0.08 nA	23	389 Gohm	0.64 nA	39	399 Gohm	0.62 nA	55	443 Gohm	0.56 nA
8	750 Gohm	0.07 nA	24	409 Gohm	0.61 nA	40	464 Gohm	0.53 nA	56	470 Gohm	0.53 nA
9	731 Gohm	0.34 nA	25	458 Gohm	0.54 nA	41	513 Gohm	0.48 nA	57	478 Gohm	0.52 nA
10	724 Gohm	0.34 nA	26	398 Gohm	0.62 nA	42	671 Gohm	0.37 nA	58	477 Gohm	0.52 nA
11	570 Gohm	0.44 nA	27	496 Gohm	0.50 nA	43	750 Gohm	0.26 nA	59	505 Gohm	0.49 nA
12	622 Gohm	0.40 nA	28	501 Gohm	0.49 nA	44	523 Gohm	0.47 nA	60	531 Gohm	0.47 nA
13	627 Gohm	0.40 nA	29	750 Gohm	0.28 nA	45	506 Gohm	0.49 nA	61	434 Gohm	0.57 nA
14	532 Gohm	0.47 nA	30	596 Gohm	0.42 nA	46	598 Gohm	0.41 nA	62	497 Gohm	0.50 nA
15	615 Gohm	0.40 nA	31	750 Gohm	0.29 nA	47	565 Gohm	0.44 nA	63	340 Gohm	0.73 nA
16	153 Mohm	1.62 uA	32	331 Gohm	0.75 nA	48	126 Mohm	1.96 uA	64	No Copper	

Table 8 – Additional Resistance Measurements of Electrically Connected Turns in Section A-B

Turn	Resistance
30-35	4.0 ohm
35-36	3.0 ohm
29-36	1.2 ohm
30-36	1.4 ohm
37-38	17.4 ohm

Turn	Resistance
36-37	16.3 ohm
37-28	15.7 ohm
28-29	1 ohm
27-28	0.7 ohm
38-39	4.4 ohm

Turn	Resistance
39-40	1.8 ohm
40-41	7.1 ohm
26-27	0.8 ohm
25-26	0.5 ohm
24-25	8.1 ohm

9.0 Vacuum Testing of Coil Sections

A low-vacuum pump was configured with a moisture/debris trap in order to selectively apply vacuum to conductor segment cooling paths (Figure 115). Each cooling path segment was vacuum tested at approximately 29 inches of mercury for 2 minutes (Table 9). One conductor segment cooling path failed to hold vacuum. The leaking conductor section was determined to be the cooling path with the internally observed void (Section A-B, Layer 3, Row 9, conductor #41).

Table 9 – Vacuum test data

Coil Section: A-B | Individual Testing: Joe Pemaula / Joe Barteau | Test Date: 10/26/16 – 10/31
Vacuum Test: IN Hg | Individual Recording: " "

Turn	1 min (Pumping)	2 Min	Turn	1 min (Pumping)	2 Min	Turn	1 min (Pumping)	2 Min	Turn	1 min (Pumping)	2 Min
1	-29.5	-29	17	N/A	N/A	33	-29.0	-28.0	49	-29.5	-28.5
2	-29.5	-29	18	-29.0	-28.5	34	-29.0	-28.5	50	-29.0	-28.5
3	-29.5	-28.0	19	-29.0	-24	35	-29.0	-28.5	51	-29.0	-28.5
4	-29.5	-29	20	-29.0	-28	36	-29.0	-28.5	52	-29.0	-28.0
5	-29.5	-28	21	-29.0	-28	37	-29.0	-29.5	53	-29.0	-28.5
6	-29.5	-28.5	22	-29.5	-27.5	38	-28.5	-28.0	54	-29.0	-28.0
7	-29.5	-28.5	23	-29.0	-28.0	39	-29.0	-28.0	55	-29.0	-28.5
8	-29.5	-28.5	24	-29.5	-29.5	ADJ 40	-29	-28.5	56	-29.5	-29
9	-29.5	-28.5	25	-29.0	-28.0	HOLE 41	-19	0	57	-29.0	-28.5
10	-29.5	-28.5	26	-29.0	-28.5	HOLE 42	-29.5	-28.5	58	-29.0	-28.0
11	-29.5	-28.0	27	-29.0	-28.0	43	-29.0	-28.5	59	-29.0	-28.5
12	-29.5	-29.0	28	-29.0	-28.0	44	-29.0	-28.0	60	-29.0	-28.5
13	-29.5	-29.0	29	-29.5	-29.5	BJ#5 45	-29.5	-28.5	61	-29.0	-28.0
14	-29.5	-28.5	BJ#2 30	-29.5	-28	46	-29.0	-28.0	62	-29.0	-28.5
15	-29.5	-28.5	31	-29.0	-29.0	47	-29.0	-28.0	63	-29.0	28.5
16	-28.5	-27.0	32	-29.0	-28.5	48	-29.5	-28.5	64	N/A	N/A

#45 - TESTED W/O PLUG & DID NOT HOLD JAC

Coil Section B-C | Individual Testing: Joe Bartzak | Test Date: 10/26-10/31/16
Insulation Test | Individual Recording:

Turn	1 min (Pumping)	2 Min	Turn	1 min (Pumping)	2 Min	Turn	1 min (Pumping)	2 Min	Turn	1 min (Pumping)	2 Min
1	-29.0	-28.0	17	N/A		33	-29,5	-29,0	49	-29.0	-28.0
2	-29.0	-28.5	18	-29,0	-28.5	34	-29.5	-28,5	50	-29.0	-28.5
3	-29.0	-28.0	19	-29,5	-29,0	35	-29.5	-29.0	51	-29.0	-28.5
4	-29.0	-28.0	20	-29,5	-28,5	36	-29.5	-28,5	52	-29.0	-28,5
5	-29.0	-28.0	21	-29,5	-28,5	37	-29.5	-29.0	53	-29,5	-29,0
6	-29.0	-28.5	22	-29.0	-28,5	38	-29,5	-28,5	54	-29,5	-28,5
7	-29.0	-28,0	23	-29,0	-28,5	39	-29,5	-28,5	55	-29.0	-28.0
8	-29,0	-28	24	-29,5	-28,5	40	-29,5	-29,0	56	-29,5	-28,5
9	-29.0	-28,5	25	-29,0	-28,5	41	-29.5	-28,5	57	-29.0	-28,0
10	-29.0	-28.5	26	-29,5	-28,5	42	-29,5	-29,0	58	-29.0	-28,5
11	-29,0	-28,5	27	-29,5	-29,0	43	-29.5	-29,0	59	-29.0	-27.5
12	-29,0	-28,5	28	-29,5	-28,5	44	-29.5	-28,5	60	-29,0	-28,5
13	-29.0	-28,5	29	-29,5	-28,5	45	-29,0	-28,5	61	-29,0	-28,5
14	-29,5	-29,0	30	-29,5	-28,5	46	-29,5	-28,5	62	-29,0	-28,5
15	-29,0	-28,5	31	-29,5	-28,5	47	-29,5	-28,5	63	-29,5	-29,0
16	-29,0	-28,5	32	-29,5	-29,0	48	-29,0	-28,5	64	-29,0	-28,5

-28,5

Coil Section C-A | Individual Testing: Joe Bartzak | Test Date: 10/26-10/31/16
Insulation Test | Individual Recording:

Turn	1 min (Pumping)	2 Min	Turn	1 min (Pumping)	2 Min	Turn	1 min (Pumping)	2 Min	Turn	1 min (Pumping)	2 Min
1	-29,0	-28,5	17	-29.0	-28.5	33	-29,0	-28,0	49	-29,0	-29,0
2	-29,0	-28,5	18	-29.0	-28.5	34	-29,0	-28,0	50	-29,0	-29,0
3	-29,0	-28,5	19	-29.0	-28.5	35	-29,0	-28,0	51	-29,0	-29,0
4	-29,0	-28,5	20	-28.5	-28.0	36	-29,0	-28,0	52	-29,0	-29,0
5	-29,5	-28,5	21	-29,5	-29,0	37	-29,0	-28,0	53	-29,0	-29,0
6	-29,0	-28,5	22	-29.5	-29,0	38	-29,0	-27,5	54	-29,0	-29,0
7	-29.0	-28.5	23	-29.0	-29.0	39	-29,0	-29,0	55	-29,0	-28,5
8	-29,0	-28,5	24	-29.5	-28.5	40	-29,0	-27,5	56	-29,0	-29,0
9	-29.0	-28.0	25	-29,5	-28.0	41	-29.0	-29.0	57	-29.0	-28,5
10	-29.0	-28,5	26	-29,0	-28, 5	42	-29,0	-28,5	58	-29,0	-28,5
11	-29,5	-29,0	27	-29,0	-28,0	43	-29,0	-28,5	59	-29.0	-28,5
12	-29, 5	-29,0	28	-29.5	-28.0	44	-29,0	-28,5	60	-29,0	-28,5
13	-29.5	-29.0	29	-29,5	-28,5	45	-29,0	-29,0	61	-29.0	-29,0
14	-29.0	-28.5	30	-29,5	-28,5	46	-29,5	-28,0	62	29,0	28,5
15	-29.50	-28.0	31	-29,5	-28,5	47	-29,0	-28,5	63	-29,0	-28,5
16	-29.0	-28,5	32	-29,5	-28.0	48	-29,0	-28,5	64		

10.0 Pressure Testing of Selected Coil Section Turns

The cooling paths of conductor segments containing braze joints and leads were tapped with a 1/8" NPT tapered thread for the attachment of pressure testing components . A 15 psi nitrogen pressure test was followed by a 400 psi hydrostatic pressure tests per ENG-014 for each tested conductor segment (Figure 116). Hydrostatic tests were repeated to vet out set-up variances, including subjecting one test set-up to an overnight leak-down. All four tested braze joints and leads passed hydrostatic testing at 400 psi. Low-pressure helium leak tests were additionally performed on the conductor segments featuring the leads, braze joint number two (2) and braze joint number three (3) in Section A-B and were unremarkable. Excerpts from the braze joint and lead(s) conductor segment hydrostatic test results are illustrated in Table 10.

Table 10 – Hydrostatic test result excerpts

TEST RESULTS: ☐ACCEPT ☐REJECT

SECTION A-B

T45 400Psi @ 10:46AM | 380Psi @ 11:16 AM | 380Psi @ 11:46AM

T30 400Psi @ 12:20 | 400Psi @ 12:50 | 400Psi @ 13:20

T45 400Psi @ 13:38 | 380Psi @ 13:48 | 380Psi @ 1358 TIGHTENED FITTING & RETAKE MEASUREMENTS

T45 400Psi @ 14:00 | 400Psi @ 14:10 | T45 400Psi @ 14:15 ~395Psi @ 14:25 ~395Psi @ 14:35 400Psi @ 14:45

TEST PERFORMED BY: JOE PEMELLA / JOE BARTZAK **DATE** 11/2/16

WITNESSED BY: I. ZATZ **DATE:** 11/2/16

TEST RESULTS: ☐ACCEPT ☐REJECT

SECTION C-A

T59 @ 400Psi @ 7:55AM | ~~380~~ 390Psi @ 8:00AM

T59 @ 400Psi @ 8:01 AM | ~~395~~ 390Psi @ 8:06AM | ~~395~~ 390Psi @ 8:11AM

TEST PERFORMED BY: JOE PEMELLA / JOE BARTZAK **DATE** 11/2/16

WITNESSED BY: THOMAS GUTTADORA **DATE:** 11/2/16

TEST RESULTS: ☐ACCEPT ☐REJECT

SECTION C-A

T16 @ 400Psi @ 7:30AM | 380Psi @ 7:35AM

T15 @ 400Psi @ 7:36AM | 380Psi @ 7:41AM | 380Psi @ 7:46AM

TEST PERFORMED BY: JOE PEMELLA / JOE BARTZAK **DATE** 11/2/16

WITNESSED BY: THOMAS GUTTADORA **DATE:** 11/2/16

TEST RESULTS: ☐ACCEPT ☐REJECT

SECTION A-B

TURN 1 – "LEAD IN" 400Psi @ 09:33 | 380Psi @ 09:43 PUMP BACKUP | 400Psi @ 09:45 | 400Psi @ 09:55

TURN 64 – "LEAD-OUT" 400Psi @ 10:15 | 400Psi @ 10:25 | 400Psi @ 10:35

TEST PERFORMED BY: JOE PEMELLA **DATE** 11/18/16

WITNESSED BY: [signature] **DATE:** 11/18/16

11.0 Summary

The forensic investigation of the failure of the PF1A-U coil produced evidence presented in a meeting held on November 3, 2016 and is summarized as follows:

1. Single Point of Failure: empirical evidence indicated one location where the cooling channel was compromised with a void and was linked to other anomalies. This location was indicated by early radiography.
2. Braze Joint Leak: empirical evidence reduced the probability of this theory. All four (4) braze joints passed vacuum tests (15 psi) and hydrostatic leak checks at 400 psi and room temperature. Braze Joint #2 and Braze Joint #3 (in Section A-B) also passed helium leak checks at room temperature.
3. Improper VPI: empirical evidence indicated numerous areas of insufficient wetting and voids in the insulation layer(s).
4. Blockage(s): empirical evidence indicated two (2) blockages proximal to braze joints. The blockage material did not originate at the blockage location. It is probable that the blockage material migrated from the electrically active void space. This was confirmed, in part, due to the ability to remove the blockages in the cooling channels by prodding with a thin tool. Once free of the obstructions, the braze joint areas where they were lodged did not show any indication that the blockage material originated there. All removed blockage material was bagged and cataloged for future analysis, if deemed necessary.
5. Over-Pressurization: empirical evidence indicated the insulation proximal to layer 2-3 experienced a pressurization event causing layer separation. Other insulation delaminations were observed with pressurization as a probable cause. Numerous delaminations were also found on the outside surface of the ground layer of the coil.
6. Foreign Material in Insulation Layer(s): no empirical evidence was observed that could confirm or eliminate this theory from consideration.
7. Design/Fabrication Deficiency: empirical evidence indicated it is probable that the execution of the design, not features inherent to the design, was causal to the observed damage. However, difficulty in executing design details may have added risk to the fabrication process.
8. Corrosion of Materials: empirical evidence eliminated the probability of this theory from consideration.
9. Excessive Temperatures: empirical evidence eliminated the probability of this theory from consideration.

12.0 Conclusions

Based on the subject investigation observations, the writers' experience, training, and education, the writers conclude the following within a reasonable degree of engineering certainty:

1. The evidence indicates a single point of failure as indicated by a void in a conductor coolant path sidewall.
2. It is probable that electrical activity at the void location resulted in molten debris that blocked the cooling path at restrictions in the conductor braze joints.
3. Communication of debris into the conductor electrical insulation system most likely resulted in the observed low-resistance connectivity to 13 other conductor segments.
4. The most probable cause of the initiating event, by process of elimination, was a conductor electrical insulation system anomaly. An insulation anomaly may have been comprised of some combination of the following:
    a. Conductive material (debris or liquid)
    b. Exposed conductor
    c. Reduced insulation thickness
    d. Dry/unwetted insulation & voids
    e. Mechanical movement/abrasion
    f. Insulation wrapping inconsistencies
5. The exact characteristic(s) of the originating anomaly is indeterminate at this time and its nature may not be able to be determined due to the failure event itself potentially having destroyed the causal evidence.
6. Further non-destructive and destructive examination of the identified failure area would be necessary to potentially augment the characteristics of the initiating event anomaly.

13.0 Recommendations

The following actions are recommendations developed by the writers to be considered by NSTX-U project leaders:

1. A team should be charged with the task of evaluating, developing, and instituting holistic methods and tools for the proactive determination of pre-installation electromagnet construction quality.
2. Actions should be taken to develop methods and tools for in-situ diagnostic evaluation of electromagnet performance in excess of existing methods. Proactive determination of infantile and progressive defects may allow for the planned mitigation of anomalous electromagnet performance if such issues were to occur in future operations of the NSTX-U program.

3. Consideration should be given to the manufacturing execution of electromagnet designs early in the design phase as to alleviate and minimize risks inherent in design fabrication challenges including manufacturer oversight.
4. Consideration should be given to further examination of the PF1A-U evidence such as additional NDT imaging and destructive excavation of the fault area.
5. Consideration should be given to purchasing a videoscope such as that used to examine the cooling paths for general use at PPPL. The writers were impressed with the quality and versatility of the rented equipment and owning such a tool would be a valued addition to the lab's quality control and diagnostic capabilities.

The writers reserve the right to amend and/or supplement this report in the event that additional investigative steps are taken and/or additional information becomes available for review.

14.0 Acknowledgements

The authors wish to acknowledge the valuable contributions made by the many individuals who assisted and participated in this investigation both inside and outside of the PPPL community. In particular, this investigation process was greatly aided through the dedicated works of the following people:

Joe Bartzak, Elliot Baer, Tom Czeizinger, Mike Dimattia, Chad Ennis, Ray Granaldi, Tom Guttadora, Bob Horner, Weiguo Que, Alexis Sanchez, Fred Simmonds, and Doug Voorhees.

15.0 References

[1] D-NSTX-SOW-134-137 Rev. 0, NSTX-U Manufacturing Statement of Work - Fabrication of Inner Poloidal Field (PF) Coils, 16 November 2012.

[2] D-NSTX-SPEC-134-137, Rev. 1, NSTX-U Manufacturing Specification – Fabrication of Inner Poloidal Field (PF) Coils, 09 December 2013.

[3] Everson Tesla Inc., Inner PF Report Log per PPPL PO# S012485-G, ET# 53156, 20 June 2014.

[4] Everson Tesla Inc., Non-Conformance Report SC14023 dated 3/20/2014 with PPPL disposition on 3/26/2014.

[5] Gerhardt, S. Personal notes titled 'Narrative on the PF1AU Troubleshooting and the Path to Restoration of Plasma Operations', 29 July 2016.

[6] Everson Tesla Inc., Manufacturing Process Outline (MPO)/Traveler for the Inner PF-1A Coils, ETI Doc. # 53156-603, 10 February 2014.

[7] D-NSTX-IP-3878, Rev. 0, Sectioning of the NSTX-U PF1A-U Coil for Forensic Destructive Testing, 30 September 2016.

[8] D-NSTX-IP-3879, Rev. 0, Forensic Testing of the Sectioned NSTX-U PF1A-U Coil, 12 October 2016.

[9] Water Dynamics, Analysis Report, 1 July 2016.

[10] B-DC11024, Rev. 2, NSTX-U Drawing 'PF1AU Study Fixture', 23 September 2016.

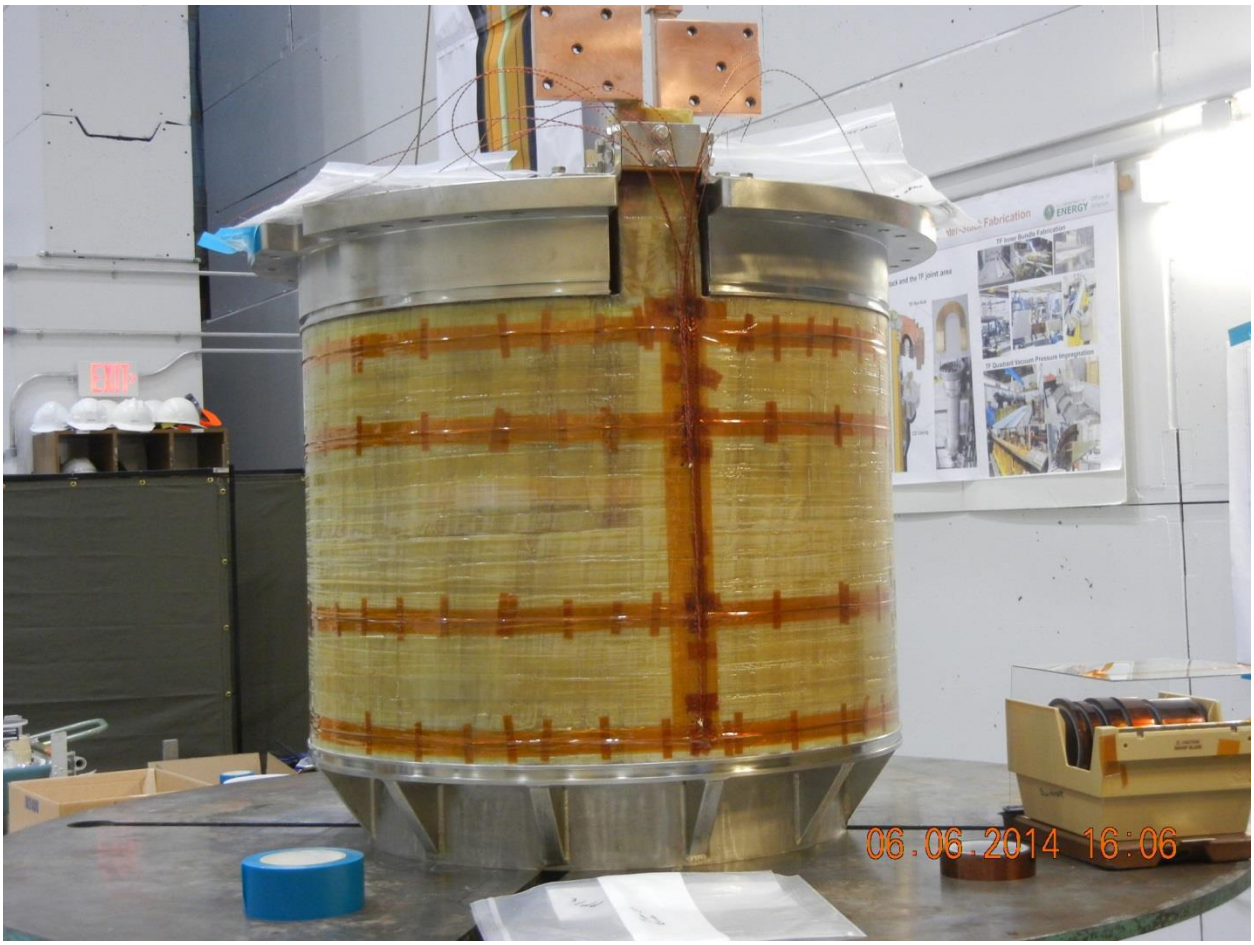

Figure 1 – The as-delivered PF1A-U coil

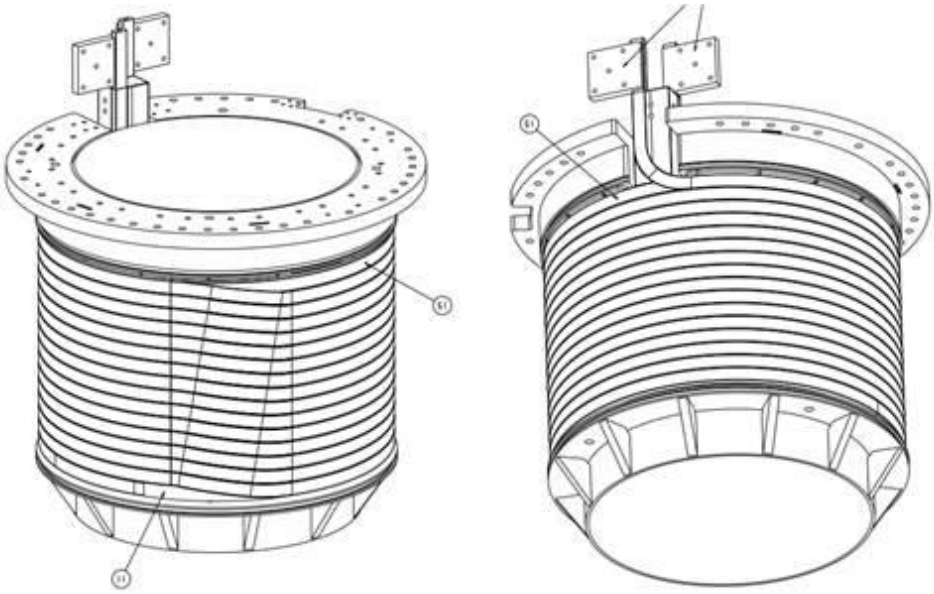

Figure 2 – Schematic of the PF1A-U coil

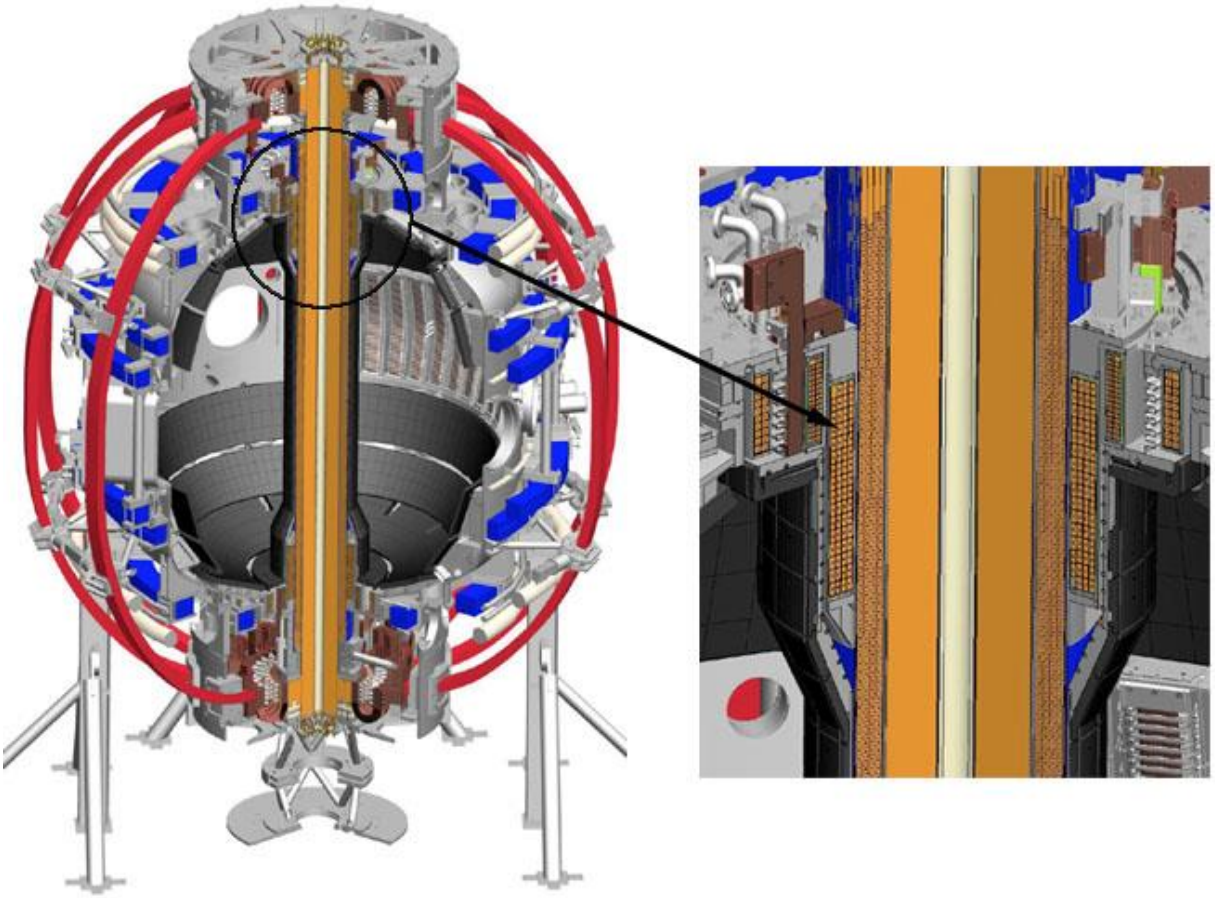

Figure 3 – Positioning of the PF1A-U coil on the NSTX-U center stack

Figure 4 – Copper/carbon slug found in flushed PF1A-U coolant compared to the size of a dime

Figure 5 – Debris found in the flushed PF1A-U coolant

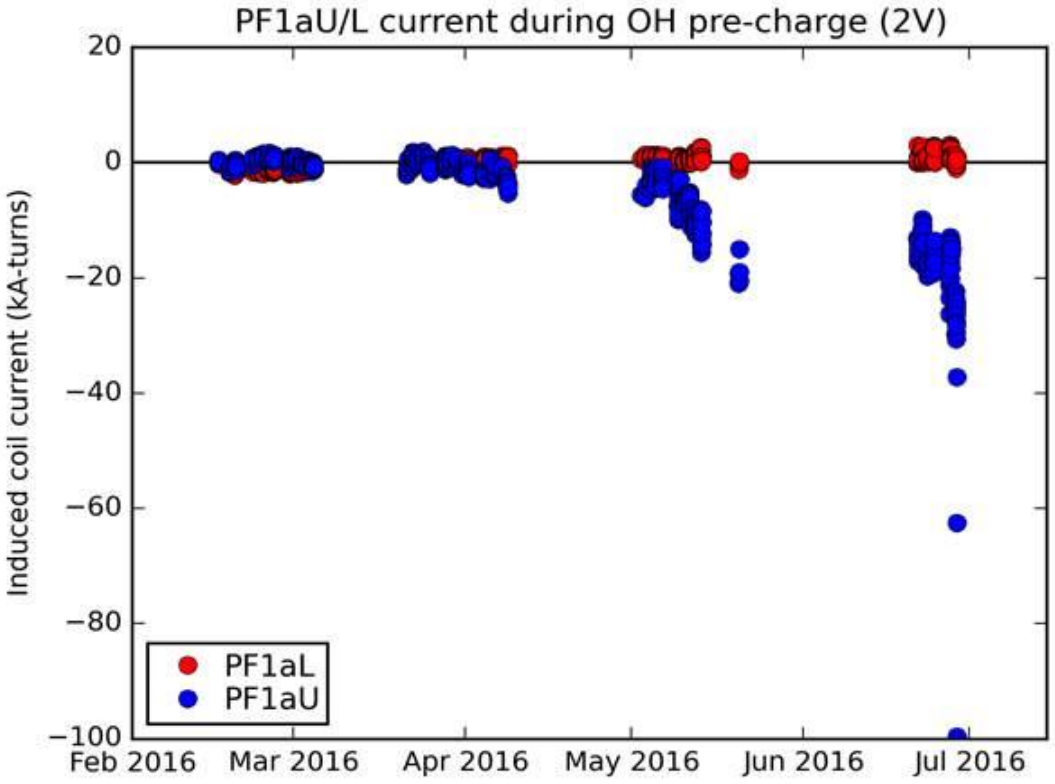

Figure 6 – Gradual change in the inductance of PF1A-U over several months

Figure 7 – Removal of PF1A-U from NSTX-U

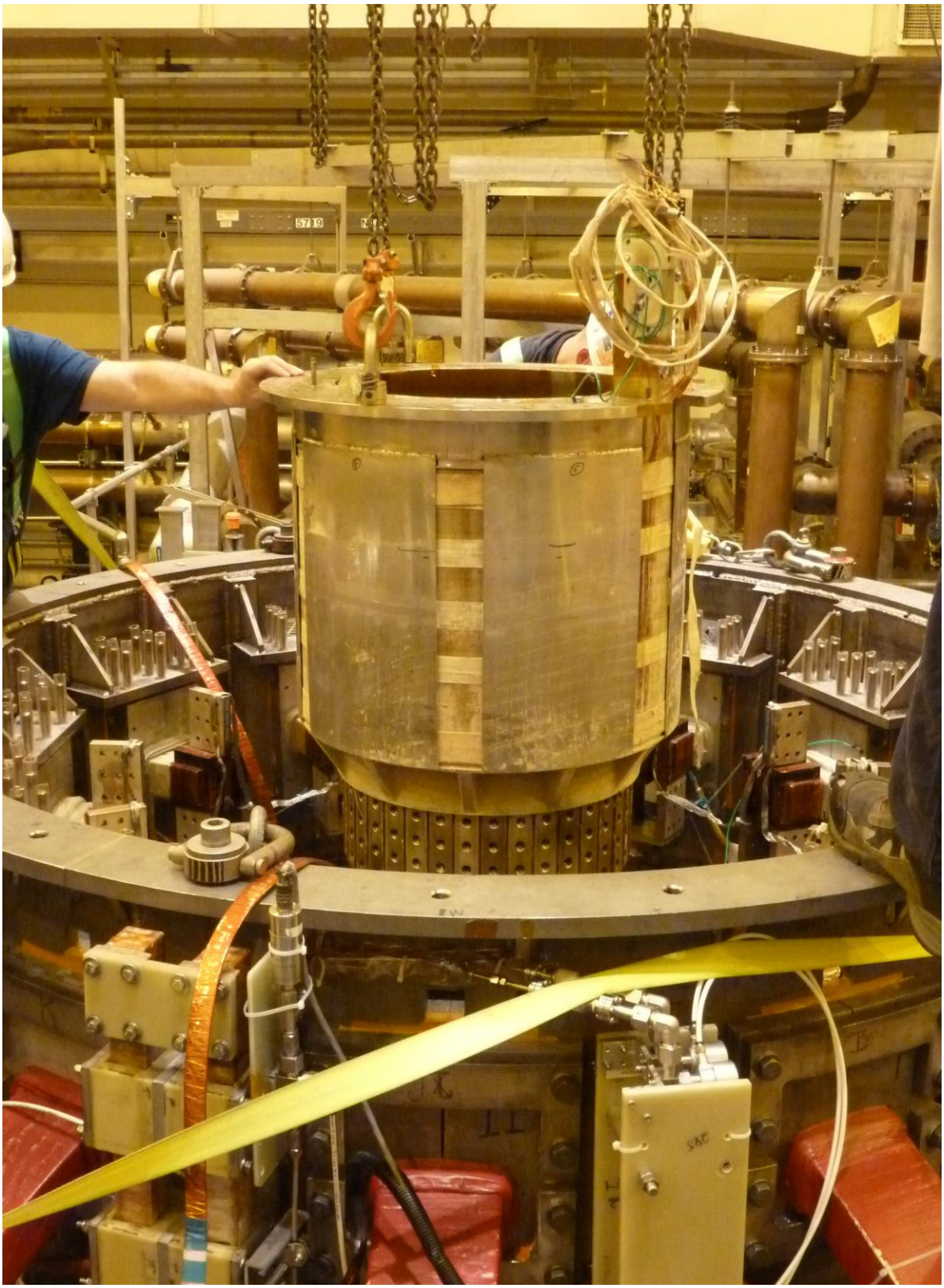

Figure 8 – Removal of PF1A-U from NSTX-U

Figure 9 – HP surveying PF1A-U post-removal

Figure 10 – PF1A-U in the south high bay

Figure 11 – Lead area

Figure 12 – PF1A-U Exterior

Figure 13 – PF1A-U Exterior

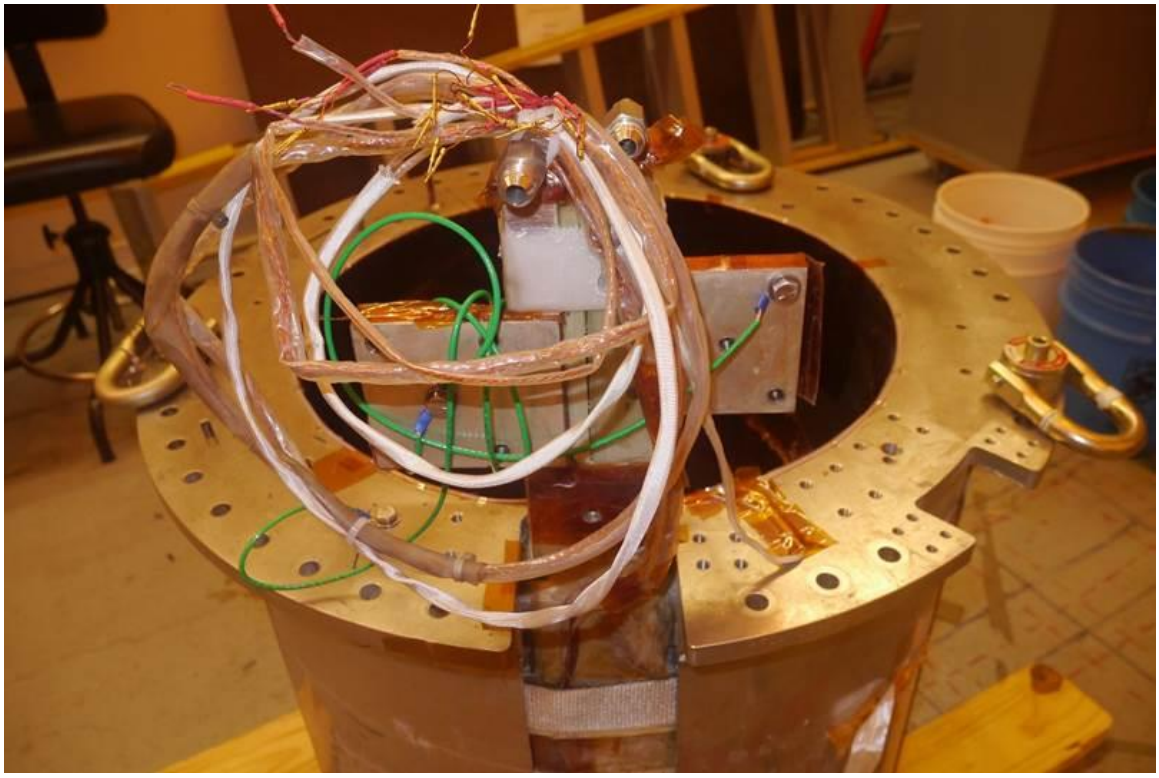

Figure 14 – PF1A-U Leads

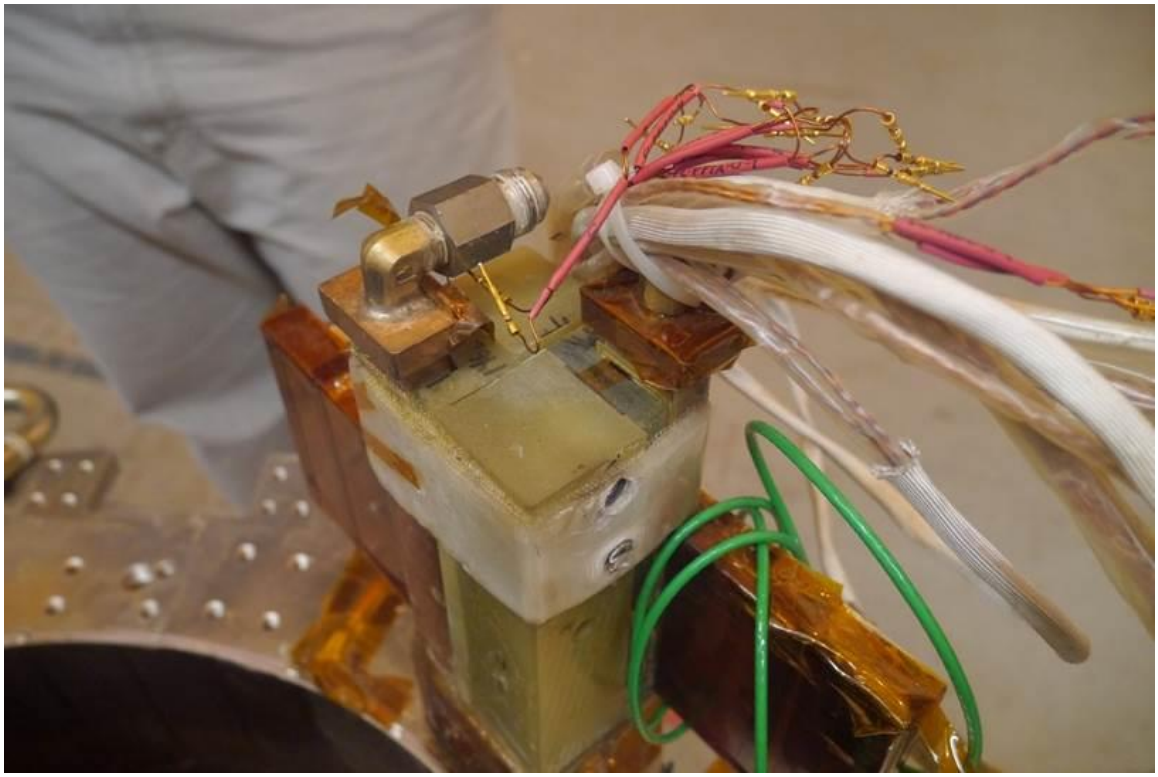

Figure 15 – PF1A-U Leads

Figure 16 – PF1A-U Exterior with shields removed

Figure 17 – PF1A-U Exterior with shields removed

Figure 18 – PF1A-U Exterior with shields removed

Figure 19 – PF1A-U Exterior with shields removed

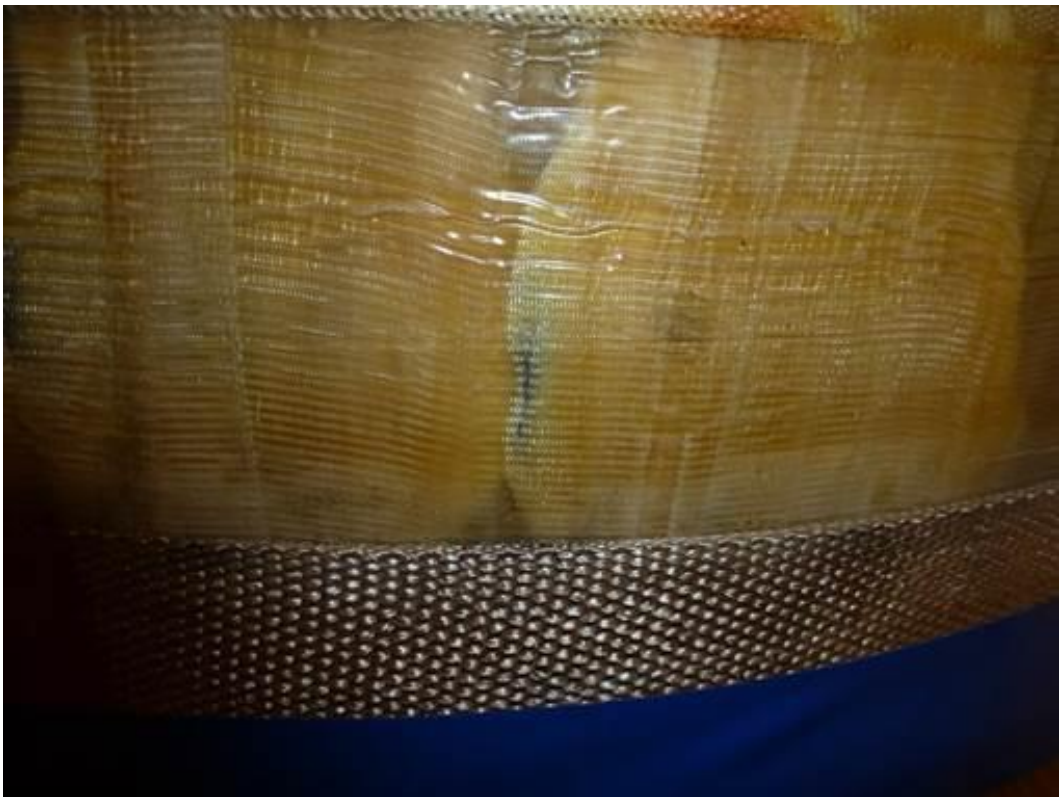

Figure 20 – PF1A-U ground wrap delamination

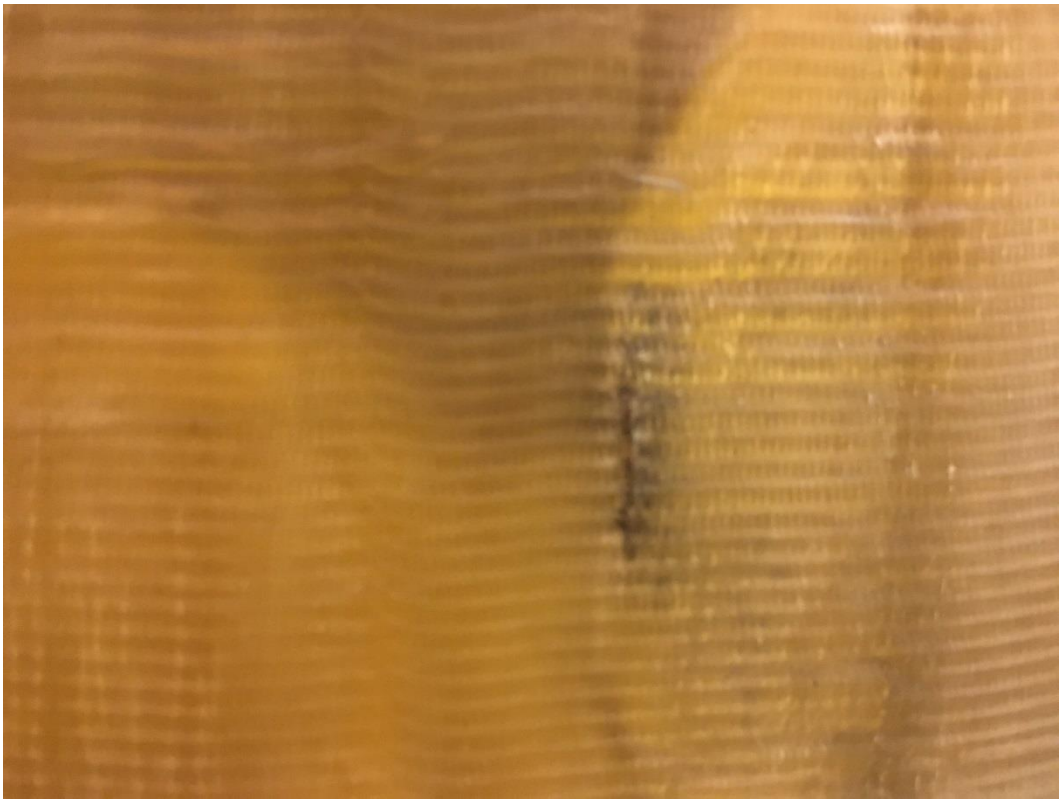

Figure 21 – PF1A-U ground wrap delamination

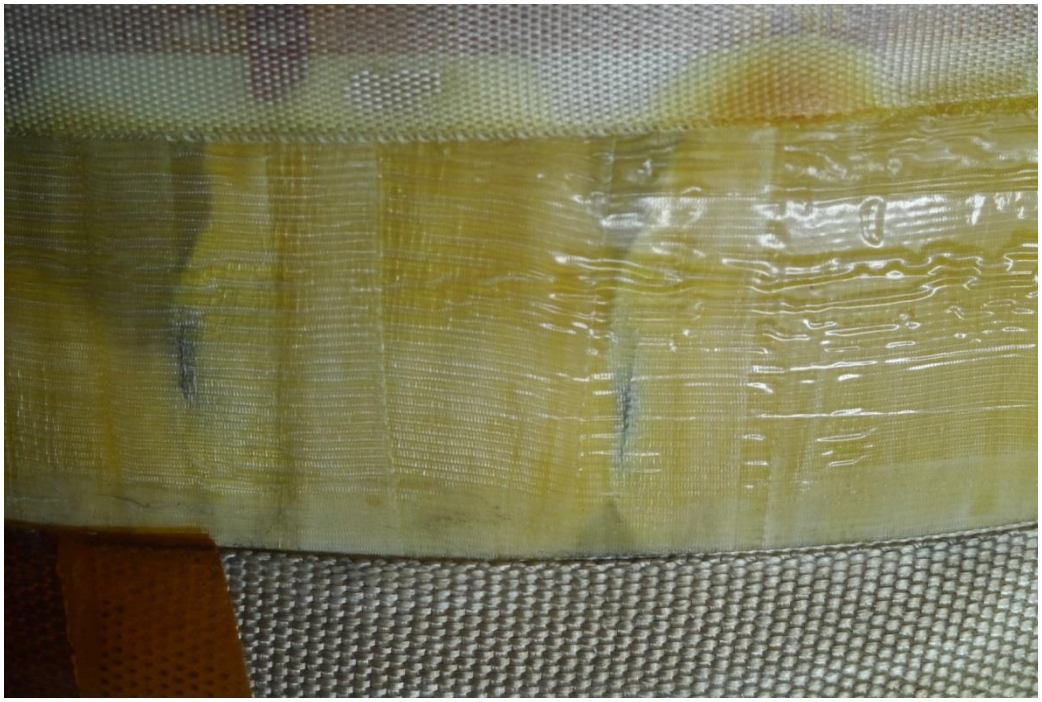

Figure 22 – PF1A-U ground wrap delamination

Figure 23 – PF1A-U ground wrap delamination

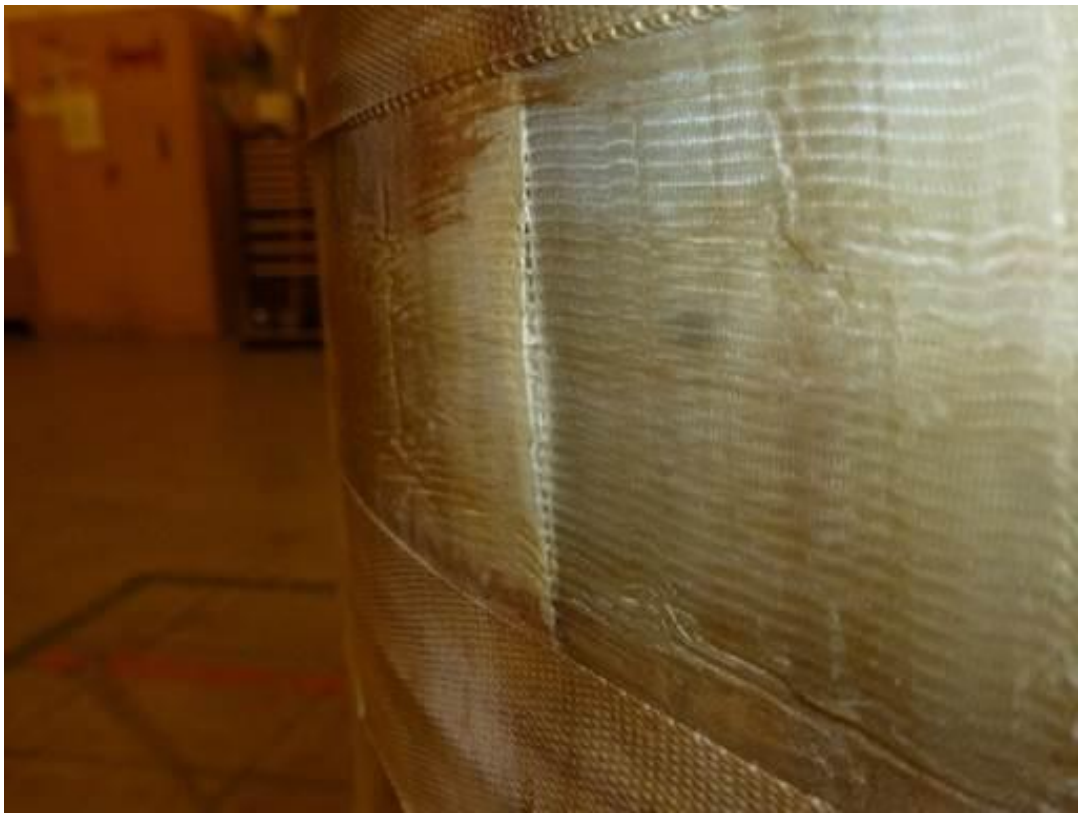

Figure 24 – PF1A-U ground wrap delamination

Figure 25 – Radiographic imaging set-up

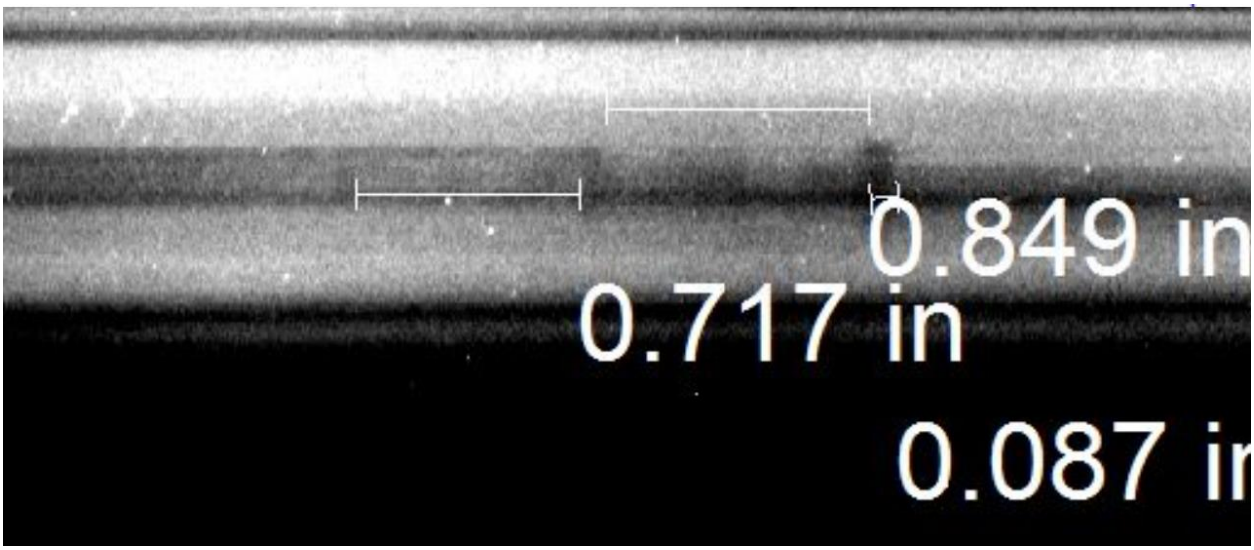

Figure 26 – Radiographic image of Braze Joint #1

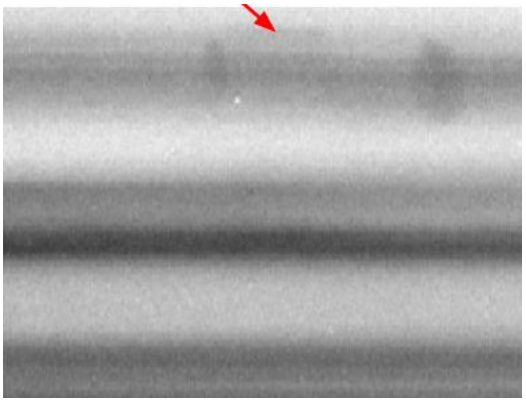
Figure 27 – Radiographic image of Braze Joint #2

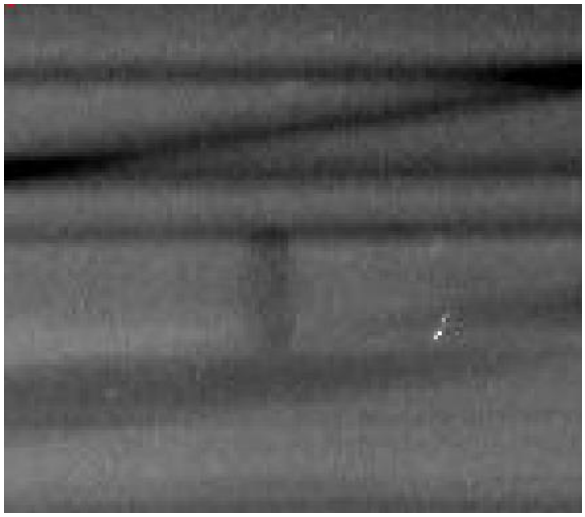
Figure 28 – Radiographic image of Braze Joint #3

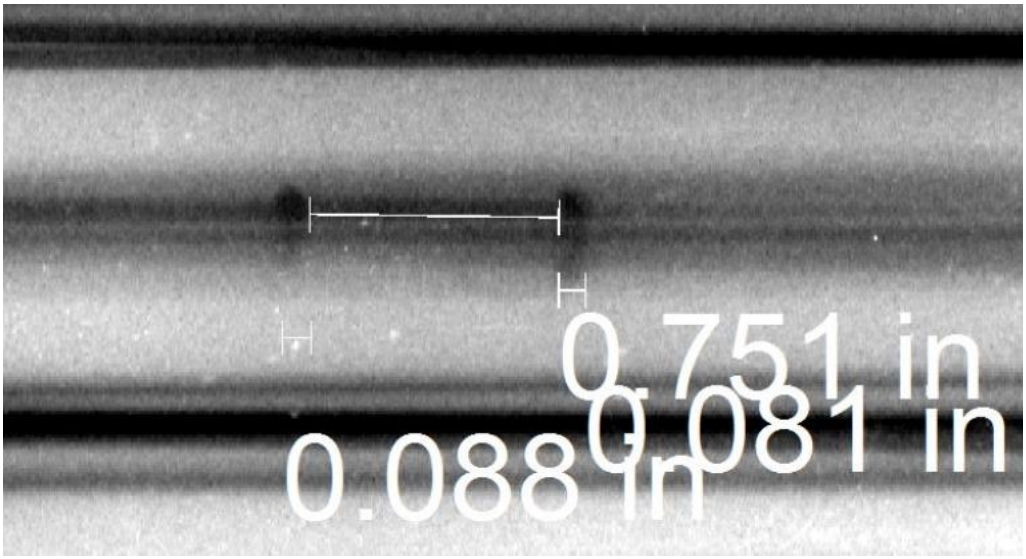

Figure 29 – Radiographic image of Braze Joint #4

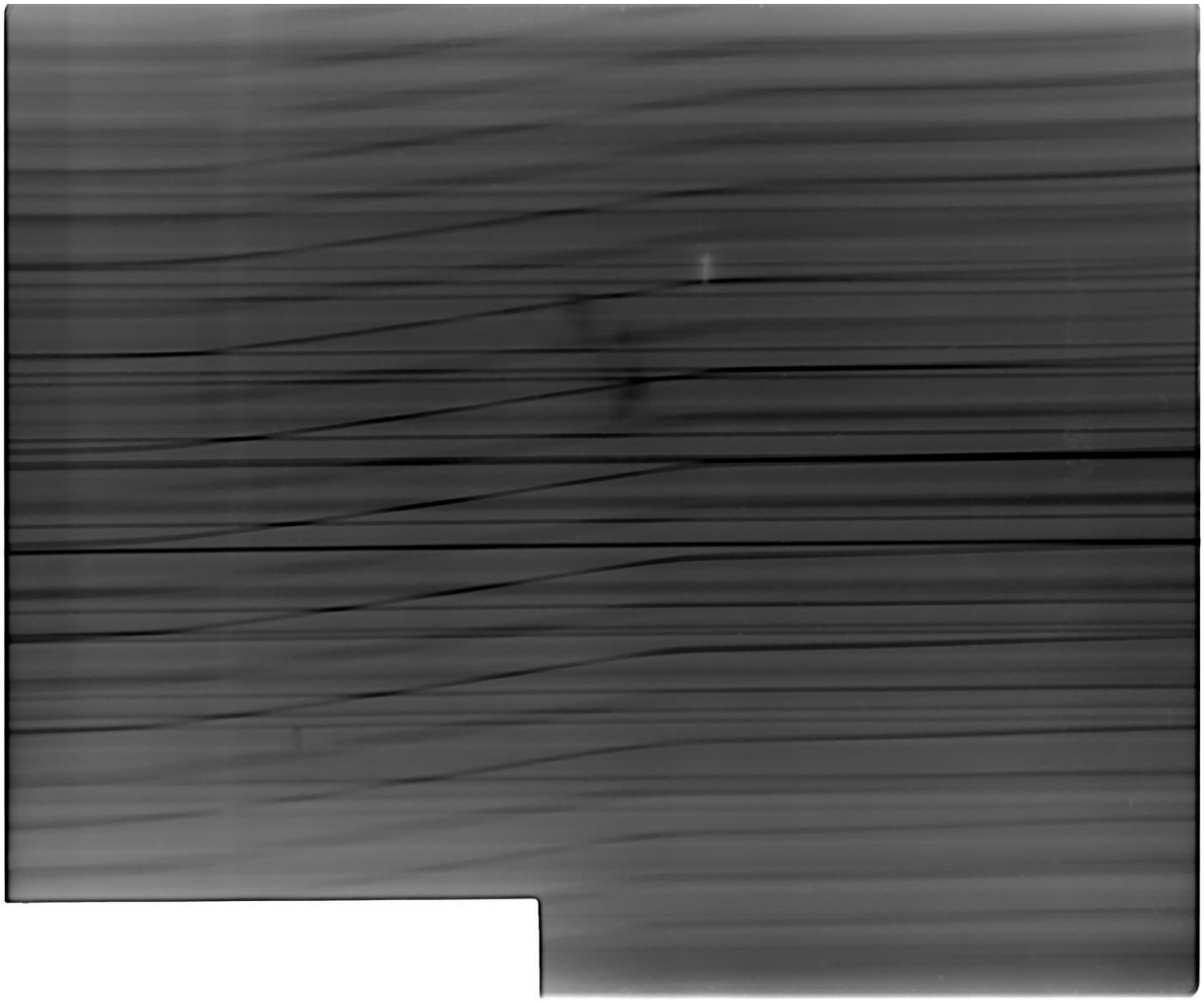
Figure 30 – Radiographic image of area “1_B”

Figure 31 – Outer radius triangulation template for anomalous region 0_1A

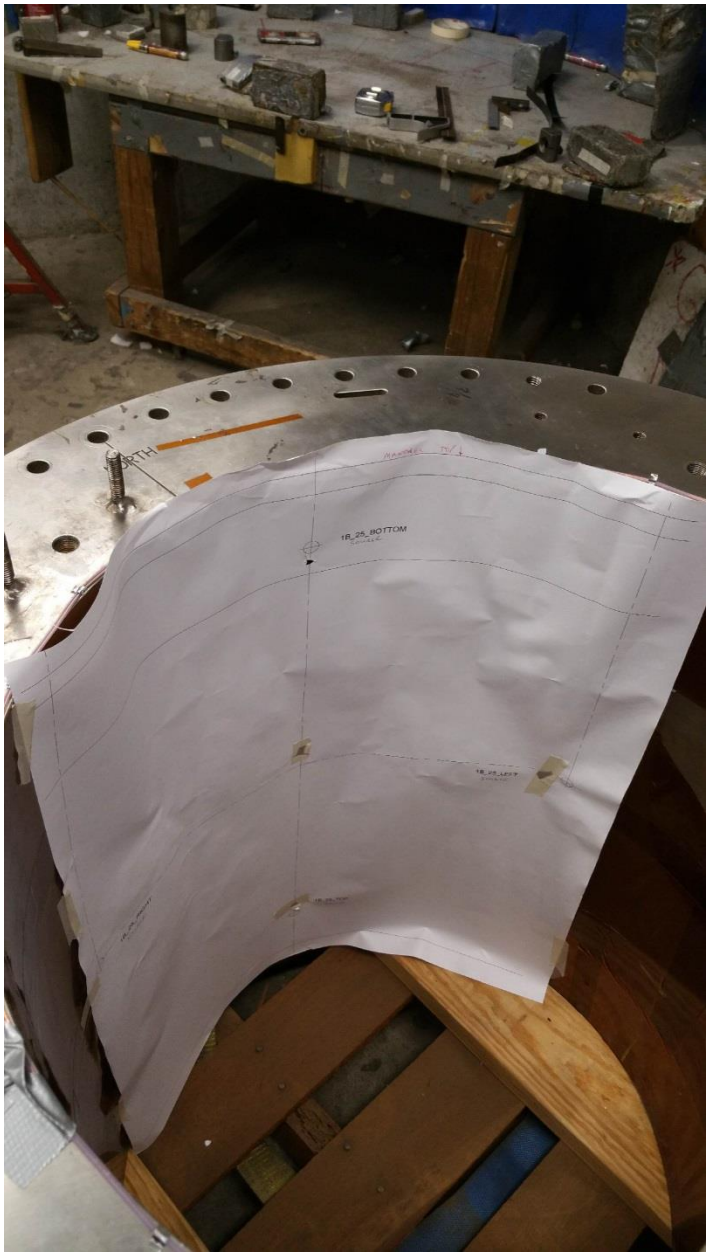

Figure 32 – Inner radius triangulation template for anomalous region 0_1A

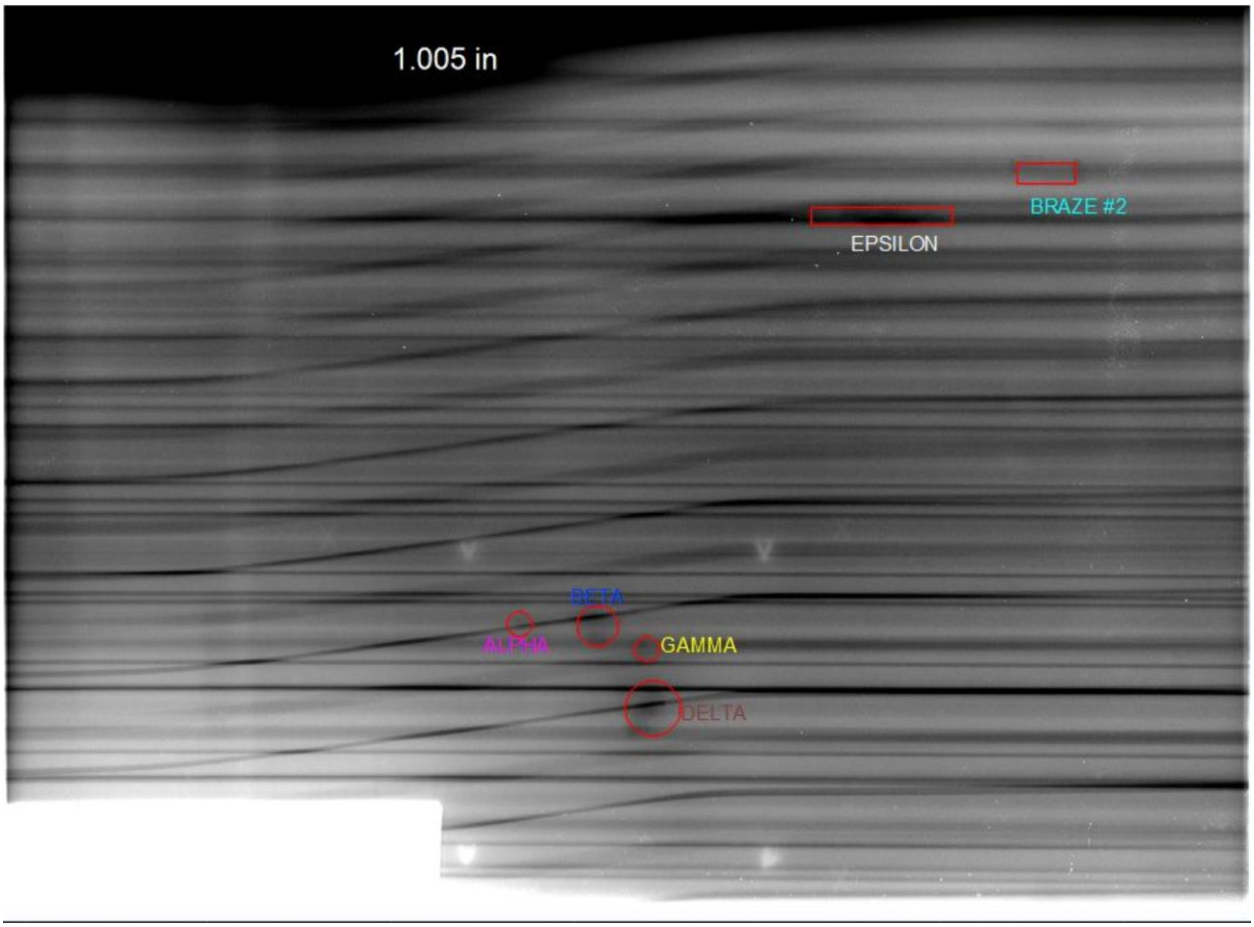

Figure 33 – Approximate references for anomalies identified in region 0_1A

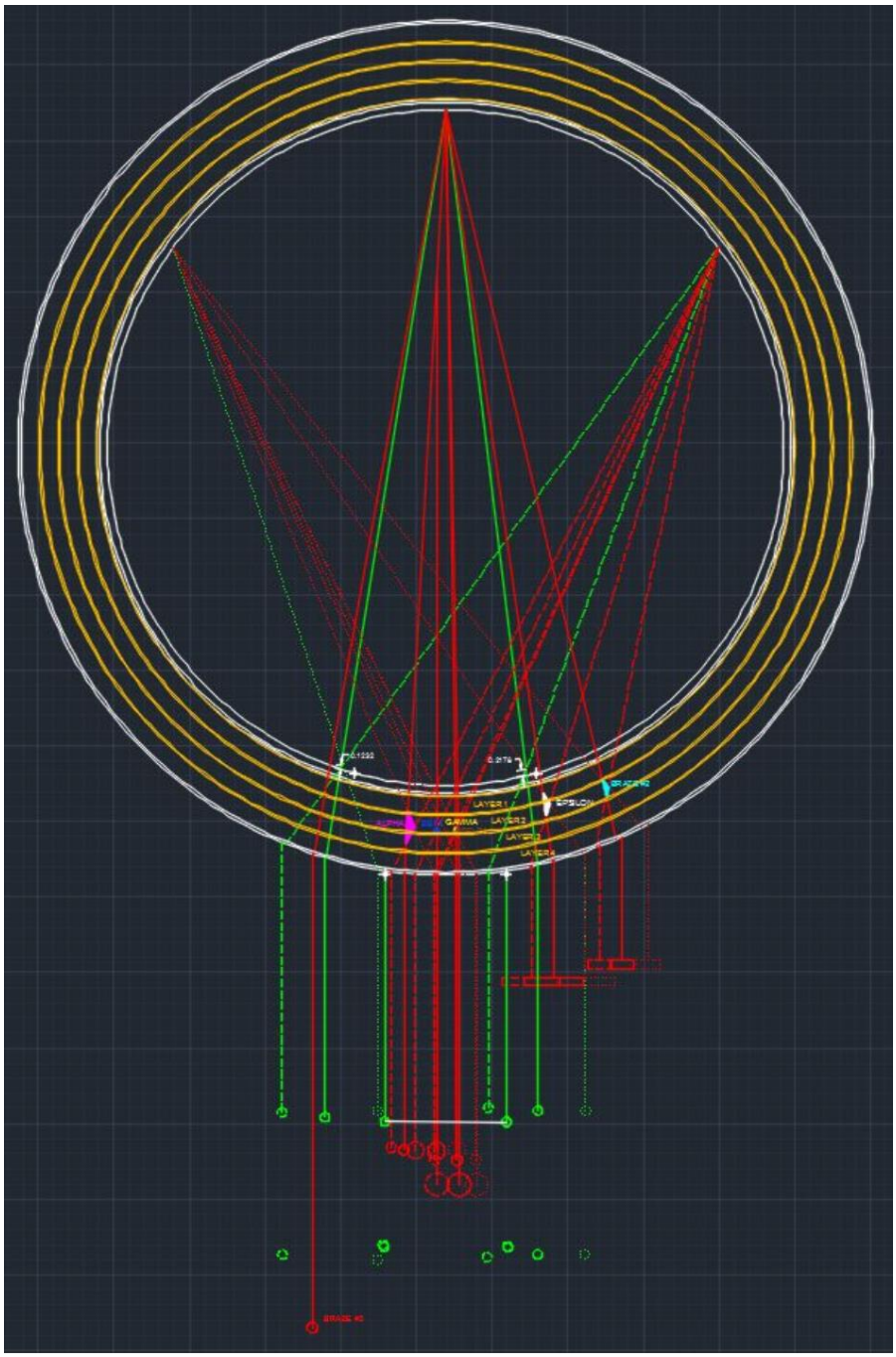

Figure 34 – AutoCAD-based triangulation of anomalous region 0_1A

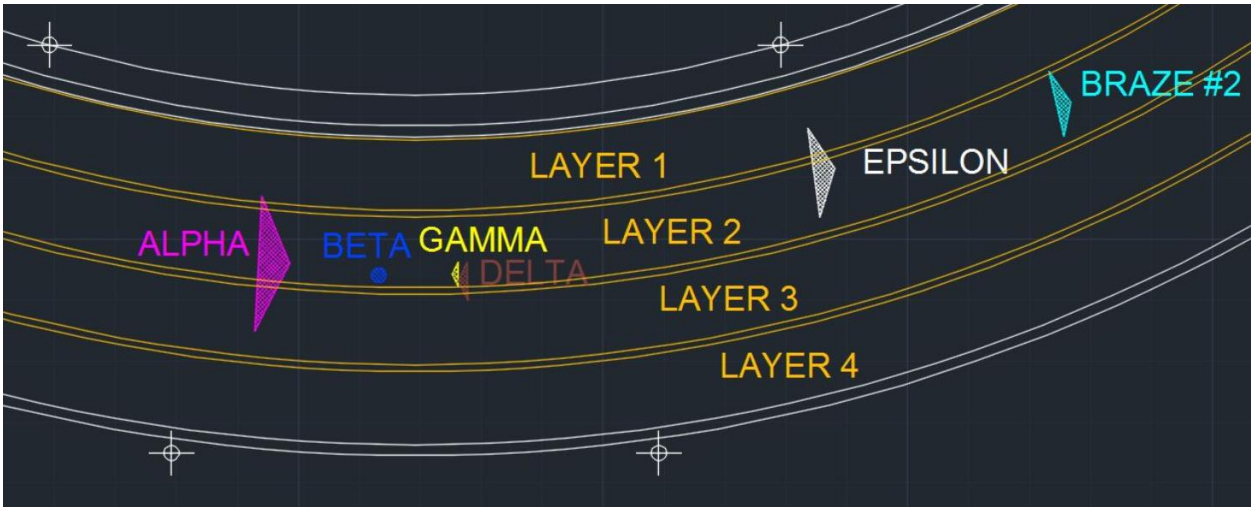

Figure 35 – AutoCAD-based triangulation of anomalous region 0_1A

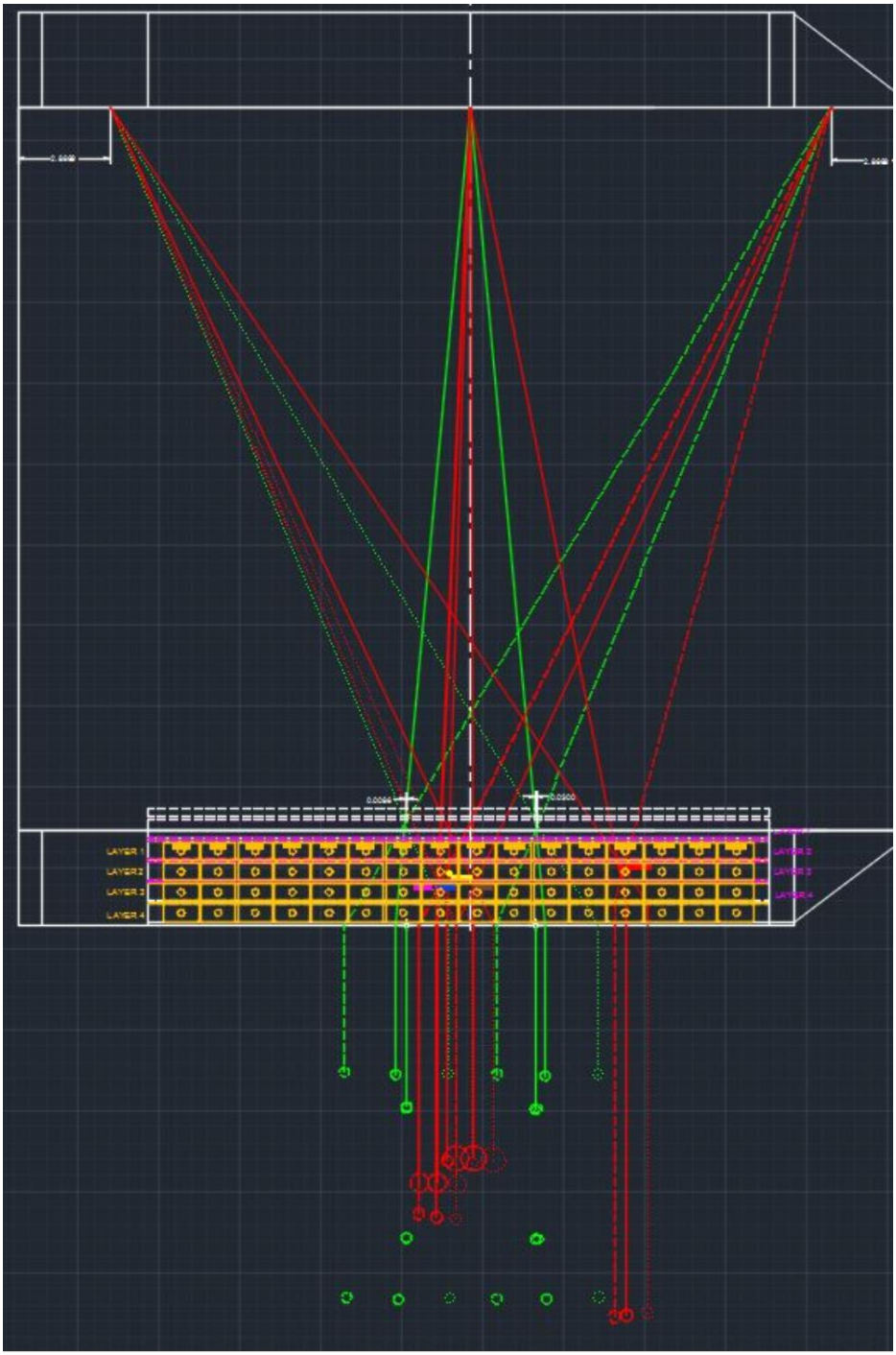

Figure 36 – AutoCAD-based triangulation of anomalous region 0_1A

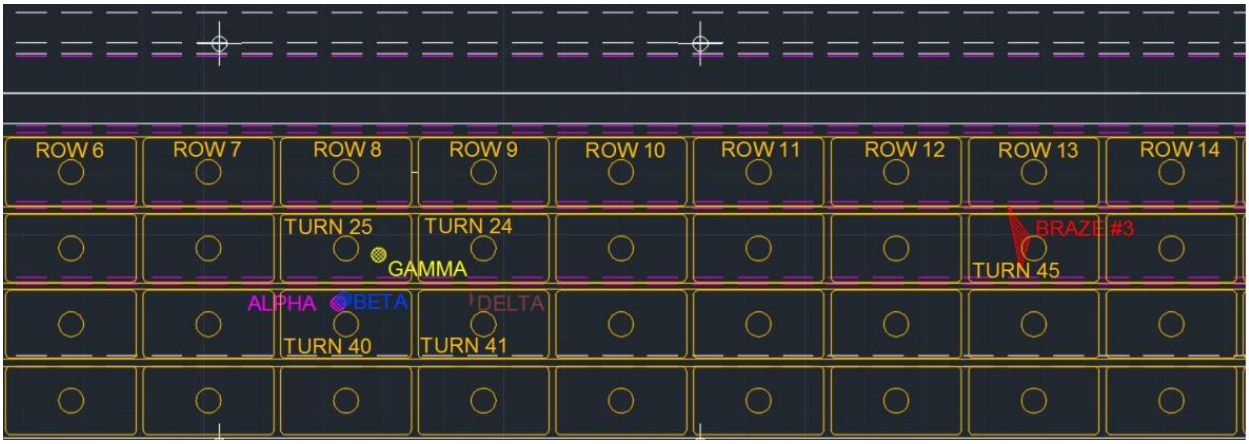

Figure 37 – AutoCAD-based triangulation of anomalous region 0_1A

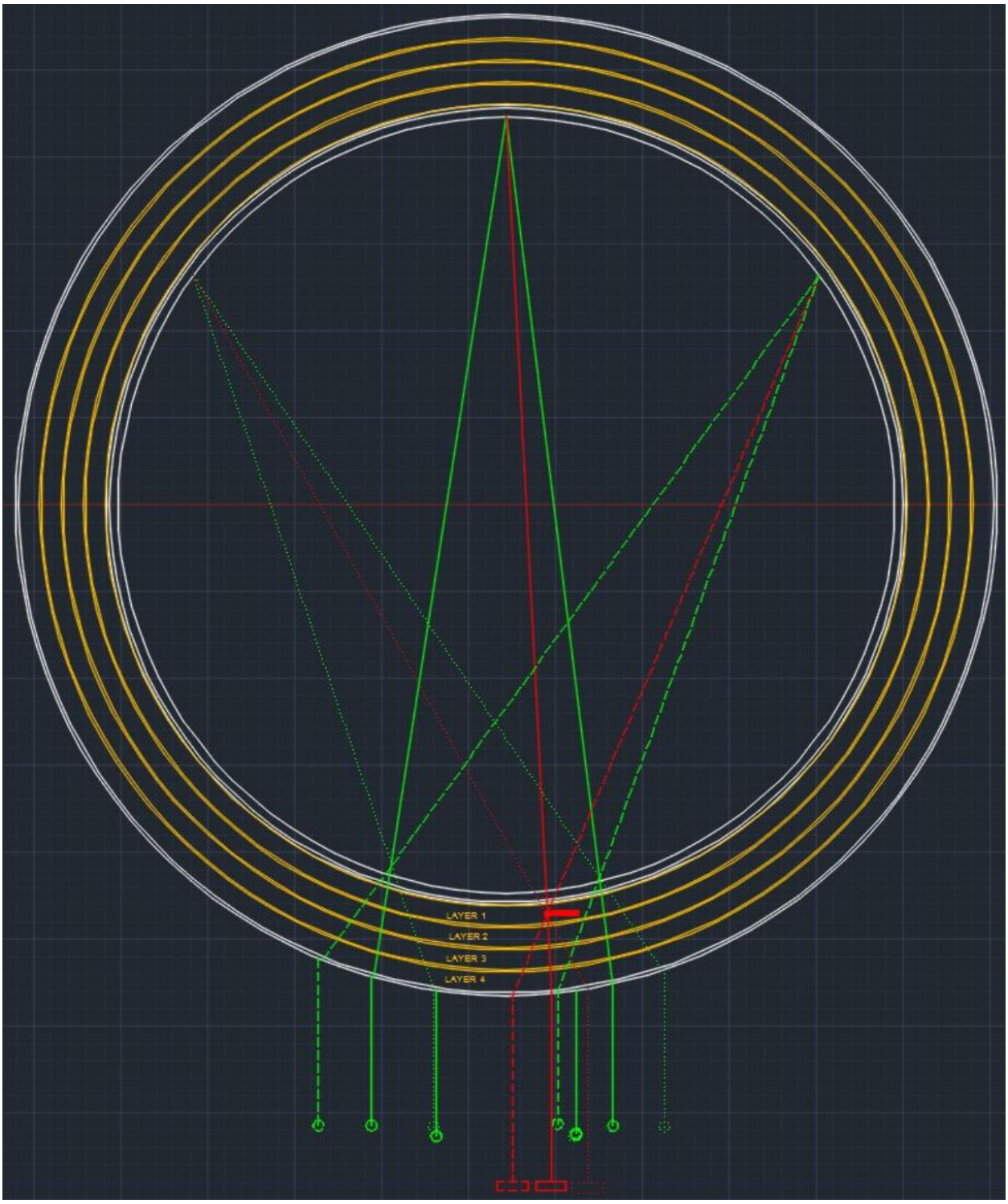

Figure 38 – AutoCAD-based triangulation of Braze Joint #1

Figure 39 – AutoCAD-based triangulation of Braze Joint #1

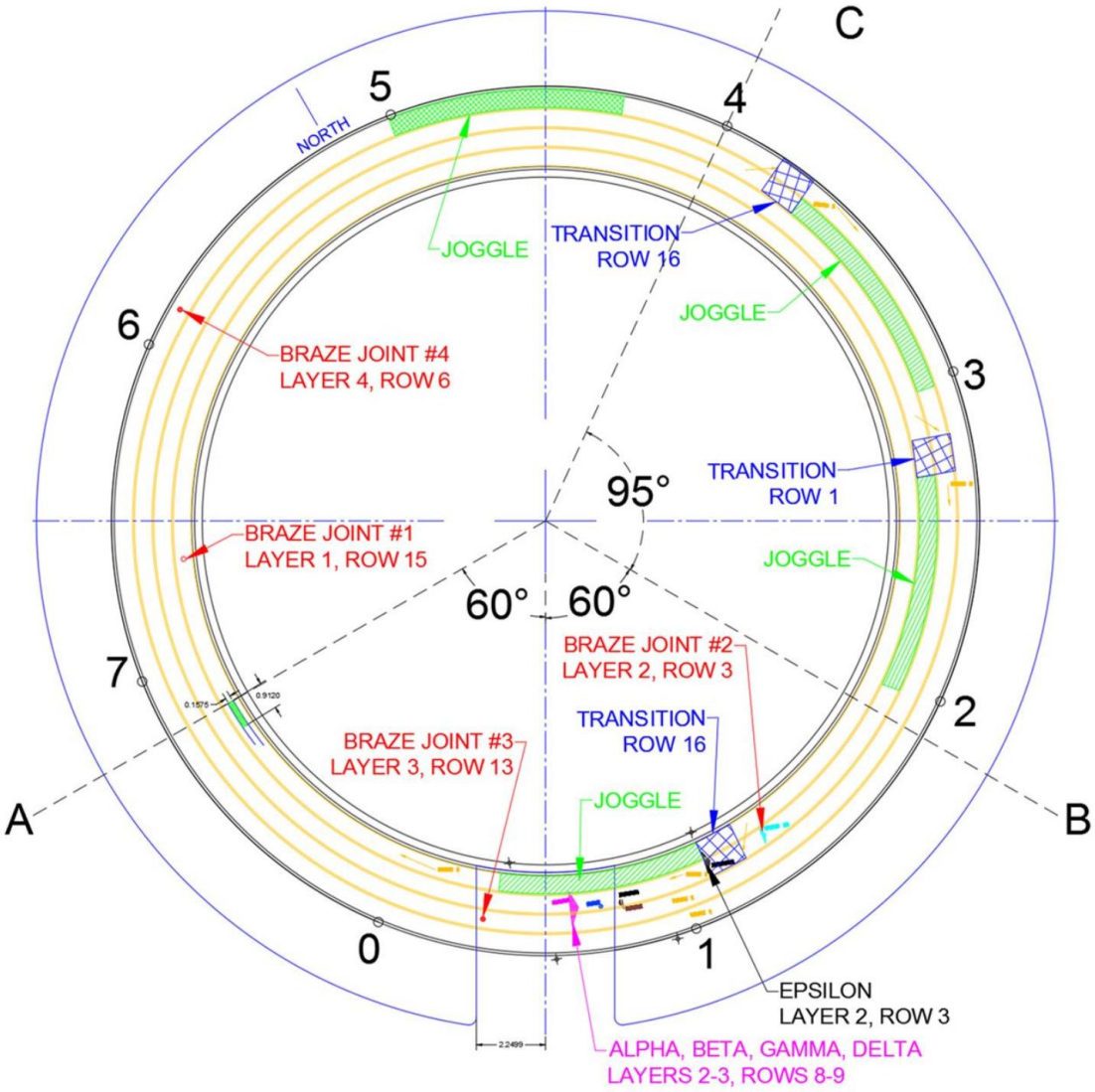

Figure 40 – Identified sectioning cuts “A, B and C”

Figure 41 – PF1A-U placement on horizontal Lucas Mill with fixtures

Figure 42 – Orientation of milling bit and shop vacuum nozzles

Figure 43 – Four flute end-mill typical of bit used to cut each segment

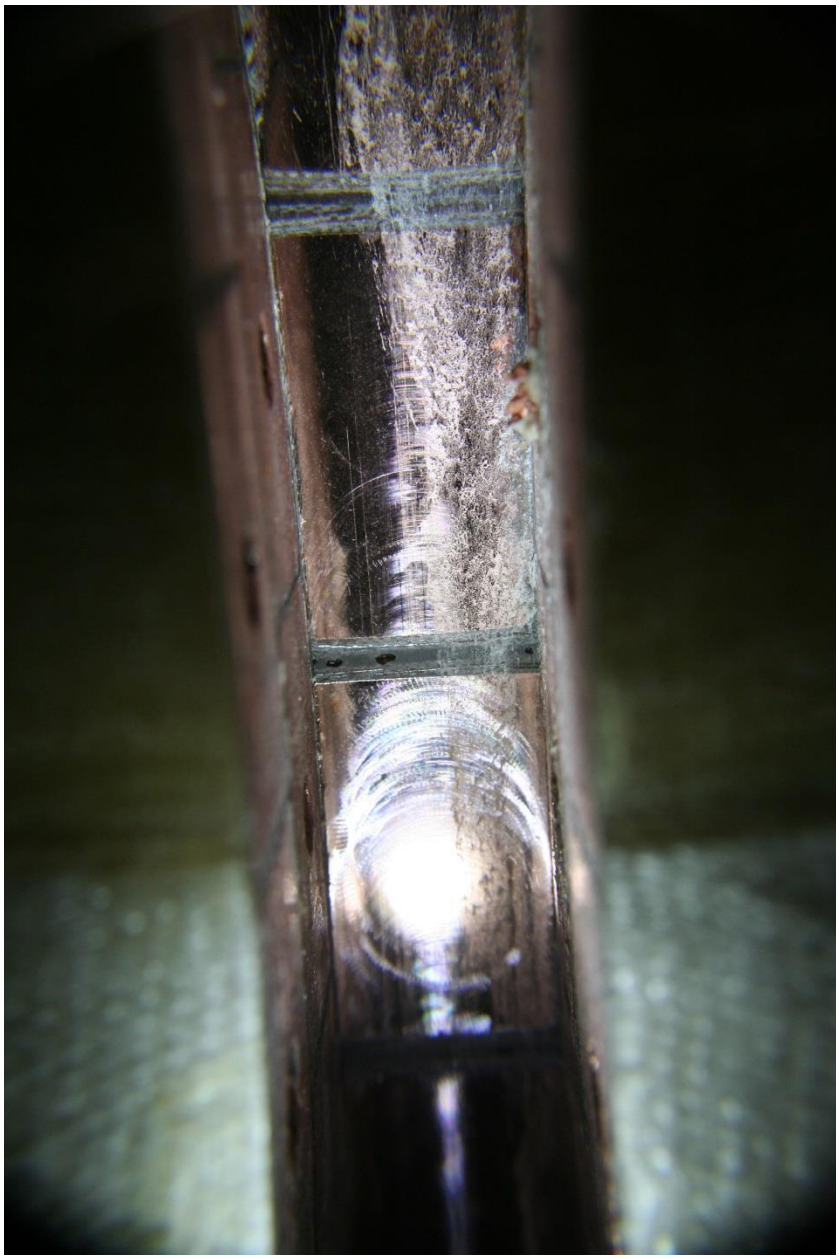

Figure 44 – Cutting Plane A void

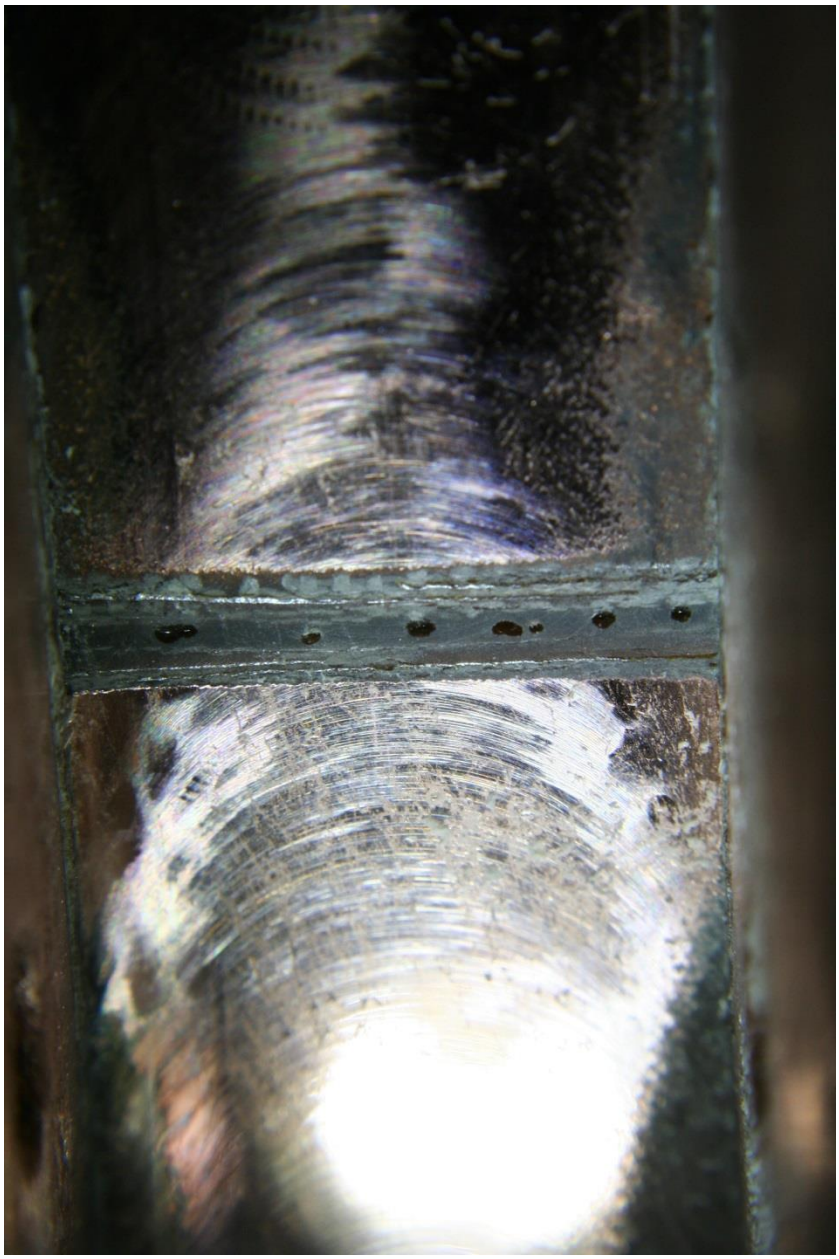

Figure 45 – Cutting Plane A void

Figure 46 – Cutting Plane A void

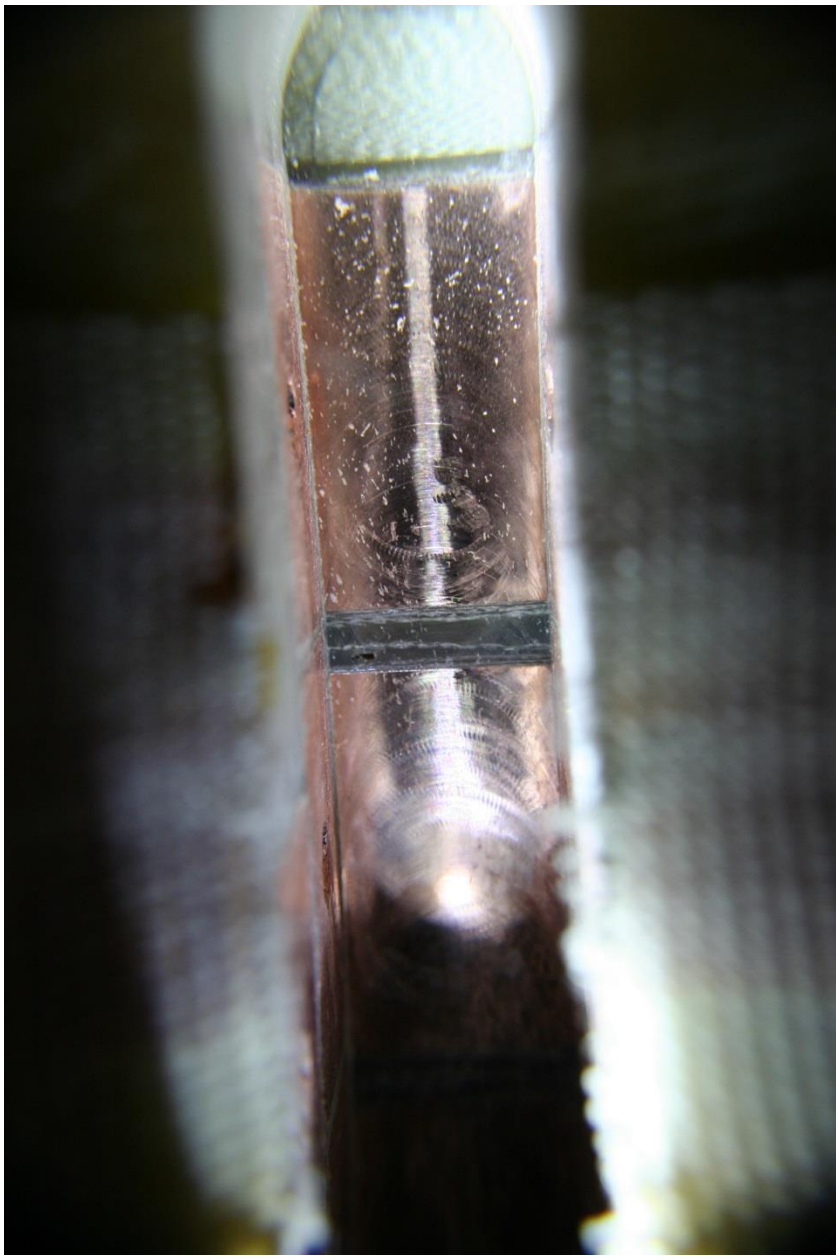

Figure 47 – Cutting Plane A half-lap ballooning

Figure 48 – Cutting Plane A adhesion issue

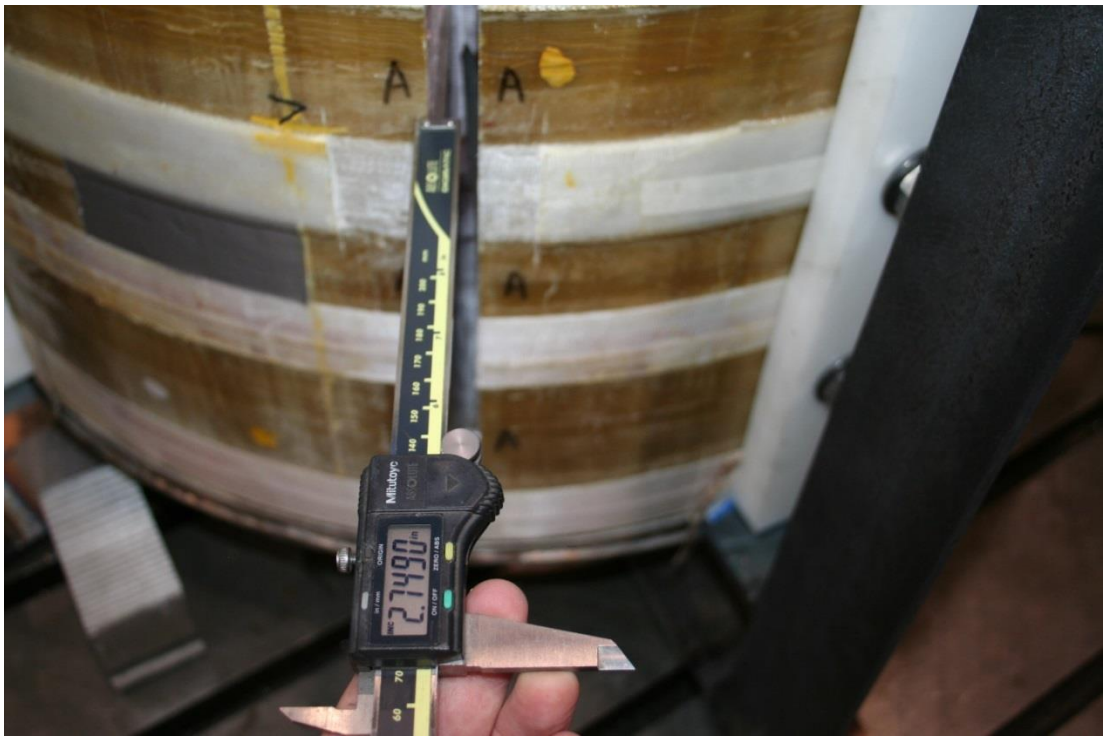

Figure 49 – Cutting Plane A coil pack depth

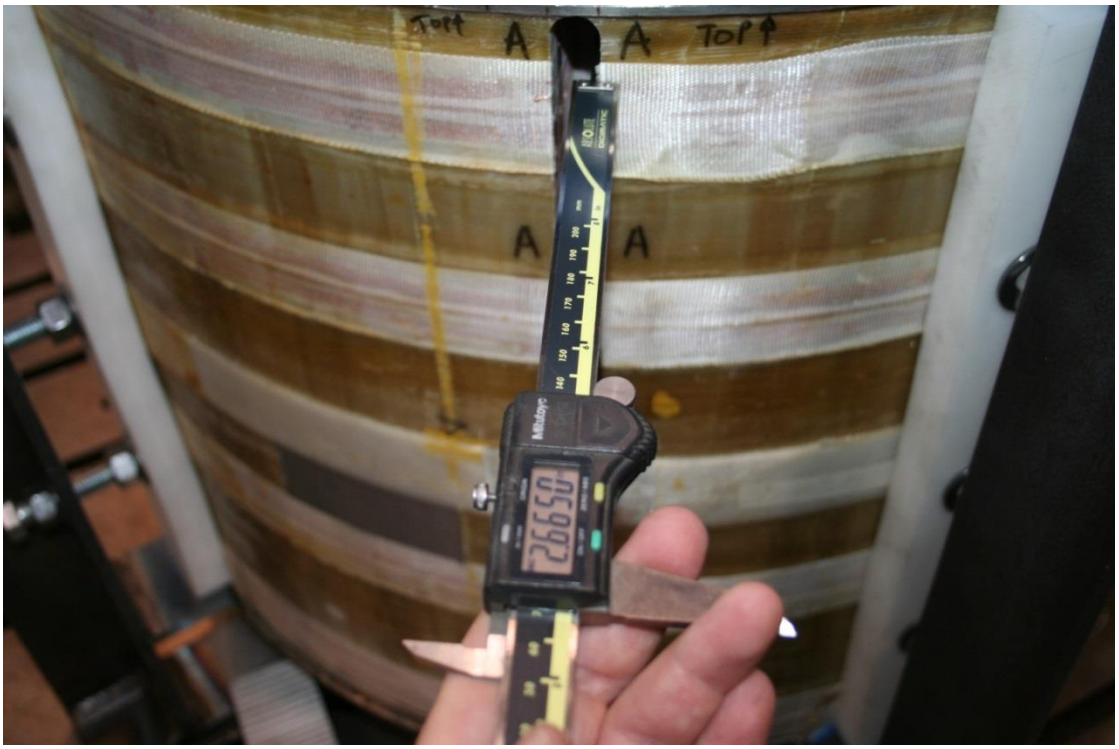

Figure 50 – Cutting Plane A coil pack depth

Figure 51 – Cutting Plane A coil pack depth

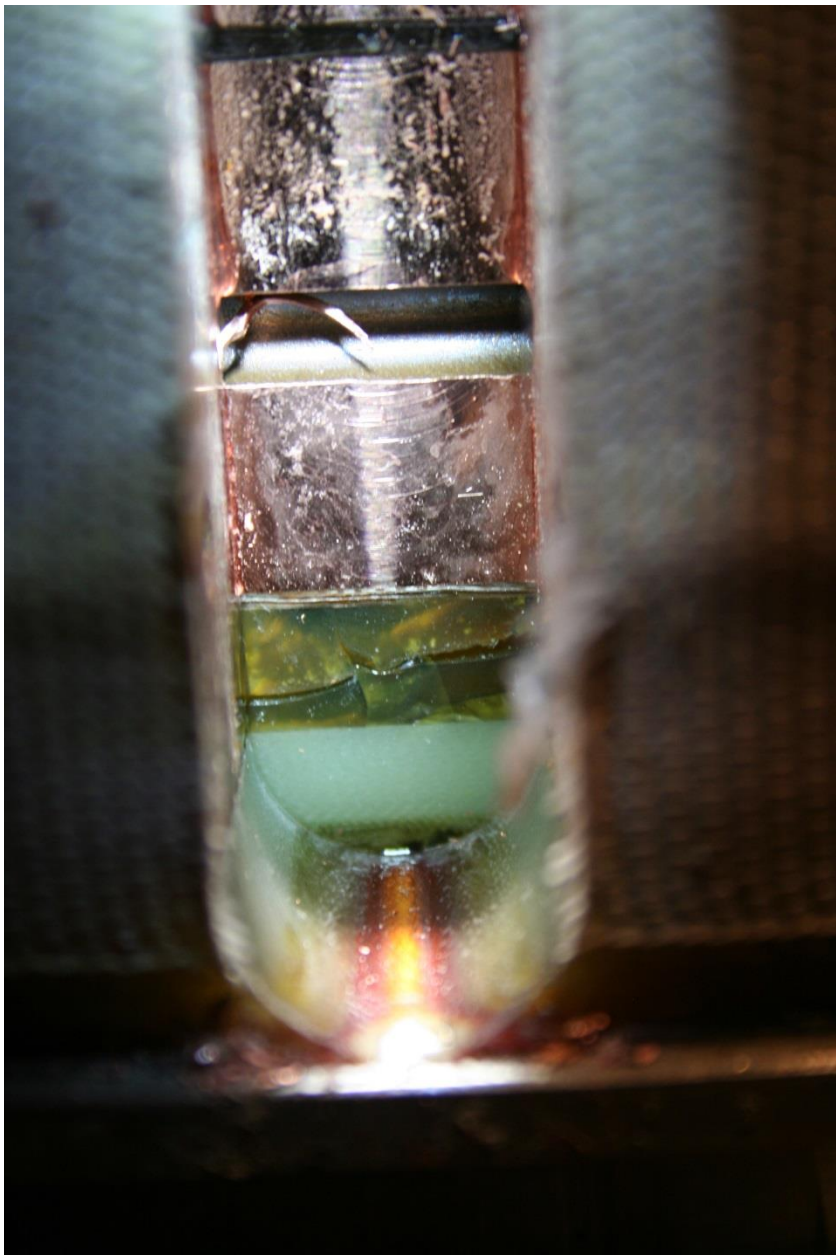

Figure 52 – Cutting Plane B resin rich area and crack

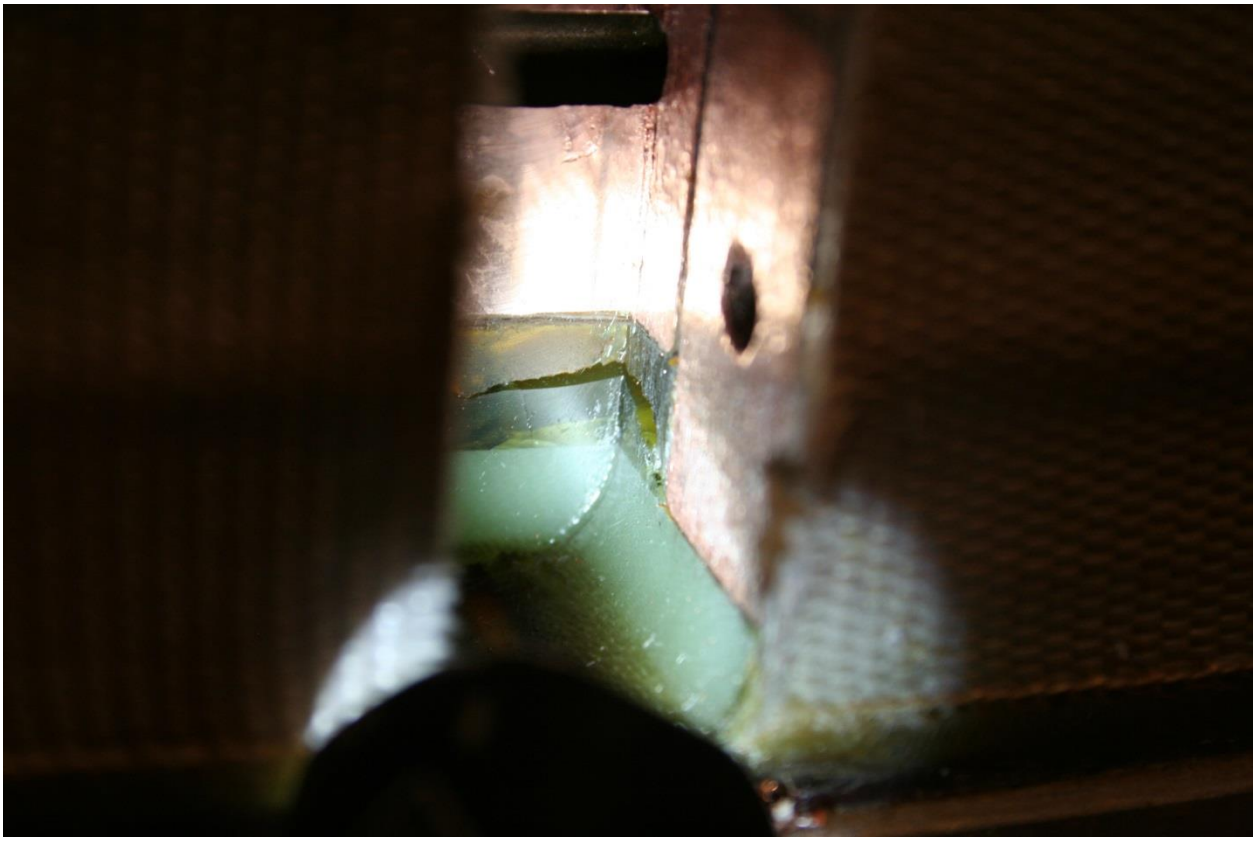

Figure 53 – Cutting Plane B resin rich area and crack

Figure 54 – Cutting Plane B delaminated region

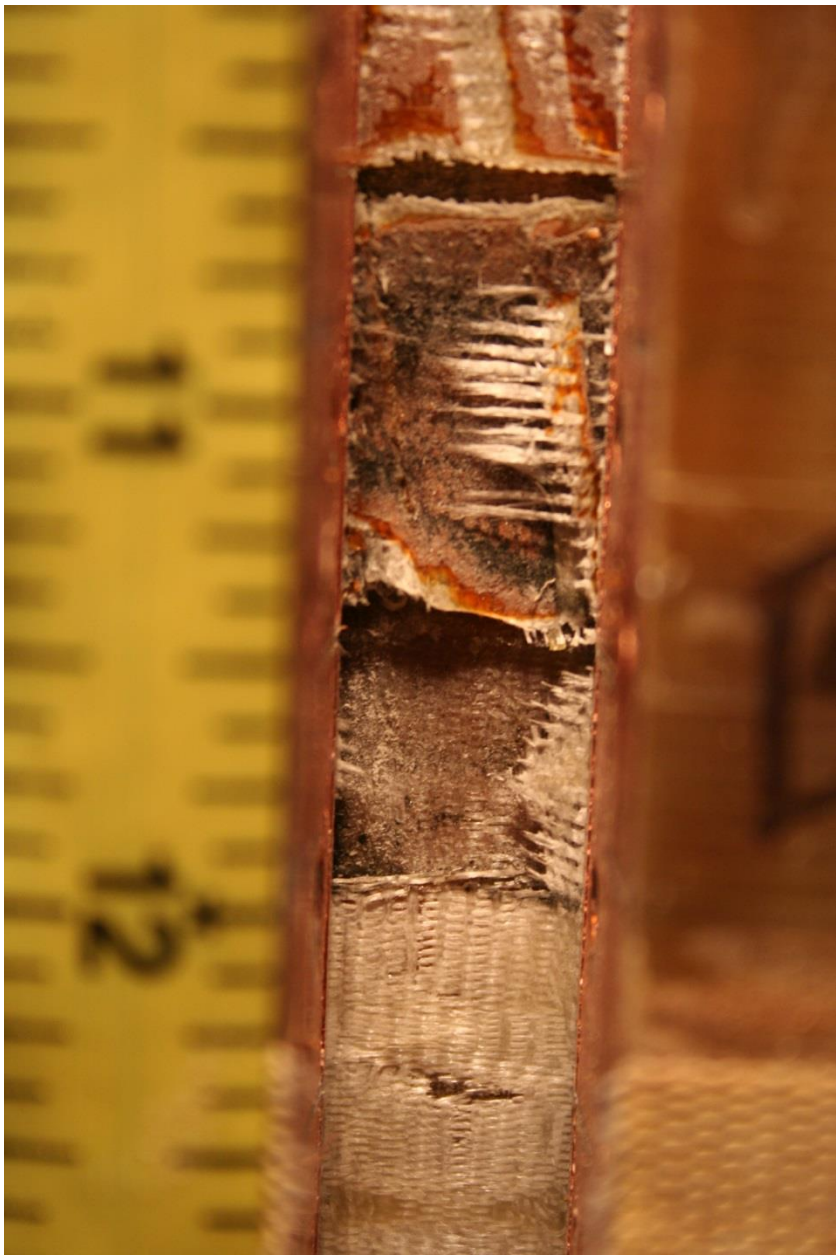

Figure 55 – Cutting Plane B unwetted region

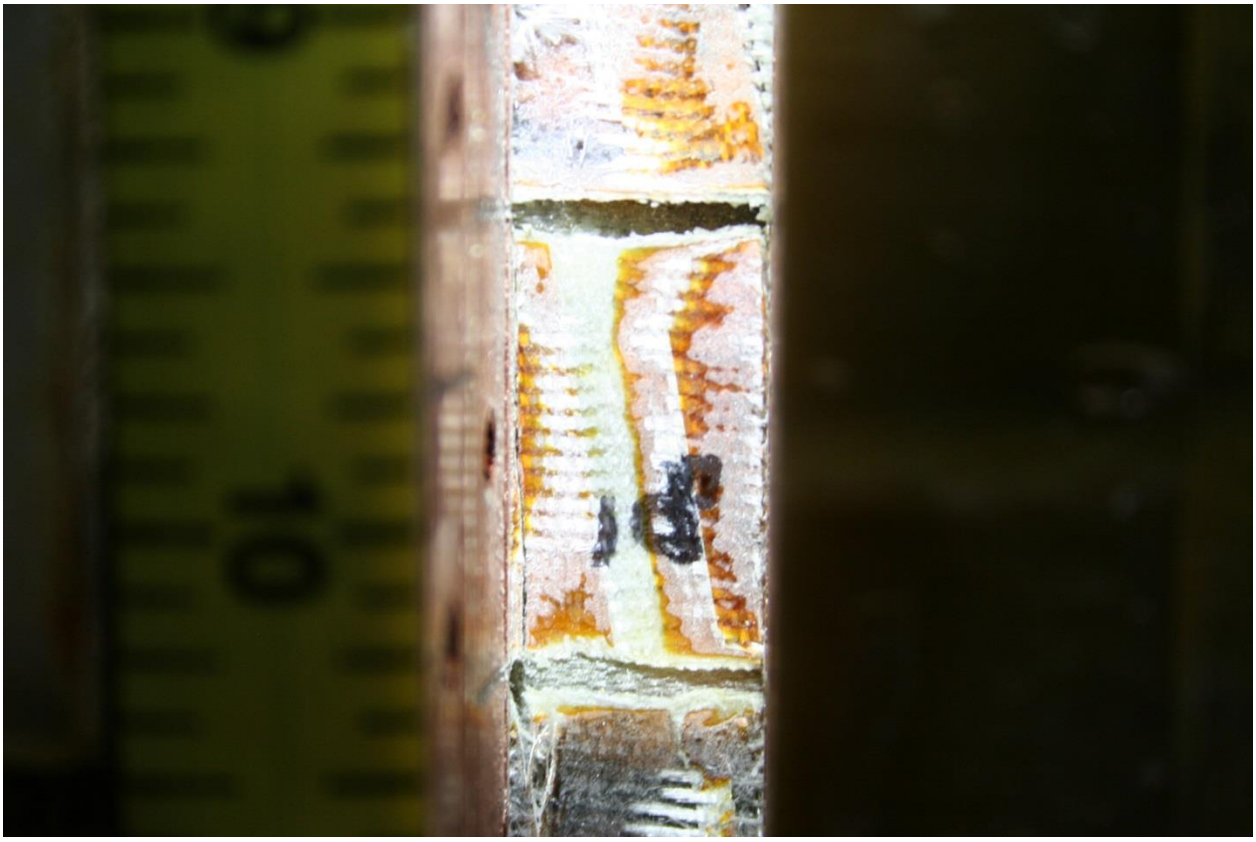

Figure 56 – Cutting Plane B sample

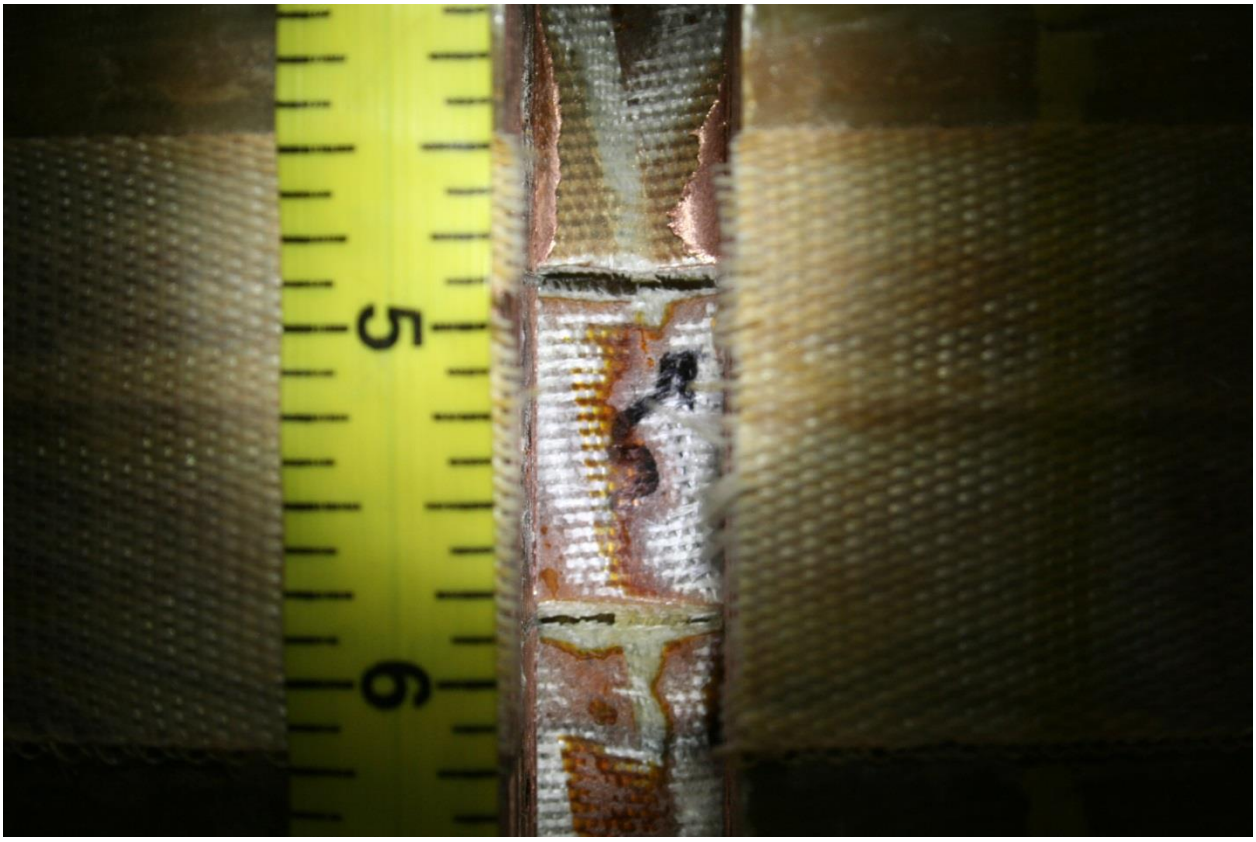

Figure 57 – Cutting Plane B sample

Figure 58 – Cutting Plane B sample

. Figure 59 – Cutting Plane B debris

Figure 60 – Cutting Plane B discolored area

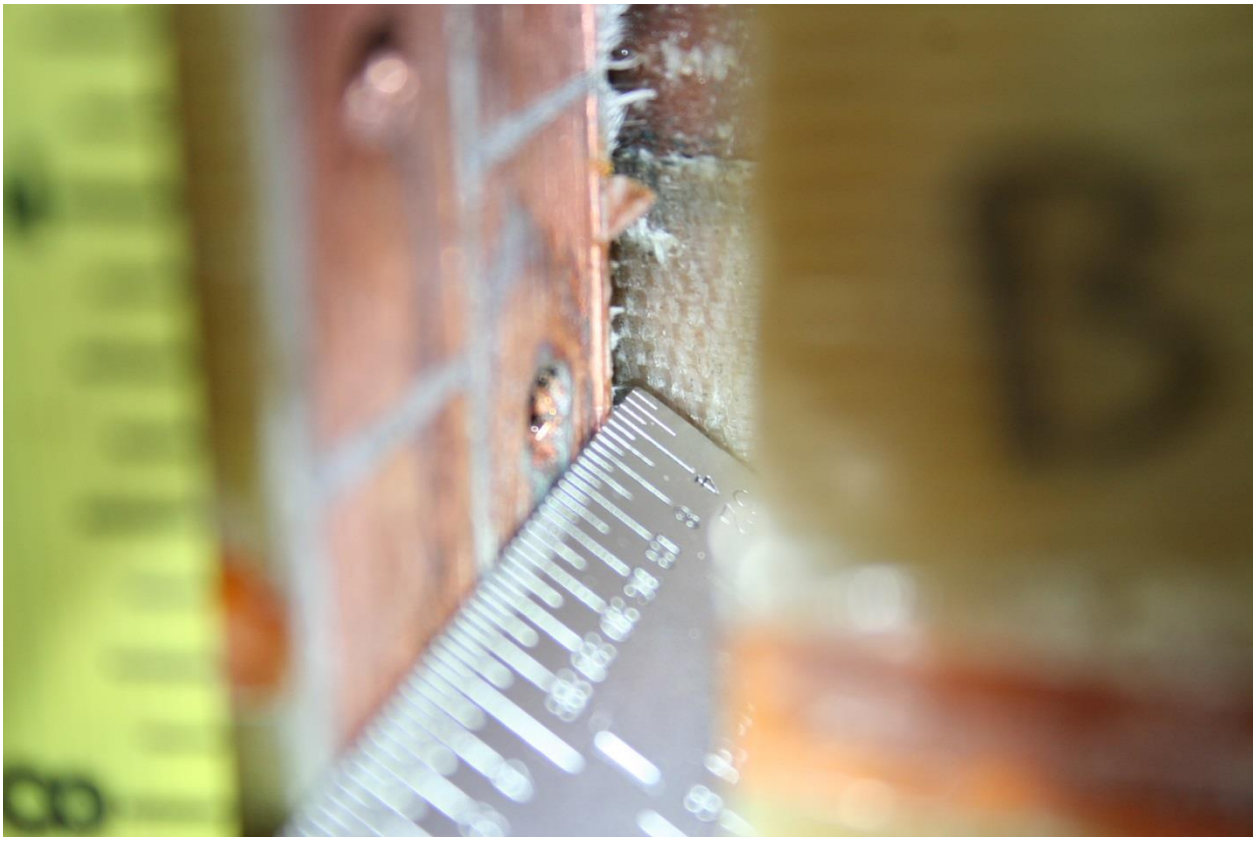

Figure 61 – Cutting Plane B gap measurements

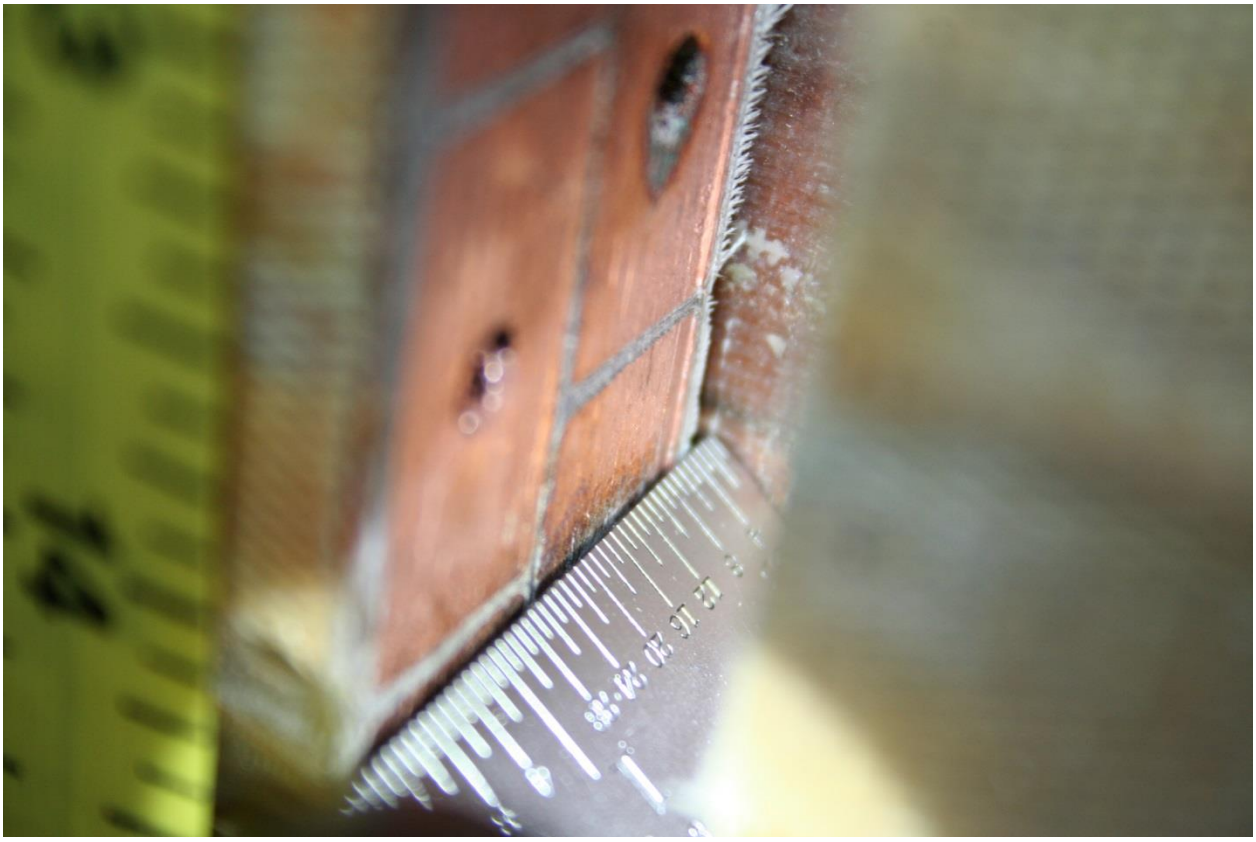

Figure 62 – Cutting Plane B gap measurements

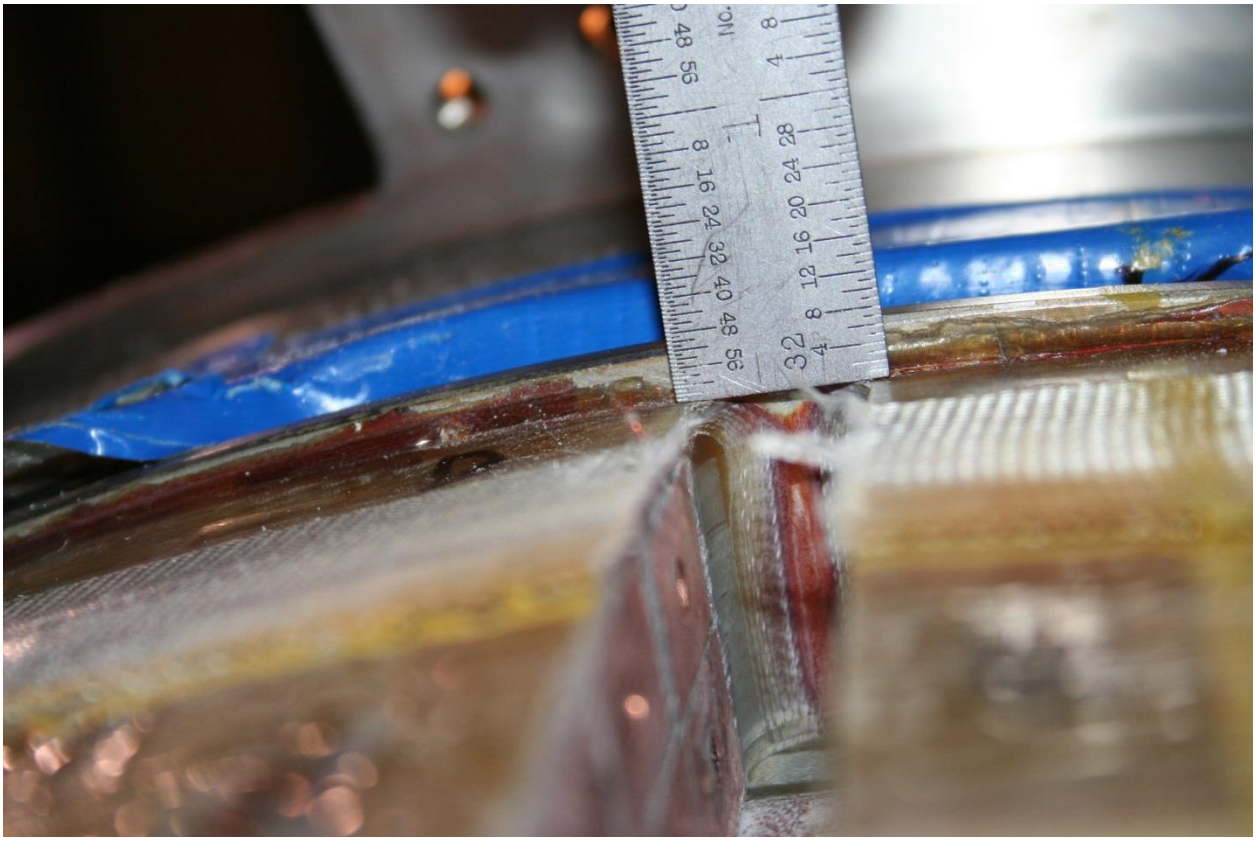

Figure 63 – Cutting Plane B top mandrel reference

Figure 64 – Cutting Plane B void

Figure 65 – Cutting Plane B coil pack depth

Figure 66 – Cutting Plane B coil pack depth

Figure 67 – Cutting Plane B coil pack depth

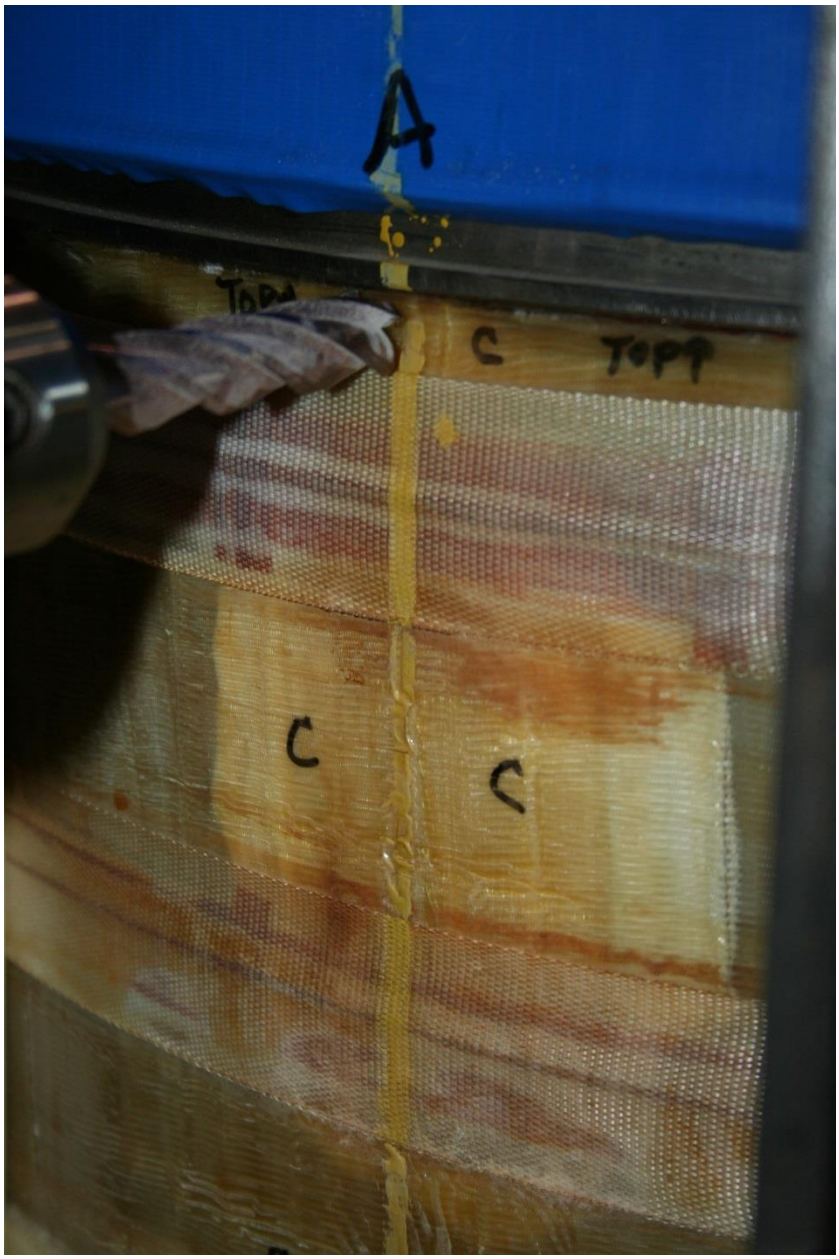

Figure 68 – Cutting Plane C ground wrap delamination

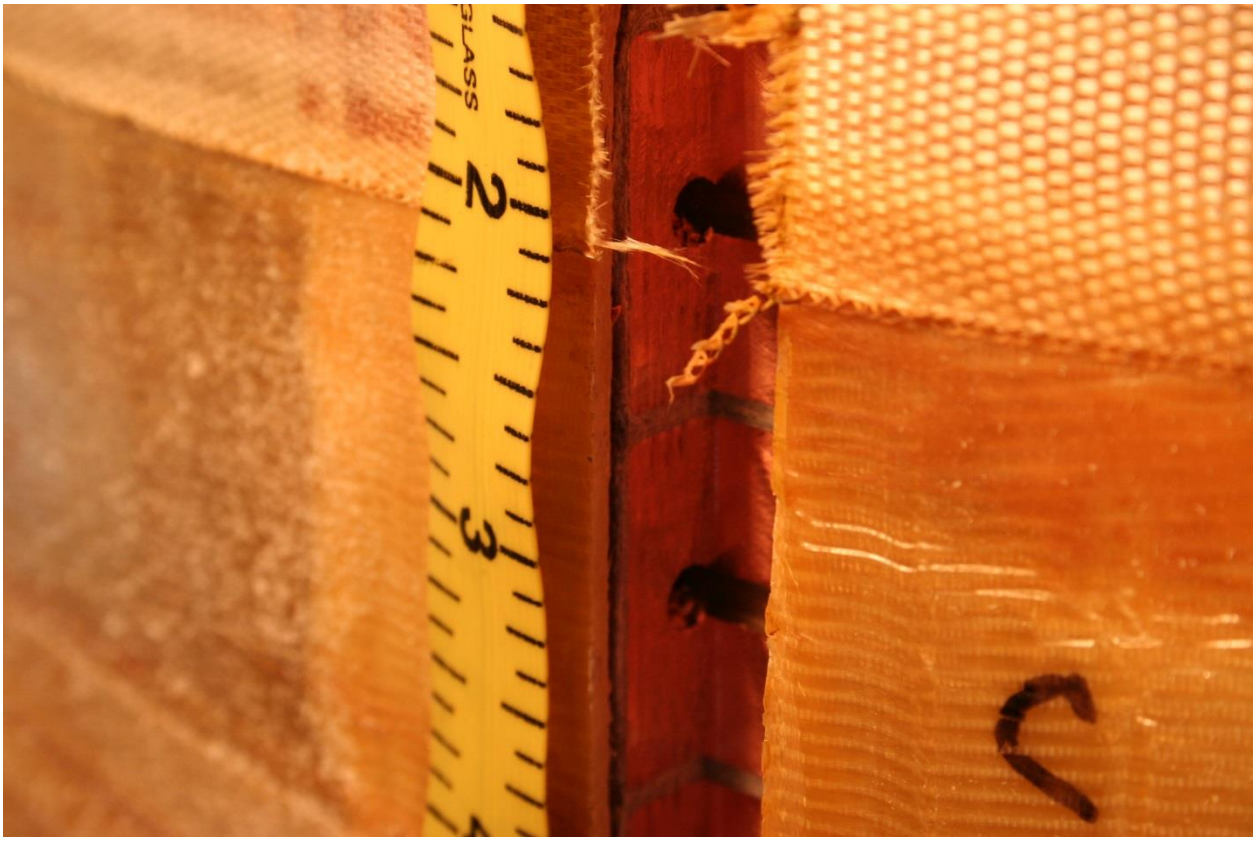

Figure 69 – Cutting Plane C ground wrap delamination

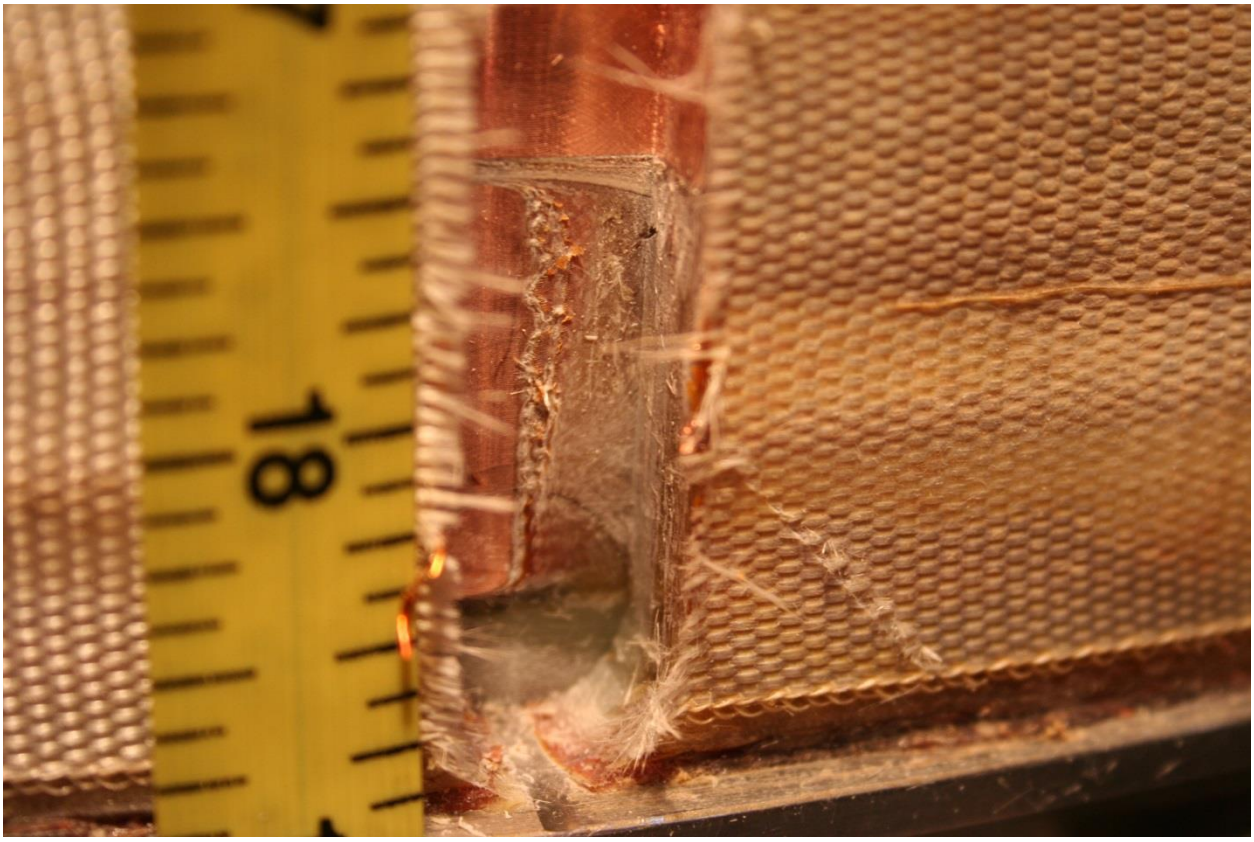

Figure 70 – Cutting Plane C layer 3 to 4 transition

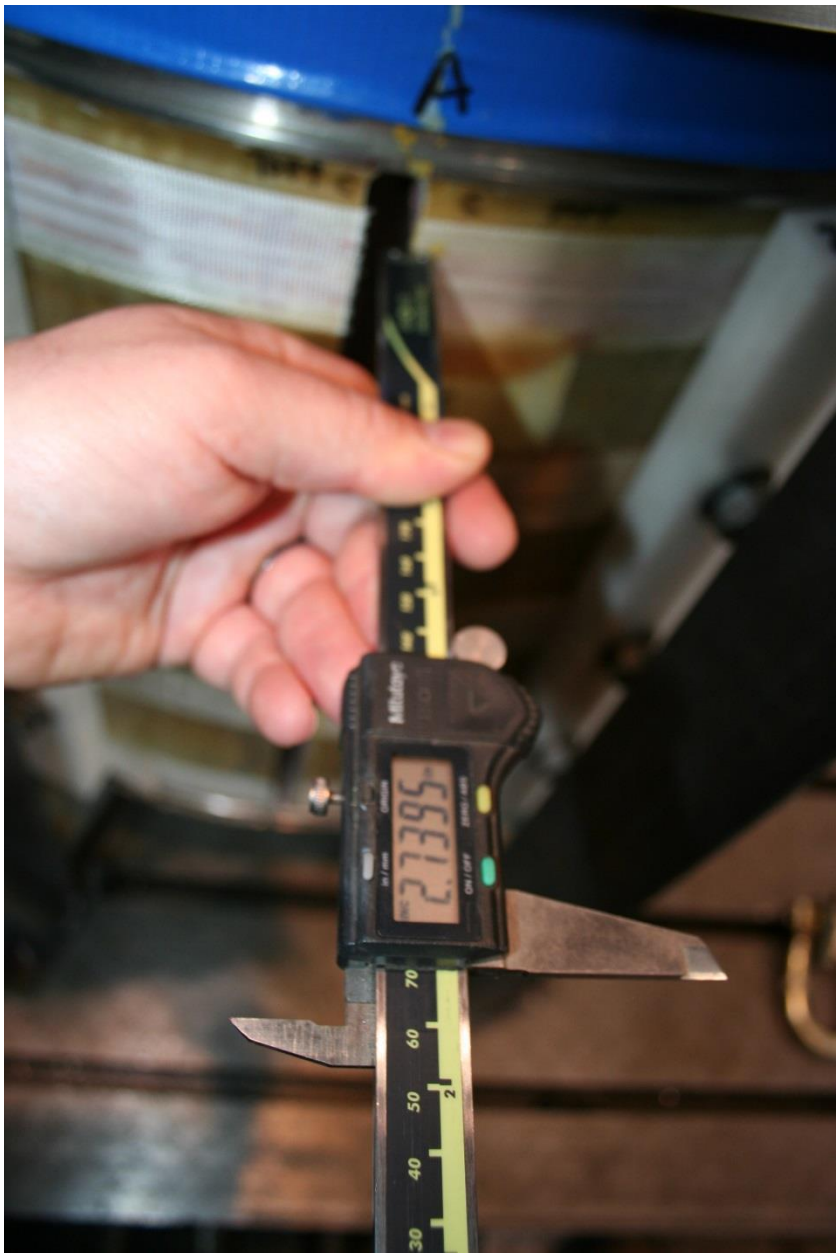

Figure 71 – Cutting Plane C coil pack depth

Figure 72 – Cutting Plane C coil pack depth

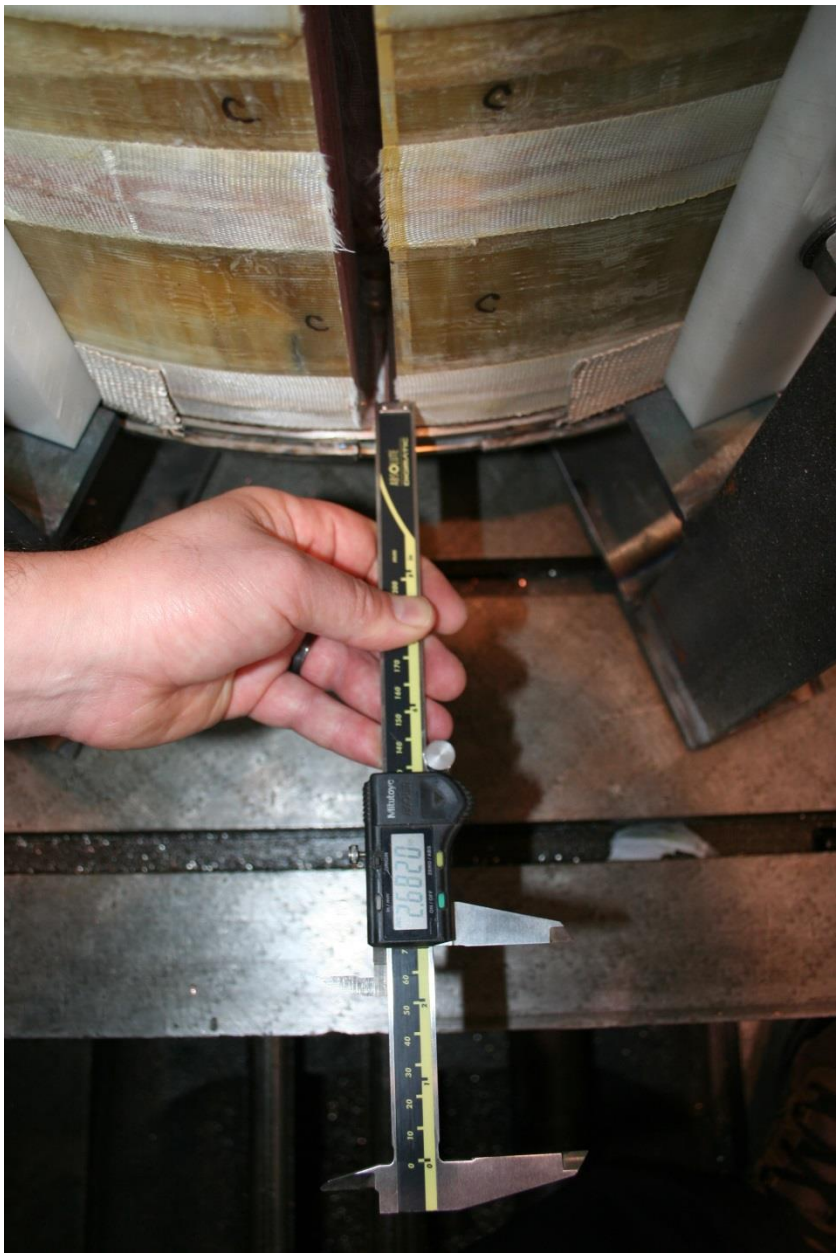

Figure 73 – Cutting Plane C coil pack depth

Figure 74 – PF1A-U Placement on Ransome table

Figure 75 – PF1A-U Placement on Ransome table

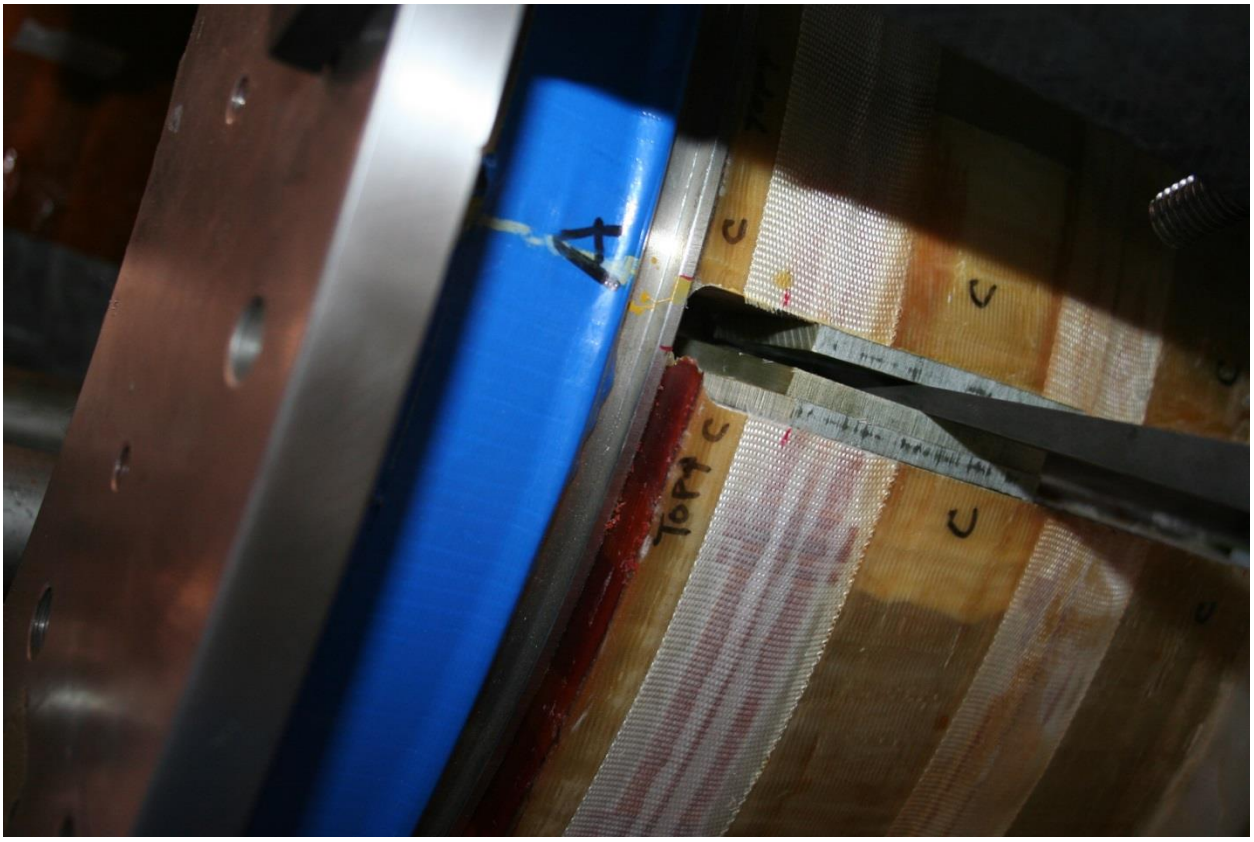

Figure 76 – Coil pack section B_C removal

Figure 77 – Coil pack section B_C removal

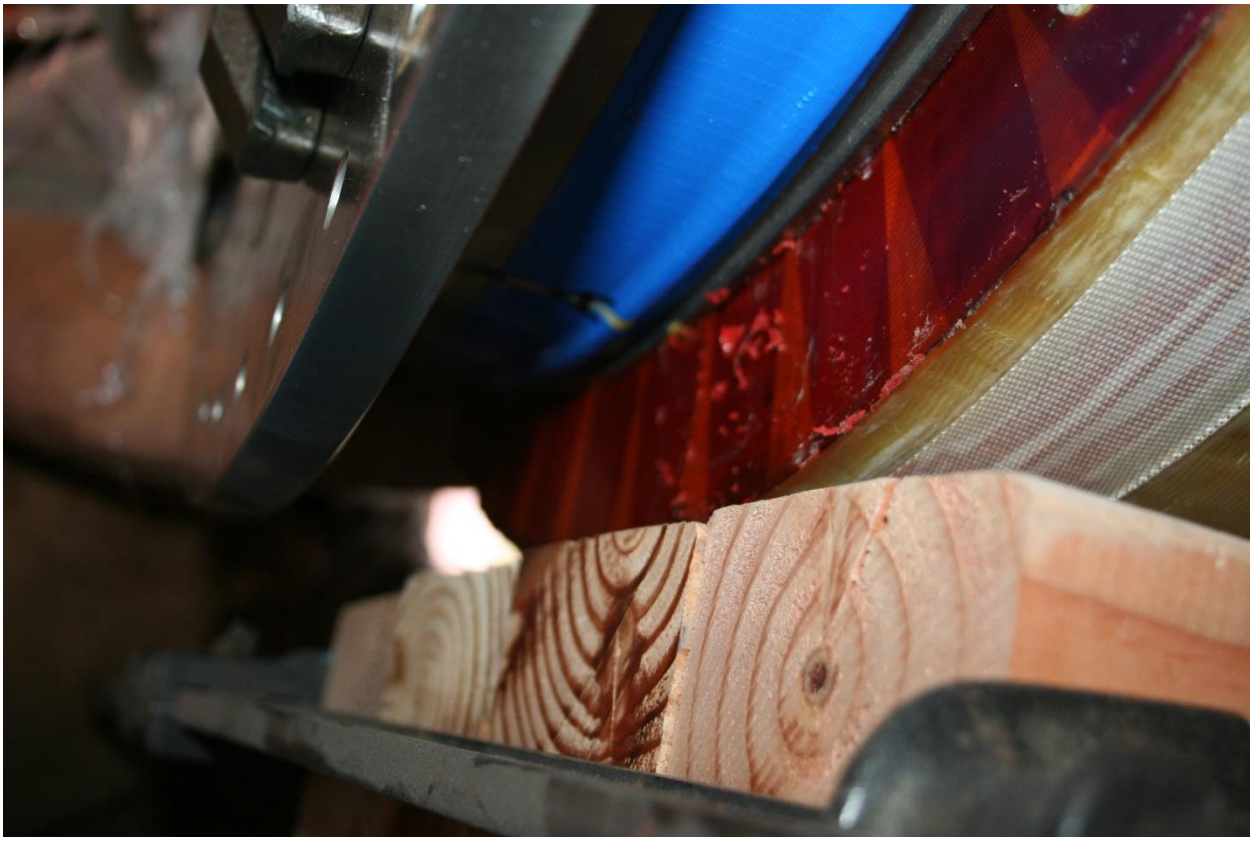

Figure 78 – Coil pack section B_C removal

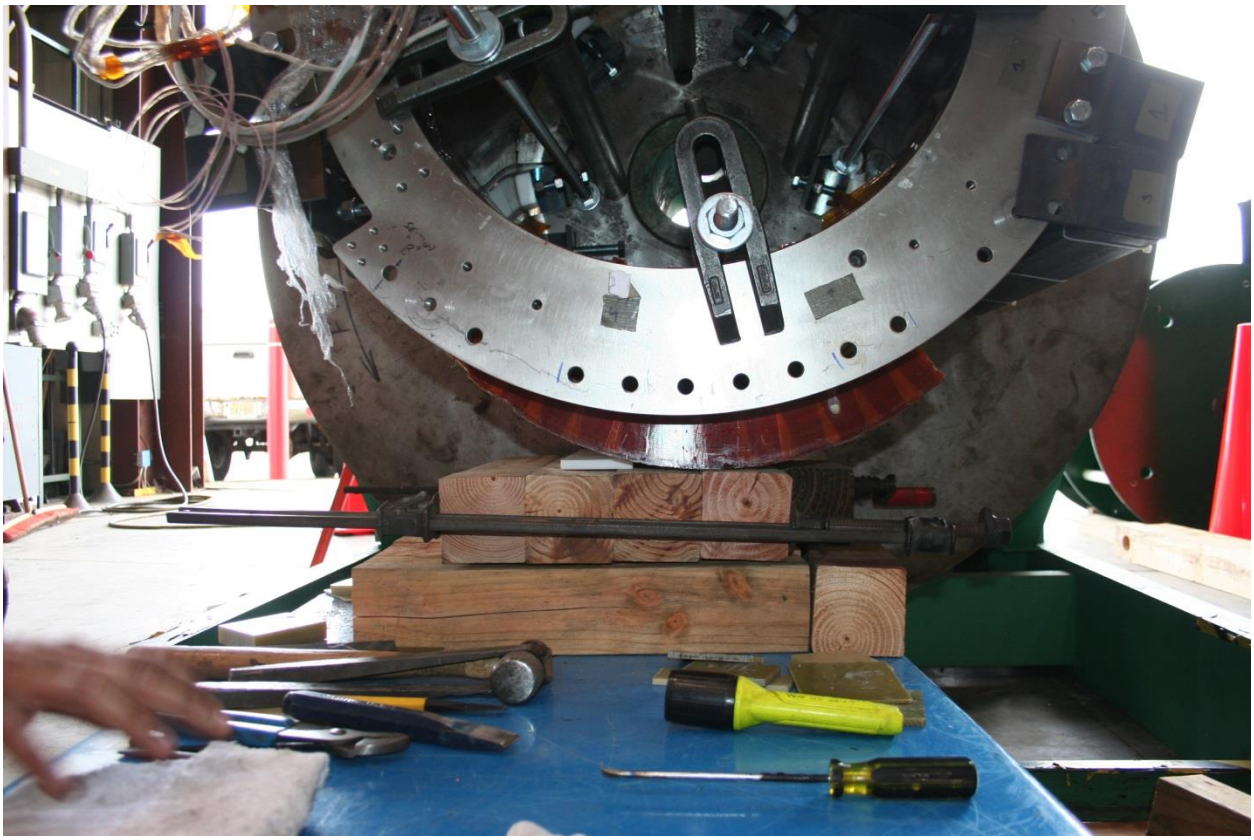

Figure 79 – Coil pack section B_C removal

Figure 80 – Coil pack section B_C removal

Figure 81 – Coil pack section B_C removed

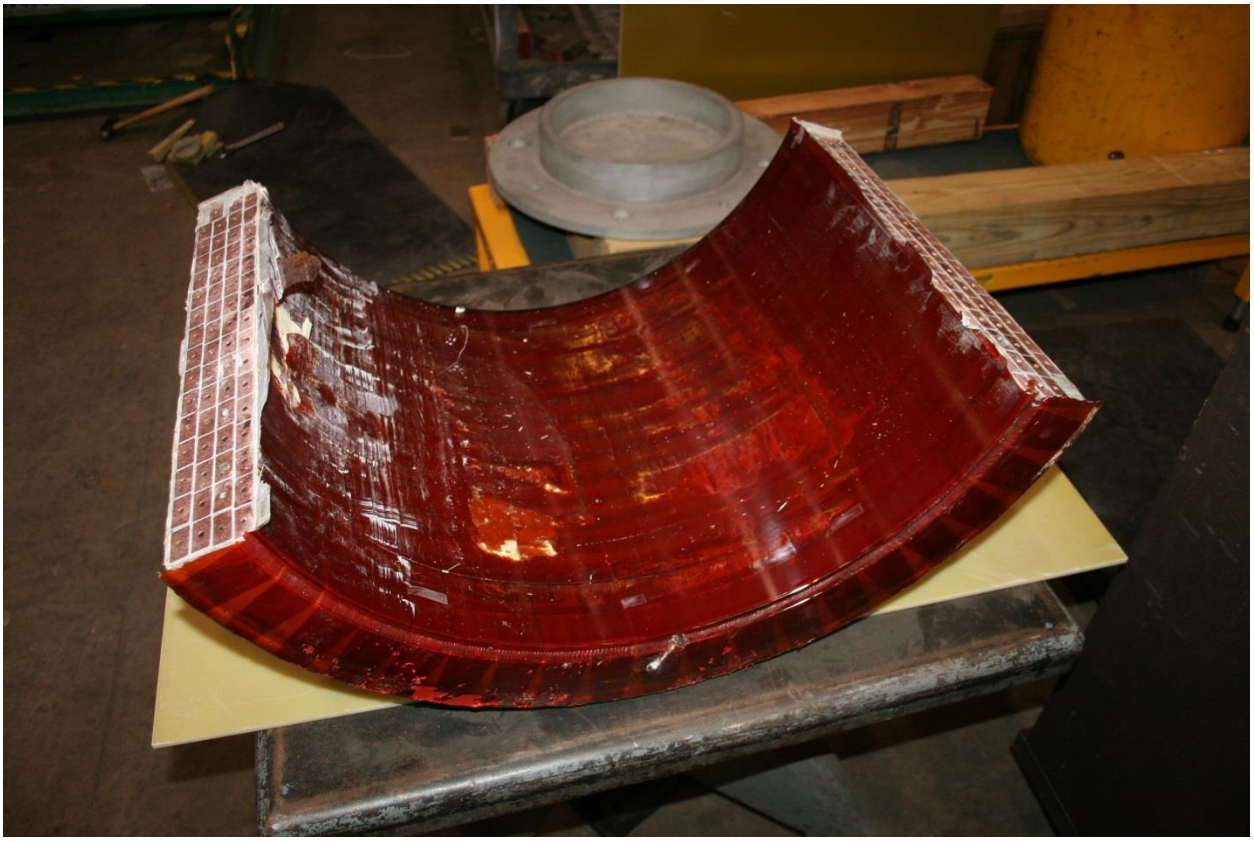

Figure 82 – Coil pack section C_A removed

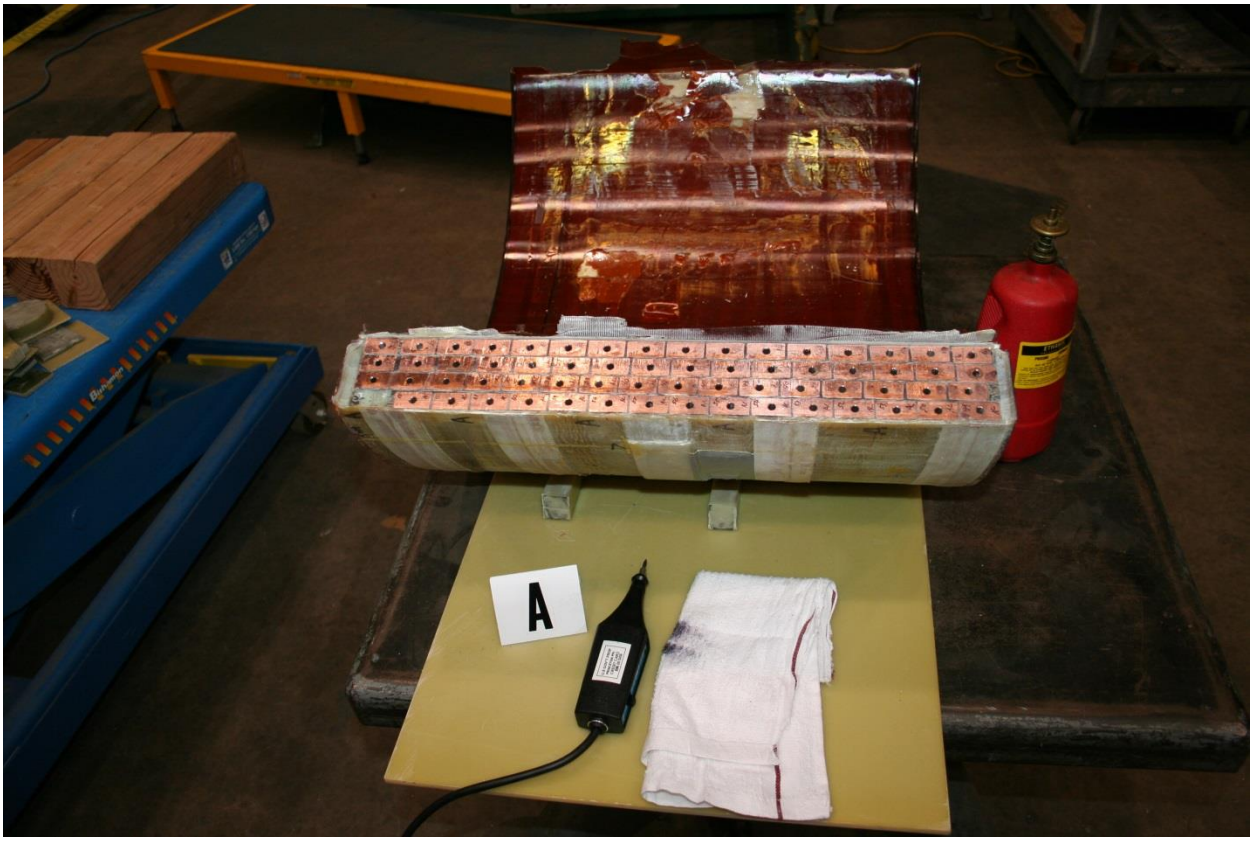

Figure 83 – Coil pack section plane A marking

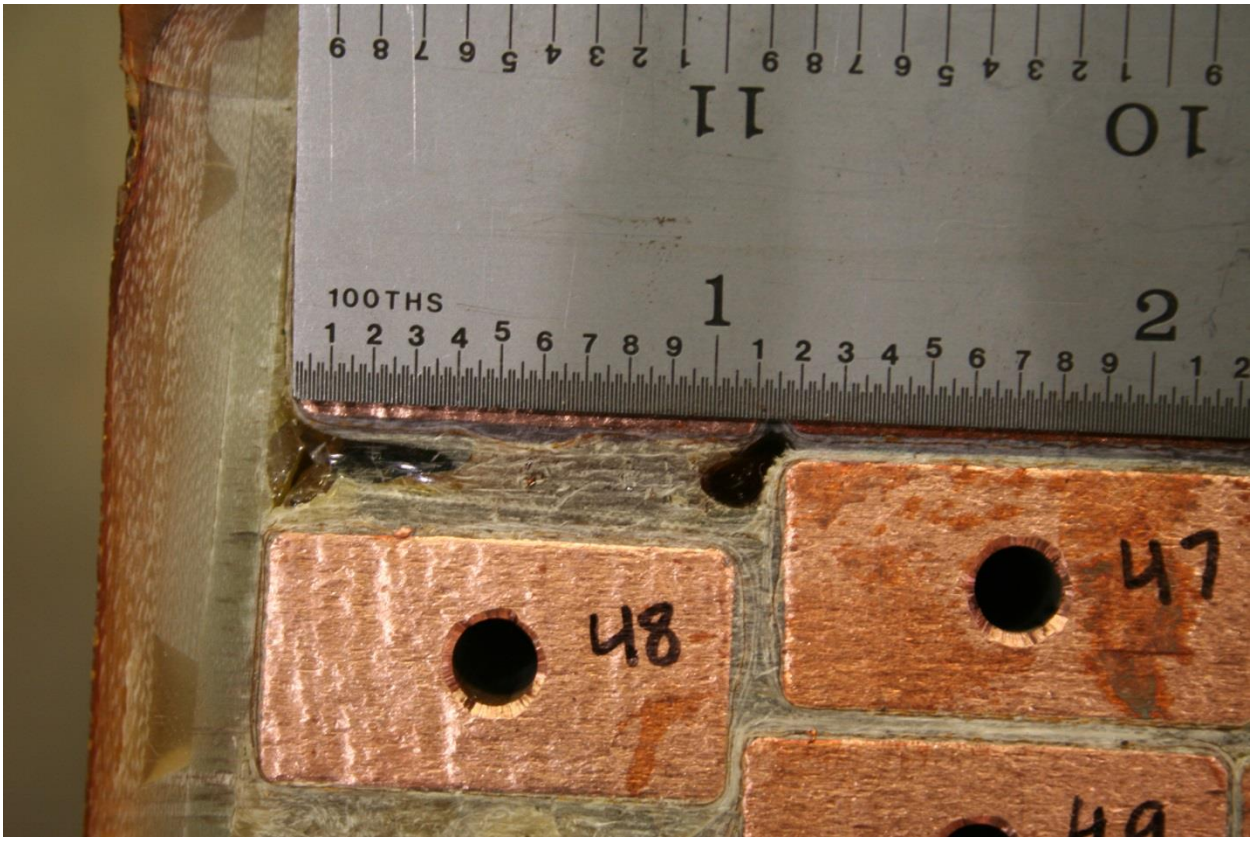

Figure 84 – Coil pack section plane C void

Figure 85 – Coil pack section plane C dry glass

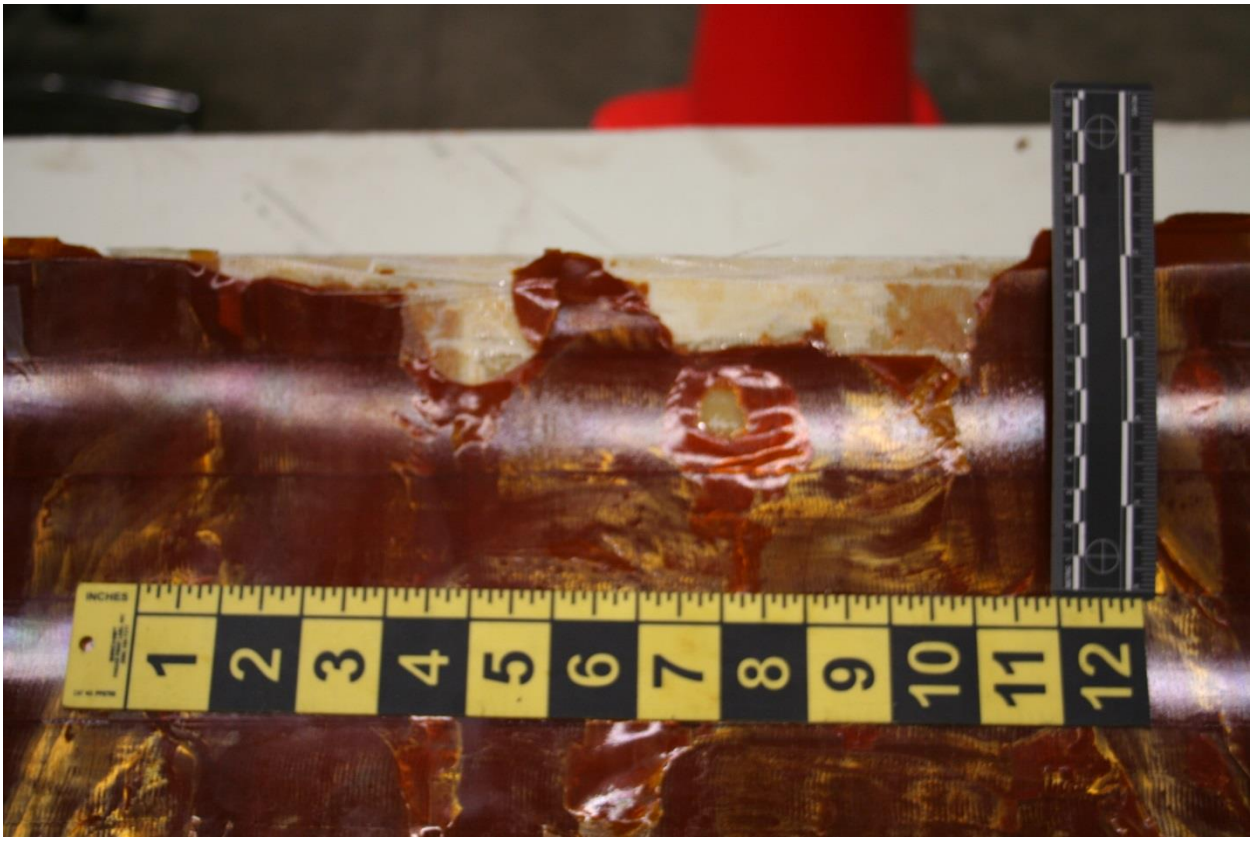

Figure 86 – Coil pack section plane B dry glass

Figure 87 – Coil pack section plane A void

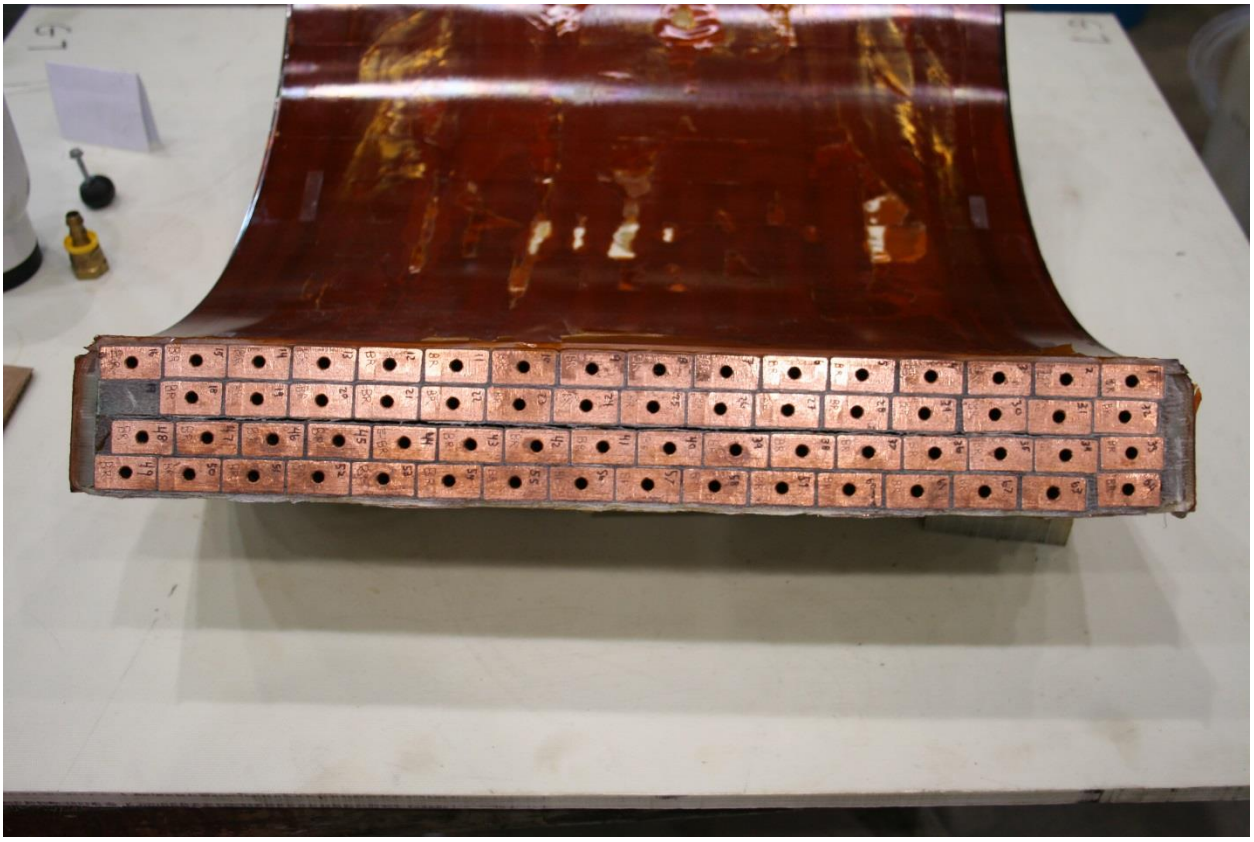

Figure 88 – Coil pack section plane B separation

Figure 89 – Coil pack section plane B separation

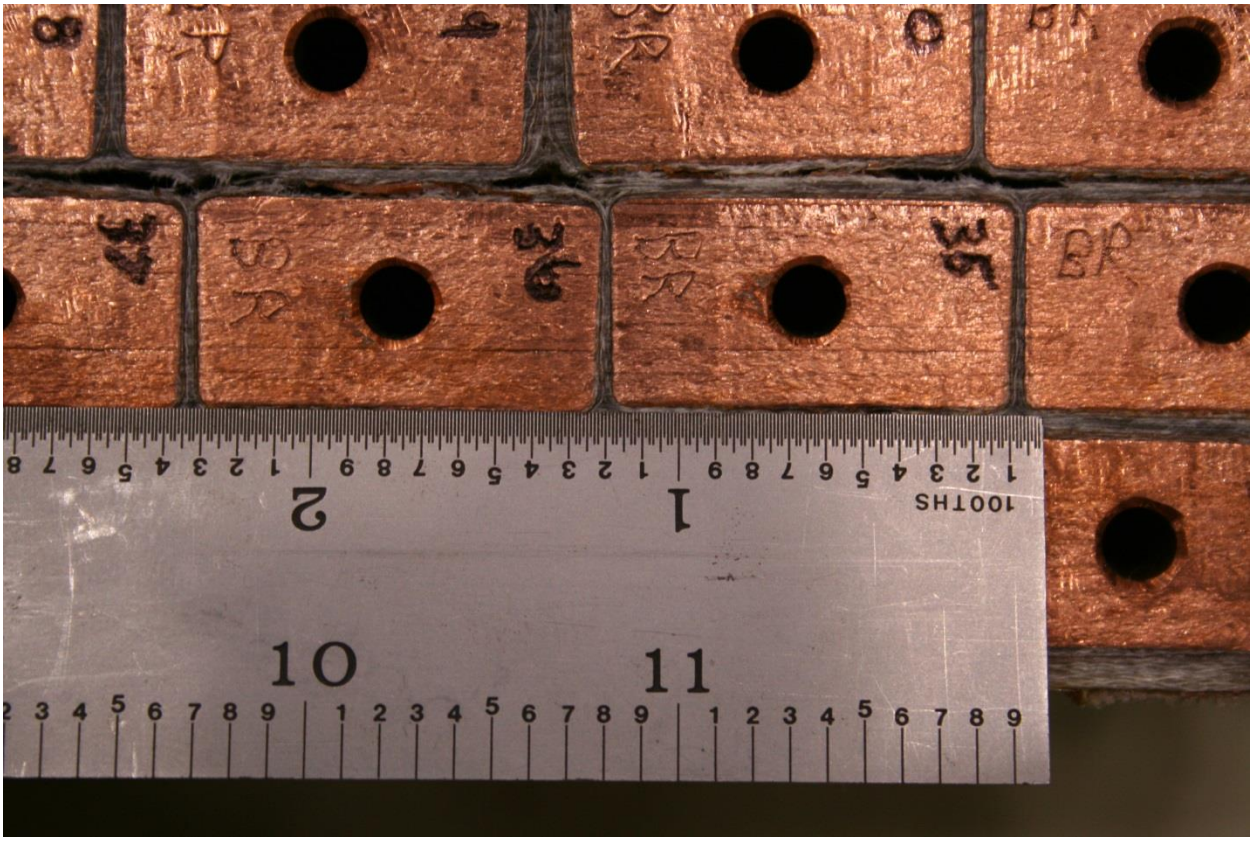

Figure 90 – Coil pack section plane B keystoning

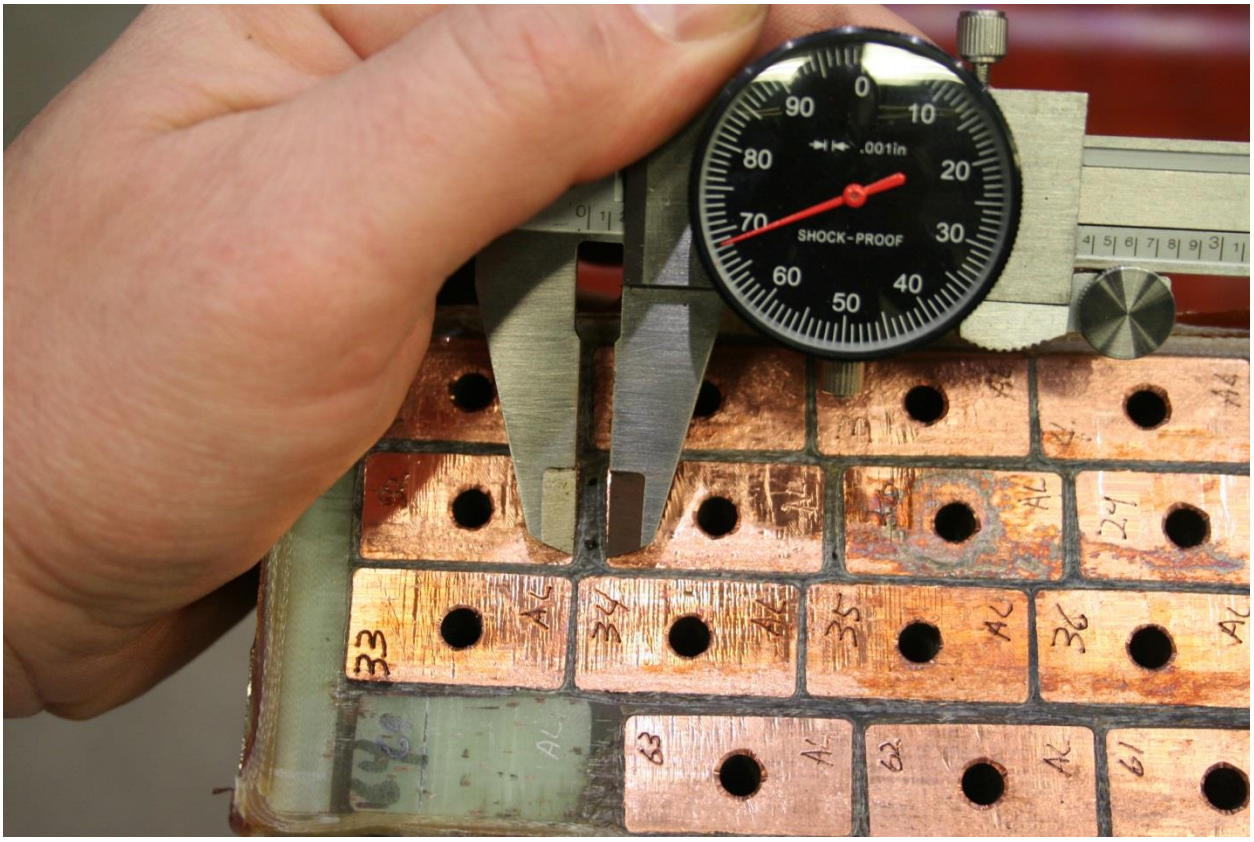

Figure 91 – Coil pack section plane A insulation spacing

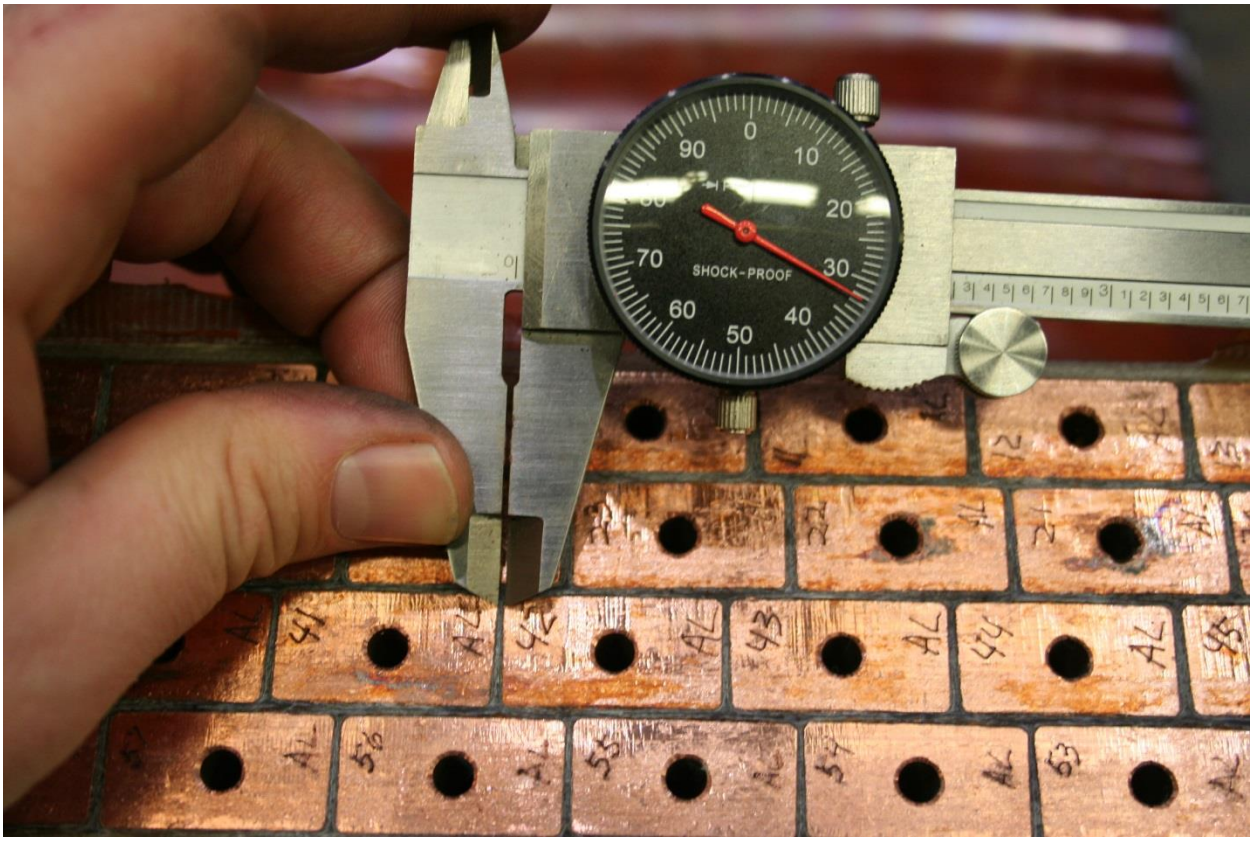

Figure 92 – Coil pack section plane A insulation spacing

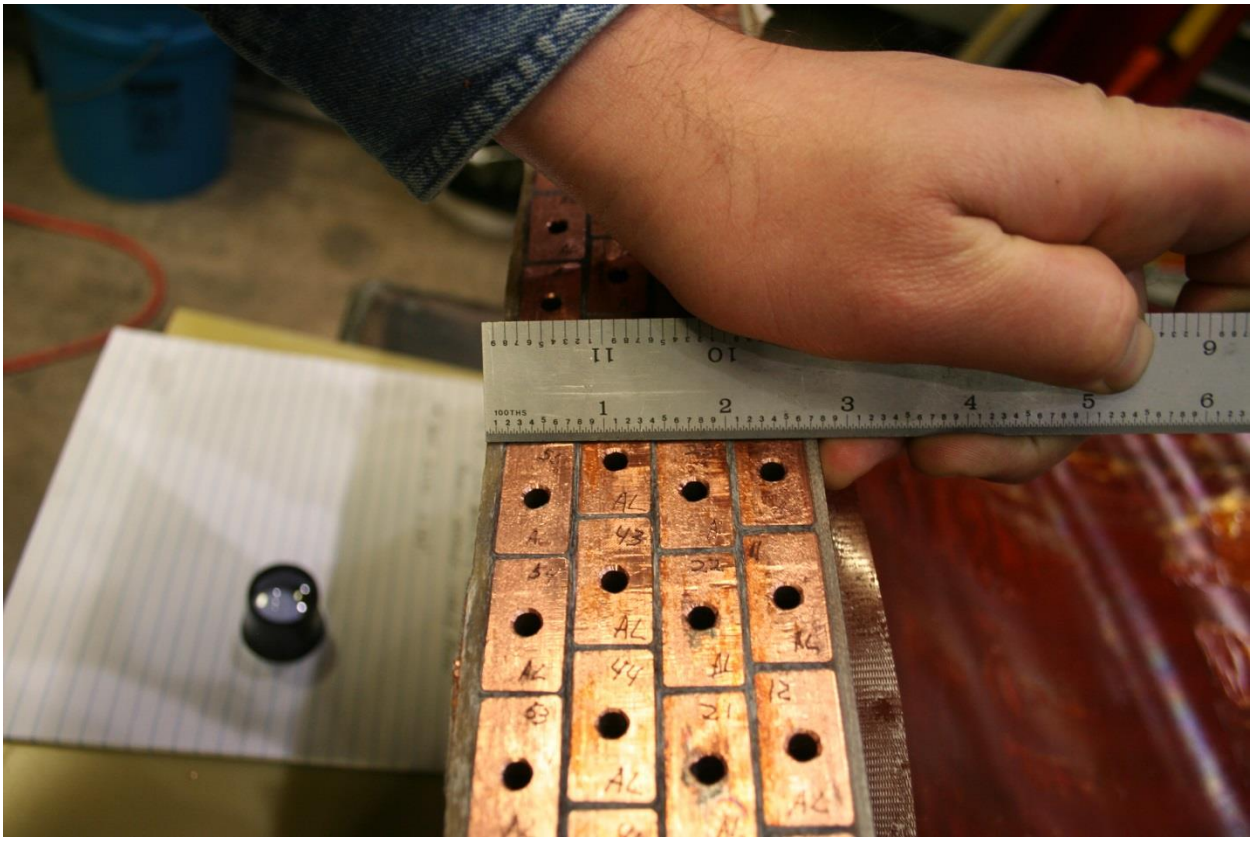

Figure 93 – Coil pack section plane A insulation spacing

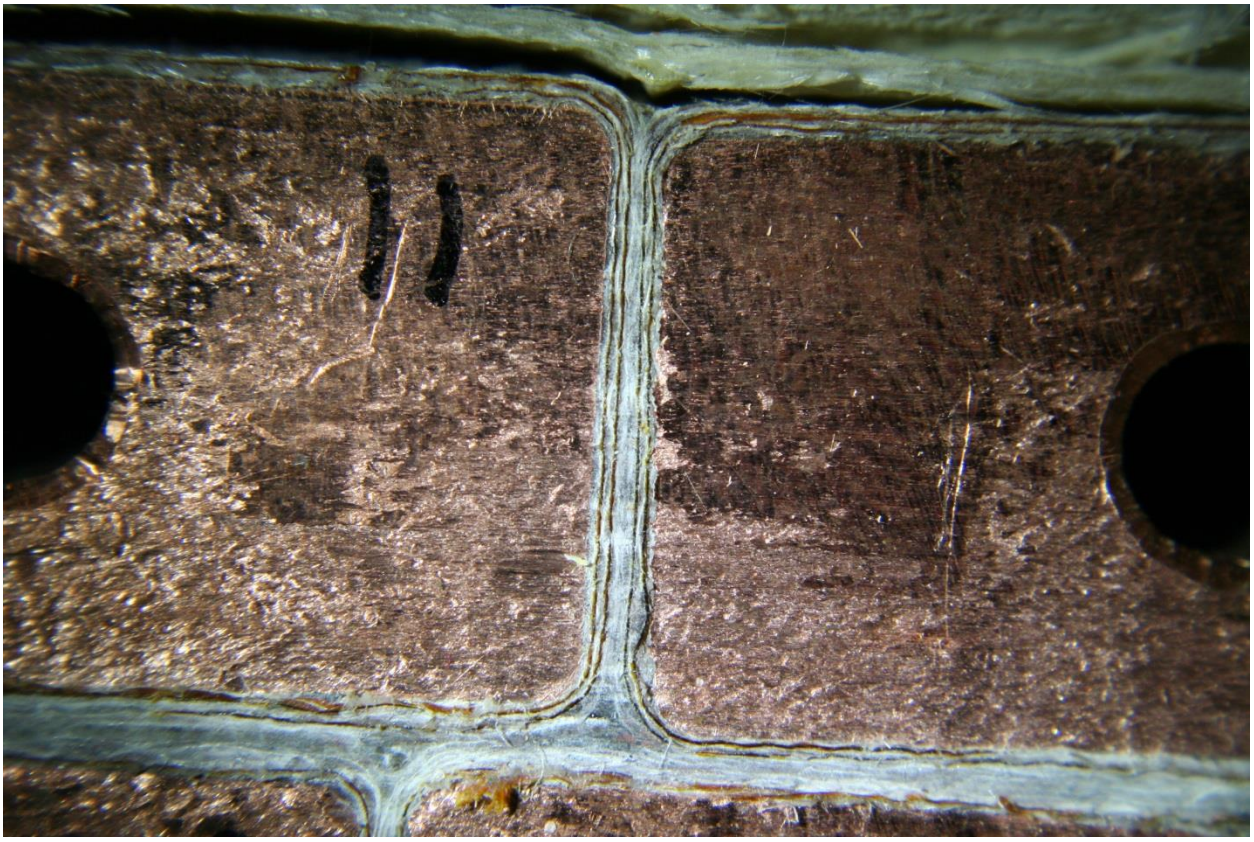

Figure 94 – Coil pack section plane C insulation lay-up

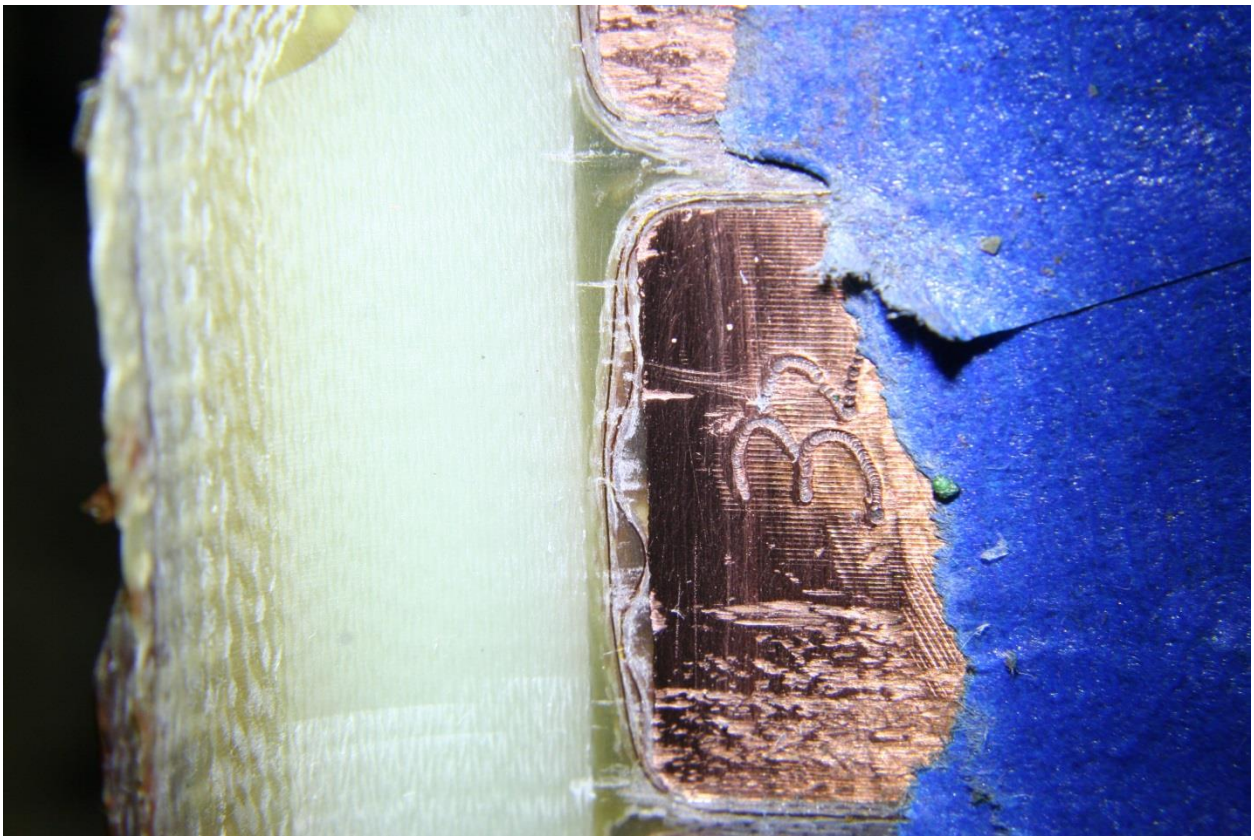

Figure 95 – Coil pack section plane A insulation lay-up

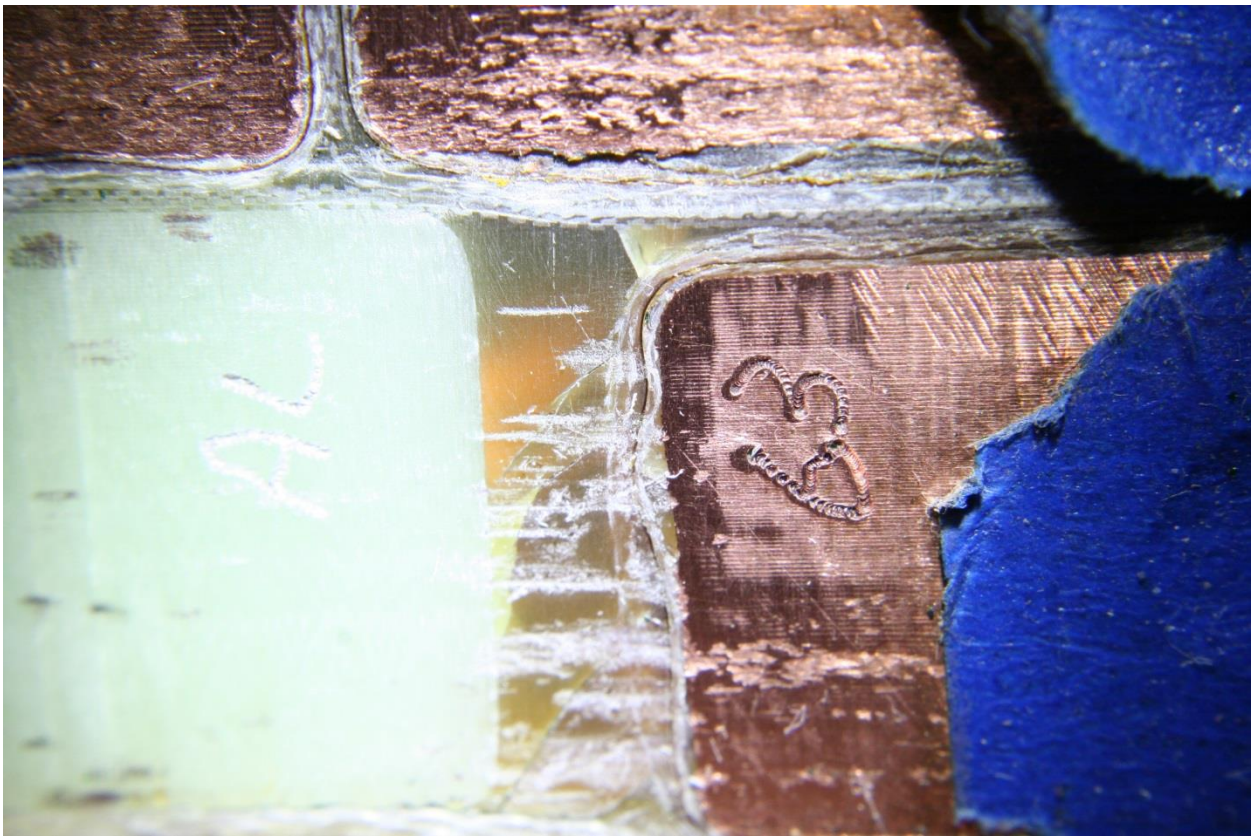

Figure 96 – Coil pack section plane A insulation layer-to-layer

Figure 97 – Braze Joint #1 with blockage – view from plane A

Figure 98 – Braze Joint #1 with blockage – view from plane C

Figure 99 – Braze Joint #1 without blockage – view from plane C

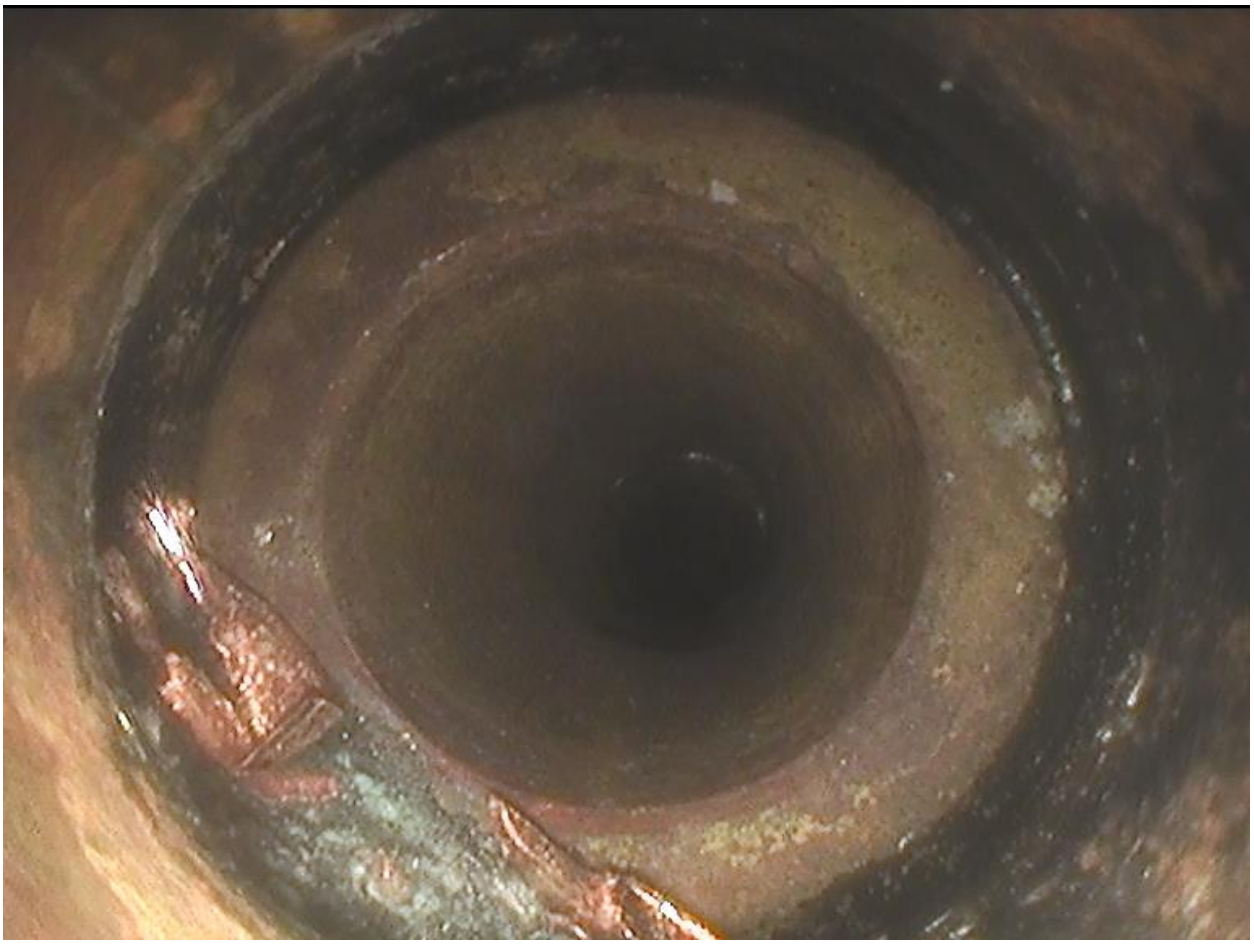

Figure 100 – Braze Joint #2 – view from plane B

Figure 101 – Braze Joint #2 void – view from plane B

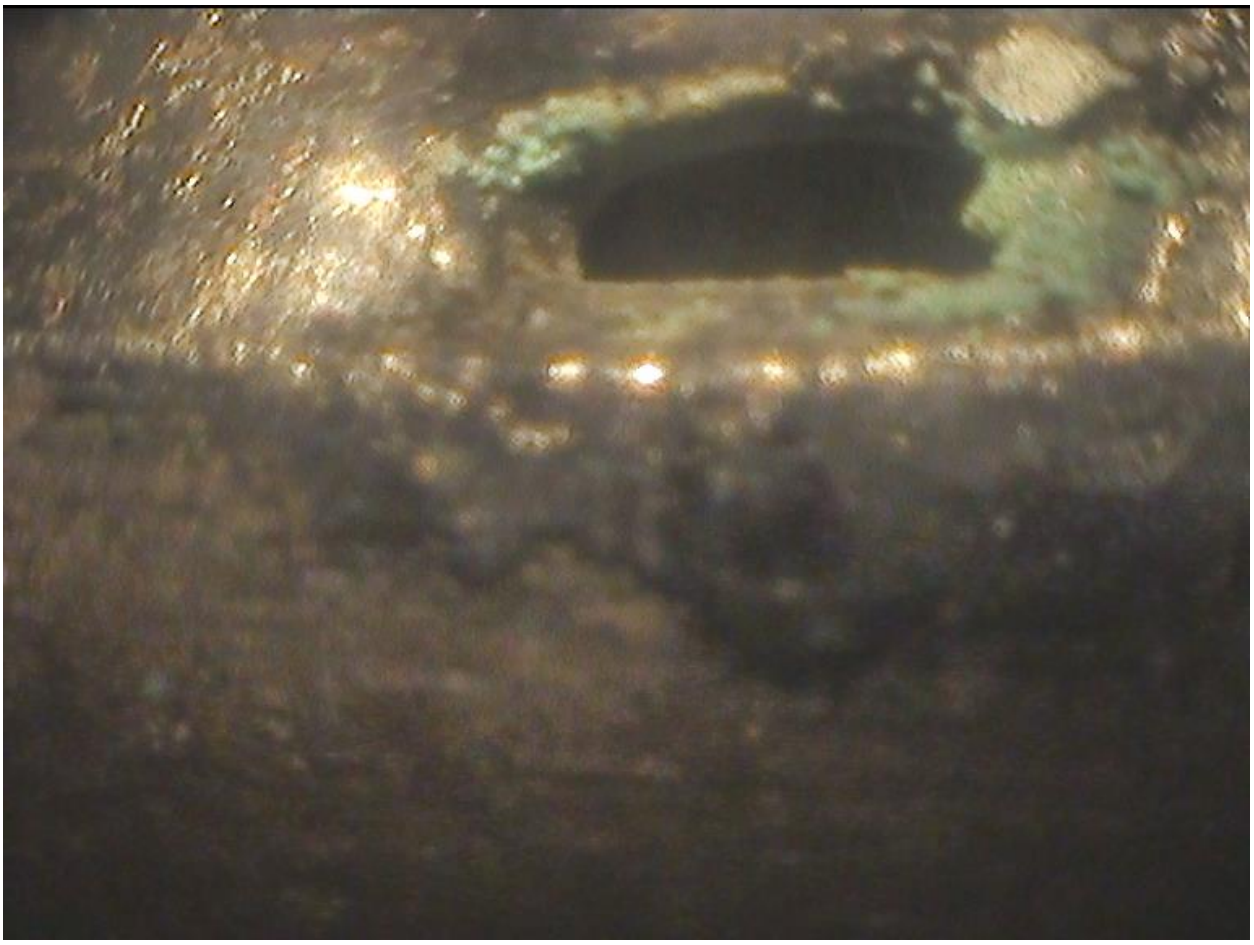

Figure 102 – Braze Joint #2 void – side view

Figure 103 – Braze Joint #3 blockage – view from plane B

Figure 104 – Braze Joint #3 blockage – view from plane A

Figure 105 – Braze Joint #3 without blockage – view from plane A

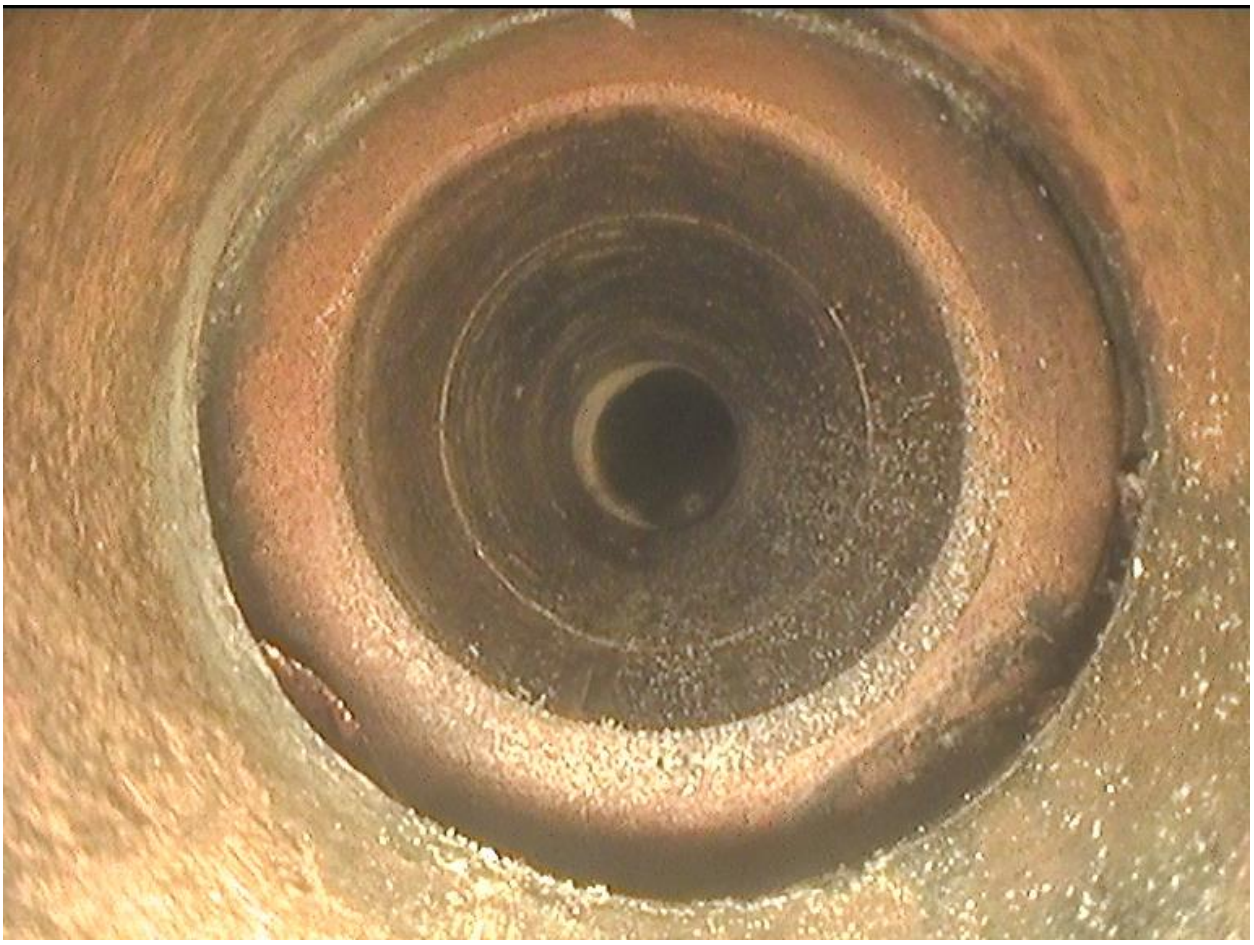

Figure 106 – Braze Joint #4 – view from plane B

Figure 107 – Braze Joint #4 misalignment – view from plane B

Figure 108 – Void – view from plane B

Figure 109 – Void – view from plane A

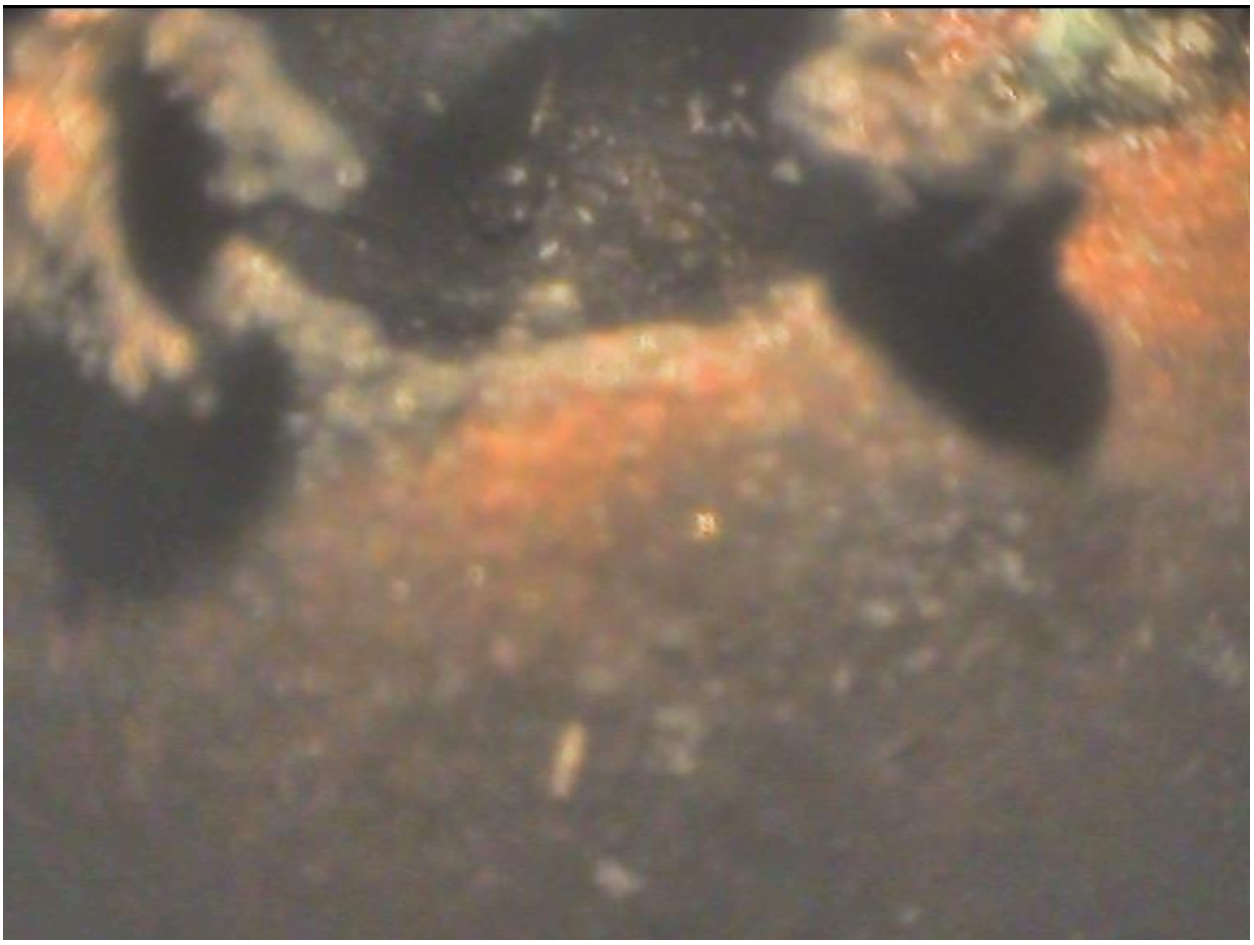

Figure 110 – Void – side view

Figure 111 – Void – side view

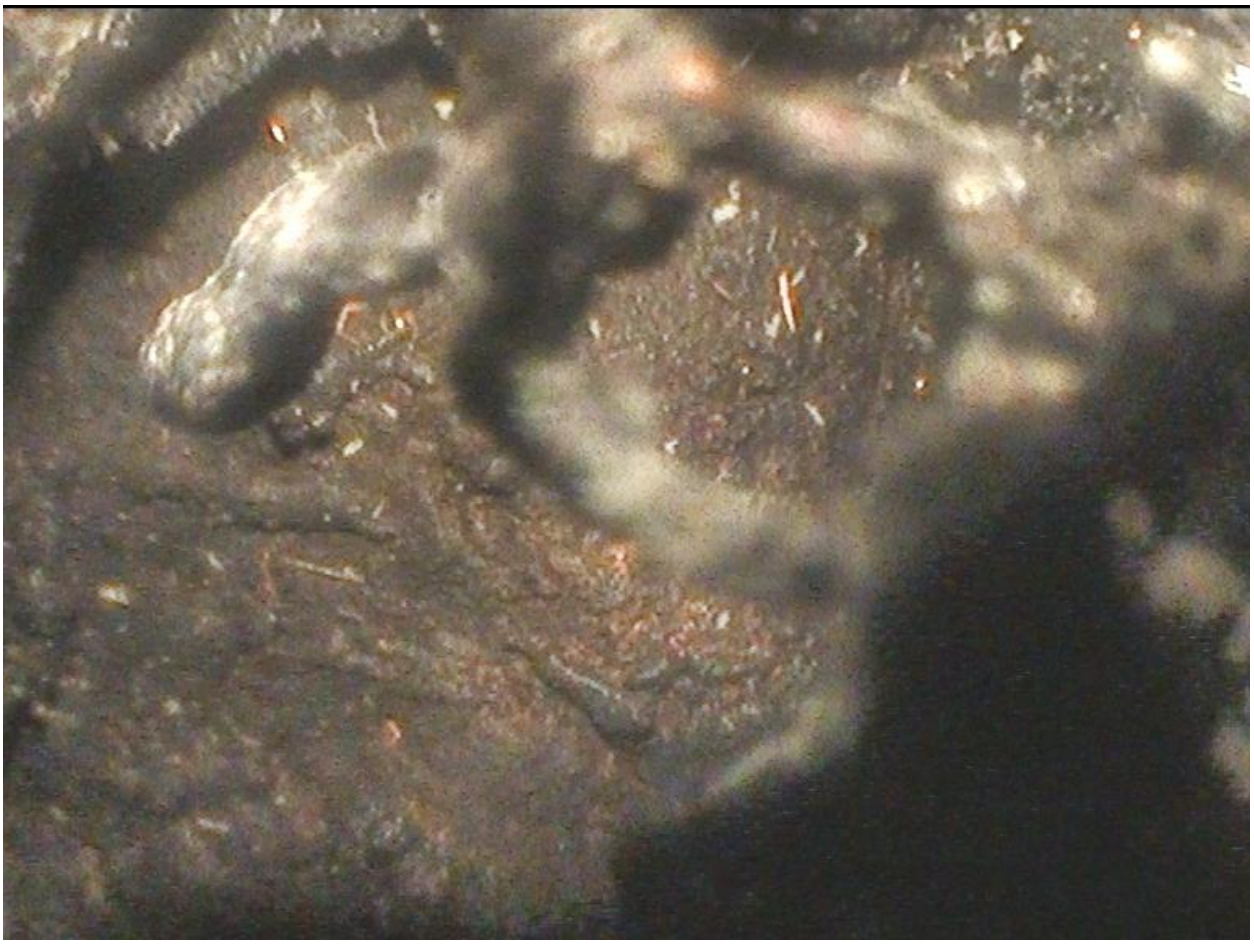

Figure 112 – Void – side view

Figure 113 – Discoloration proximal to void in adjacent cooling path

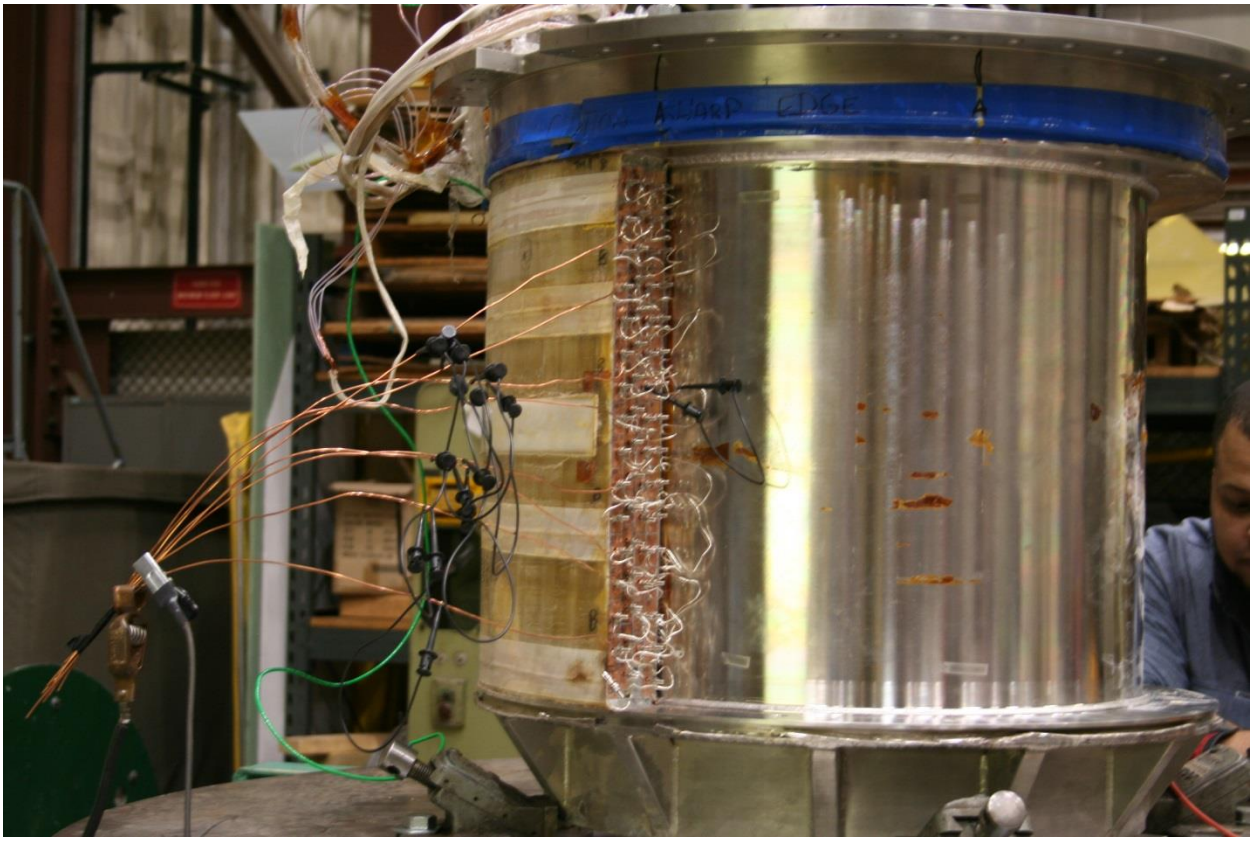

Figure 114 – Electrical testing set-up example

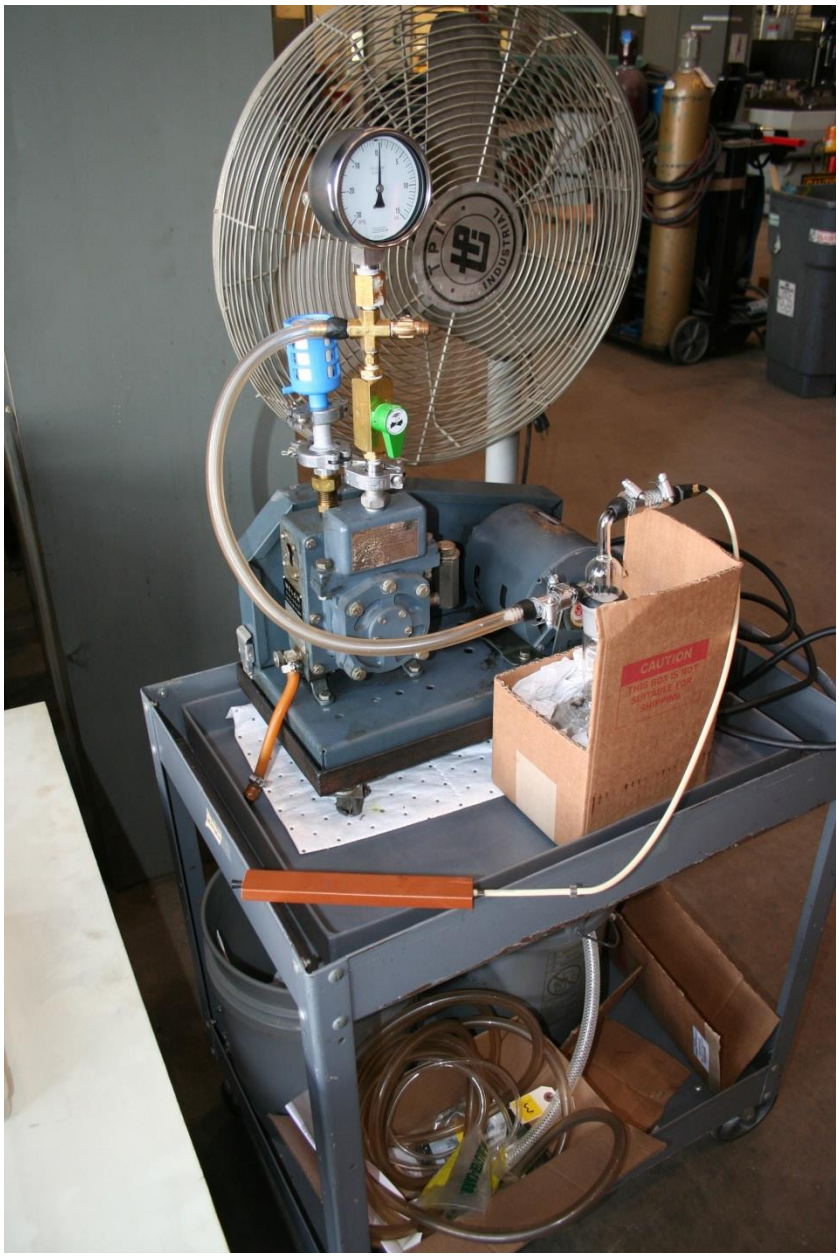

Figure 115 – Vacuum testing apparatus

Figure 116 – Pressure testing set-up example